High Performance Disturbance Observer Based Control System Design for Permanent Magnet Synchronous AC Machine Applications

A thesis submitted in partial fulfilment for the degree

of Doctor of Philosophy

By

Bayandy Sarsembayev

Supervised by:

Dr Tatiana Kalganova

Dr Ton Duc Do (Nazarbayev University, Kazakhstan)

Department of Electronic and Computer Engineering

College of Engineering, Design and Physical Sciences

Brunel University London

November 2022

Acknowledgements

The work presented in this thesis is the results of my PhD study at the Department of Electronic and Computer Engineering, Brunel University London and research done in the Laboratory of Power Conversion and Motion Control, Nazarbayev University (Kazakhstan).

I would like to express my sincere gratitude to my supervisors, Dr Tatiana Kalganova and Dr Ton Duc Do for their time, expertise and knowledge they have given during the fulfilment of the PhD study.

It would not be possible without the beliefs to my potential and financial supports of my wife, and my parents, therefore I express my gratitude and love to them.

I would like to thank the Center for International Program “Bolashak” of the Ministry of Education and Science Republic of Kazakhstan for granting me a President of Kazakhstan Republic’s scholarship to study master programme and following extending of my fulfilment of the scholarship obligations due to commencing PhD study. Thanks to all members of Laboratory of Power Conversion and Motion Control at Nazarbayev University for their supports. Thanks for external and internal examiners for valuable comments during viva examination.

Abstract

An electrical machine is one of the main workforces in different industries and serves them in various applications. Machine drive control design involves many technical issues for efficient and robust exploitation. Over several decades, Permanent Magnet Synchronous Motor (PMSM) is getting preferred for industrial applications over its counterpart Squirrel Cage Induction Motor (SCIM) drive, because of their higher efficiency, power density, and higher torque to inertia ratio.

In the prospective that PMSM drives are considered the drives of the future, there are still technical challenges and issues related to PMSM control. Many studies have been devoted to PMSM control in the past, but there are still some open research areas that bring worldwide researchers' interests back to PMSM drive control. One of the approaches that may facilitate better performance, higher efficiency, and robust and reliable work of the control system is the disturbance observer-based control (DOBC) with linear and nonlinear output feedback control for PM synchronous machine applications. DOBC is adopted due to its ability to reject external and internal disturbances with improving tracking performance in the variable speed wind energy conversion system (WECS) to maximize power extraction. The high order disturbance observer (HODO) is utilized to estimate the aerodynamic torque-based wind speed without the use of a traditional anemometer, which reduces the overall cost and improves the reliability of the whole system. Also, this method has been designed to improve the angular shaft speed tracking of the PMSM system under load torque disturbance and speed variations.

The model-based linear and nonlinear feedback control are used in the proposed control systems. The sliding mode control (SMC) with switching output feedback control law and integral SMC with linear feedback and state-dependent Riccati equation (SDRE) based approaches have been designed for the systems. The SDRE control accounts for the nonlinear multivariable structure of the WECS and is approximated with Taylor series expansion terms. The chattering inherited from SMC is eliminated by the continuous approximation technique. The sliding mode is guaranteed by eliminating the reaching mode in the proposed integral SMC. The model-free cascaded linear feedback control system based on the proportional-integral (PI) controllers use a back-calculation algorithm anti-windup scheme. The proposed speed controllers are synthesized with HODO to compensate for the external disturbance, model uncertainty, noise, and modelling errors. Moreover, servomechanism-based SDRE control, a near-optimal

control system is designed to suppress the model uncertainty and noise without the use of disturbance observers.

The proposed control systems for PMSM speed regulation have demonstrated a significant improvement in the angular shaft speed-tracking performance at the transients. Their performances have been tested under speed, load torque variations, and model uncertainty. For example, HODO-based SMC with switching output feedback control law (SOFCL) has demonstrated improvement by more than 78% than the PI-PI control system of the PMSM. The performance of the HODOs-based Integral SMC with SDRE nonlinear feedback is improved by 80.5% under external disturbance, model uncertainty, and noise than Integral SMC with linear feedback in the WECS. The HODO-based SDRE control with servomechanism has shown an 80.2% improvement of mean absolute percentage error under disturbances than Integral SMC with linear feedback in the WECS. The PMSM speed tracking performance of the proposed HODO-based discrete-time PI-PI control system with back-calculation algorithm anti-windup scheme is improved by 87.29% and 90.2% in the speed commands and load torque disturbance variations scenarios respectively. The simulations for testing the proposed control system of the PMSM system and WECS have been implemented in Matlab/Simulink environment. The PMSM speed control experimental results have been obtained with Lucas-Nuelle DSP-based rapid control prototyping kit.

Table of Contents

List of Figures

List of tables

List of abbreviations

ARE – Algebraic Riccati Equation

AW – Anti-Windup

BIBO – Bounded-Input and Bounded-Output

DOBC – disturbance observer-based control

DSP – Digital Signal Processing

FOC – Field-Oriented Control

FODO – First Order Disturbance Observer

FPGA – Field Programmable Gate Arrays

HODO – High Order Disturbance Observer

IDO – Intelligent Disturbance Observer

ISMC – Integral Sliding Mode Control

LDO – Linear Disturbance Observer

LQR – Linear Quadratic Regulator

MIMO – Multi-Input and Multi-Output

NDO – Nonlinear Disturbance Observer

OC – Optimal Control

PI - Proportional-Integral controller

PMSG – Permanent Magnets Synchronous Generator

PMSM – Permanent Magnets Synchronous Motor

PWM – Pules Width Modulation

SDRE – State-Dependent Riccati Equation

SISO – single input single output

SMC – Sliding Mode Control

SVPWM – Space Vector Pules Width Modulation

VC –Vector Control

VSI – Voltage Source Inverter

WECS – Wind Energy Conversion System

WT – Wind Turbine

List of symbols

$x \in R^n$	State vector
$u \in R^m$	Control input vector
$d \in R^m$	Disturbance vector
$y \in R^l$	Output vector
A,B, C and D	A system, input, output, and feed-forward matrices
$\hat{d}$	Estimated disturbance
z	An internal variable of the observer
L	Observer gain matrix
F^+	Pseudo inverse matrix of F.
$\Gamma_0 = \mathrm{diag}(\xi_{01} \ldots \xi_{0r})$	Positive disturbance observer gain matrix
$K_A(t), K_B(t), K_C(t)$	AC motor variables
α-β	Stationary reference frame
d-q	Rotating reference frame
Ψ_s	Stator magnetic flux
θ_m	Mechanical angle
Ψ_d	Magnetic flux leakage in d-axis
Ψ_q	Magnetic flux leakage in q-axis
ε_d	Back electro-motive force (EMF) in d-axis
ε_q	Back electro-motive force (EMF) in q-axis
T_p	Produced torque of PMSM
ω_{max}	The maximum rotor speed of PMSM
$E_{s\,max}$	Maximum induced phase voltage in PMSM
$(\dot{\ldots})$	Denotes derivatives of argument function;
ω	Angular rotor speed
ω_d	Desired angular rotor speed
i_d and i_q	d-axis and q-axis currents
V_d and V_q	d-axis and q-axis voltages
T_L	Rated load torque
$\hat{T}_L$	Estimated load torque
P	Number of poles pairs
R_s	Stator resistance
L	Stator inductance
J_{ri}	Rotor inertia
B_{vf}	Viscous friction coefficient
λ_m	Magnet flux linkage
ρ	Air density
R	WT rotor radius
v	Wind speed
C_p	Power coefficient of the wind turbine
λ	Tip-speed ratio
β	Pitch angle
ω_t	Angular shaft speed of the turbine.
n_{gb}	Gearbox ratio
T_a	Aerodynamic torque
T_{gs}	Generator side angular torque
T_e	Electromagnetic torque

ΔR_s and ΔL	Variations of stator resistance and inductance
d_{qn} and d_{dn}	Noise and modeling errors
$P \in R^{n\times n}$	Positive-definite matrix
σ	Sliding surface
λ_{opt}	Optimal tip-speed ratio
C_p^{max}	Maximum power coefficient corresponding to optimal tip-speed Ratio and pitch angle
Q, R	Tuning gain matrices
$\tilde{\omega}$	Electrical rotor speed error
$\tilde{T}_e$	Electromagnetic torque error
δ	Small positive constant.
L_1, L_2, L_3	HODO observer gains
V	Positive candidate Lyapunov's function
k	Positive scalar
z_p	number of poles,
b	Viscous damping coefficient
c_{ed}	Eddy currents coefficient
C_f	A static moment of friction
C_{hys}	Hysteresis losses coefficient
d_{ed}	Eddy currents damping coefficient
Ψ_{dq}	DQ frame magnetic flux linkage
$inSat$	The input of the saturation block
$\overline{+}Sat$	The output of the saturation block
out	The output of the PI controller
$inAW$	The input of the anti-windup block
$\overline{+}AW$	The output of the anti-windup block
$eSat$	An error of saturation block
eAW	An error of the anti-windup block
K_p	Proportional gain of PI controller
T_i	Integrator time
T_s	Sampling time
$\frac{1}{z}$	Unit delay
K_{back}	Back-calculation gain
d_T^{cogi}	The amplitude of the i^{th} -order harmonic cogging torque
θ_e	The electrical angle of the rotor position
λ_{mi}	The amplitude of the 6^{th}-order harmonic flux
d_T^{flux}	Torque disturbance due to flux harmonics
I_{max}	Maximum stator current
e	Error signal
u_c	Compensating term of the control input signal
$u_{SDRE}(t)$	SDRE-based the nominal control part
$u_1(t)$	Integral-based discontinuous part
$K(x)x$	The state-dependent near-optimal gain matrix
G	Design matrix in ISMC
$w(t)$	Integral term in ISMC
$d_u(t,x)$	Input disturbance
N	Number of the SDRE terms computed offline
$k_{Piq}$and k_{Iiq}	PI gains of the q-axis current controller

k_{Pid}, k_{Iid}	PI gains of the d-axis current controller
$k_{P\omega}$and $k_{I\omega}$	PI gains of the speed controller

Chapter 1: Introduction

1.1.Background information

There have been several applications where permanent magnet (PM) synchronous AC machines are becoming popular due to the preferable characteristic. They can be used in applications such as traction motors in electric vehicles (EVs), part of wind energy conversion systems (WECSs), heating, ventilation, and air condition (HVAC) appliances, etc. Although induction motors (IMs) still are widely used in the mentioned applications, the PMSMs are replacing them due to their advantages, such as higher power density, higher torque to inertia ratio, and higher efficiency.

As one application, a variable-speed drive or servo drive system, speed or position feedback is used for precise control of electric machines. The response time, and fewer errors in transient and steady-state times with which the machine follows the commanded speed and position are considered important performance characteristics. Industrial drive technology has changed in recent years from conventional DC or two-phase AC motor drives to less maintenance three-phase vector-controlled AC drives for all motor applications where quick response, light weight, and large continuous and peak torques are required. Moreover, the recent advances in power electronics have enabled them to reduce their cost by half per kilowatt

PMSMs combine some of the desirable advantages of conventional induction and synchronous motors and deserve special attention. They can be classified into two categories, one group is sinusoidally excited, known as PMSM and the other is square wave (trapezoidal excited) motors, known as brushless DC (BLDC). Each one has its advantages in different applications.

Machines with a sinusoidal excitation are fed with three-phase sinusoidal waveforms and operate on the principle of a rotating magnetic field. They are simply called sinewave motors or permanent magnet synchronous machines (PMSMs) [1]. All phase windings conduct current at the same time.

The square wave excited machines are also fed with three-phase waveforms shifted one from another by 120◦, but back EMF wave shapes are rectangular or trapezoidal as shown in Figure 1.1 (b). Such a shape is produced when the armature current is precisely synchronized with the rotor's instantaneous position and frequency (speed). The most direct and popular method of providing the required rotor position information is to use an angular position sensor mounted on the rotor shaft. Such a control

scheme or electronic commutation is functionally equivalent to the mechanical commutation in DC motors.

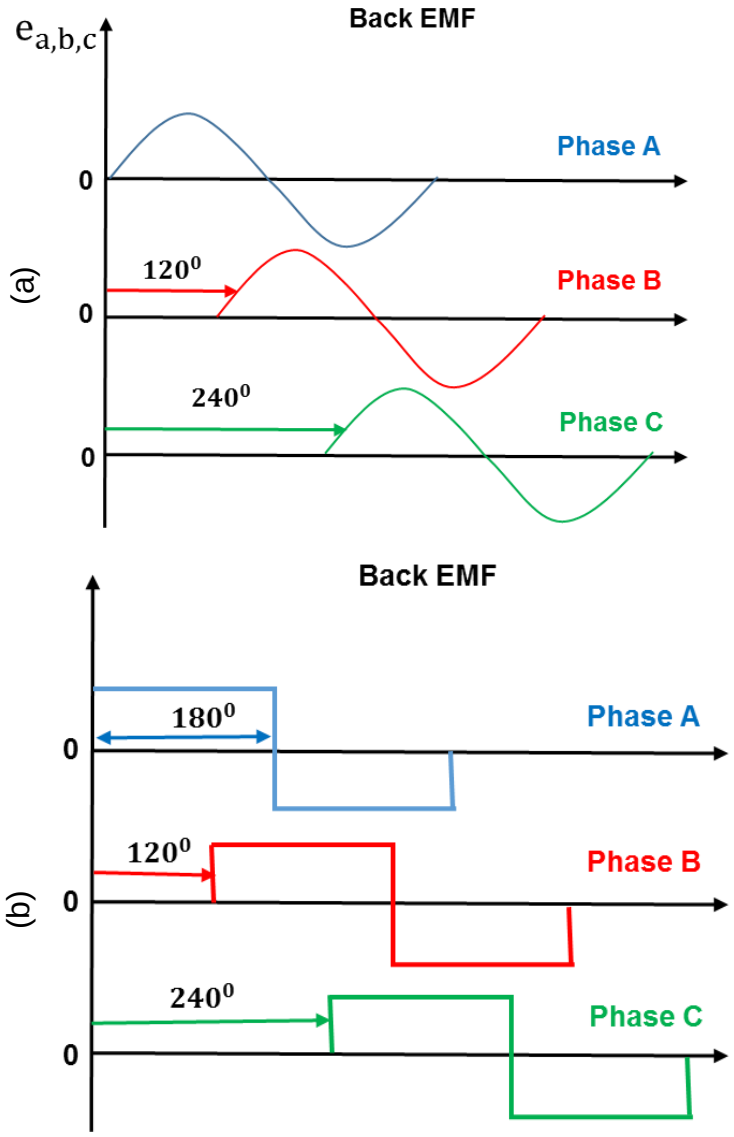

Figure 1.1. Basic excitation waveform, back EMF for (a) sinusoidal (b) trapezoidal courtesy of [1]

This explains why motors with square-wave excitation are called brushless DC motors (BLDC). These two kinds of permanent magnet motors are different in performance and control. In this research, the emphasis was placed on PM synchronous machines with sin wave excited back-EMF.

The use of PMSM in electrical drives has become a more attractive option than induction motors. The improvements made in the field of semiconductor drives mean that the control of PMSM has become easier and cost-effective with the possibility of operating the machine over a large speed range and still maintaining good efficiency and power

factor. The price of rare earth magnets is also coming down making these motors more popular [6].

For the variable speed, motor drives pulse width modulation (PWM) techniques are used to produce variable AC voltage with variable frequency from a voltage source inverter (VSI) connected to a DC power source. The commonly used PWM technique is space vector PWM (SVPWM). The basic idea of PWM is to modulate the duration of the pulses to achieve controlled voltage/current/power and frequency. The fast digital signal processing (DSP), microcontrollers, and field programmable gate arrays (FPGA) have made the implementation of complex PWM algorithms easier.

The variable-speed direct-driven WECS is another application of PM synchronous machines as a generator to produce a carbon-free energy source for electrical appliances and storage. While aerodynamic design and power converters topology of wind turbines play important role in the quantity and quality of energy production, the control system can maximize its efficiency during partial load as well as in fault conditions. Moreover, this configuration of WECS can work in standalone mode and grid-tied or in hybrid modes.

The harvesting of the electrical energy from converting the endless energy of wind through mechanical torque rotating permanent magnet synchronous generator (PMSG) installed in wind turbines (WTs) on-shore or off-shore is a quite promising technological application of PM synchronous machine. For example, 5 kW WT can produce over 18.3 kWh of energy a year with a 42% capacity factor. The energy generated by such WTs can be maximized via robust control systems developed by the research community. However, the fast-changing nature of the wind, measurement errors, parameter uncertainties, and faults of the sensors of the system may cause termination or inefficient operation of a control system of WECS. Therefore, the design control system tolerant to the fault of wind speed sensors and robust to model uncertainty is important for this application.

1.2.Problem statement

The DSP-based microcontrollers as well as advancing power electronics made various complex control designs possible to implement for the efficient operation of PM electric machines in various applications. The traditional linear techniques with closed-loop control are quite straightforward. However, the presence of various sources of disturbances such as external disturbance, parameters uncertainties, nonlinearities,

modelling errors, and noise degrades the control system's performance significantly Therefore, the design of robust, active disturbance-rejecting control systems for various PM electric machine applications are important for the research community.

1.3.Research aim and objectives

The main aim of this research is to design control systems insensitive to various sources of disturbances in the PM electric machine applications, namely servo motor speed control and WECS with PMSG. The aim of this project will be achieved through the fulfilment of the following objectives:

- Review of active disturbance observer-based control techniques to attenuate various sources of disturbances for improving tracking performance in the PM electric machines;
- Analyzing and understanding the dynamic equations of PMSM by deriving error dynamics and state-space model of the PMSM system;
- Design of robust switching output feedback control law (SOFCL) -based SMC for PMSM speed regulation;
- Investigation of tracking performance of the SOFCL-based SMC for PMSM speed regulation under speed variations, load torque disturbance, and model uncertainty;
- Understanding the dynamic equations of PMSG and its important relations in the 5 kW WECS with deriving nonlinear error dynamics and state-space model of the system;
- Design of robust nonlinear output feedback, state-dependent Riccati equation (SDRE) control based Integral SMC law for PMSG-based WECS to facilitate maximum power extraction from wind energy via efficiently controlling generator side power converter;
- Investigation of tracking performance of the SDRE-based Integral SMC for PMSG based WECS under the presence of vast-varying disturbance, model uncertainty, nonlinearities;
- Design of servomechanism-based SDRE control with HODO for estimation of wind speed in the variable speed WECS to facilitate maximum power extraction from wind energy via efficiently controlling generator side power converter;

- Investigation of the performance of servomechanism-based SDRE control with HODO for estimation of wind speed in the variable speed WECS under the presence of vast-varying disturbance, model uncertainty, nonlinearities, noise;
- Understanding of the dynamics of 300 W servo PMSM prototyping kit;
- Design of HODO-based discrete-time PI-PI control system with back-calculation algorithm anti-windup scheme to compensate total disturbance in the speed controller of servo PMSM;
- Investigation of performance and comparison of cascaded discrete-time HODO-based PI-PI control system for PMSM speed regulation under speed variations and load torque disturbance.

1.4.Research methodology

This thesis's methodology is based on an analysis of the most advanced approaches in PMSM speed control applications which are less sensitive to the various sources of disturbances such as model uncertainty, external disturbance, and modelling errors. The most important parameter relationships in the PMSM and WECS systems have been analysed. The models according to operation conditions and type of electric machine have been updated. The state-space models of the systems have been derived. The nonlinear terms as well as parameters that may vary have been identified. The potential noise quantity has been defined. The derived control laws have been tested under nominal operational conditions and parameter variations of the systems. Finally, the proposed control laws synthesised with HODOs have been analysed and compared with conventional control systems with/without disturbance observers.

1.5.Principal contributions to knowledge

The principal contributions to the knowledge presented in this thesis can be summarized as follows:

1. HODO based SOFCL based SMC has been proposed for improvement of the PMSM's angular shaft's speed tracking performance under speed variations and load torque disturbance. Presented in Chapter 5 and the contents of which have been published in the Proceedings of International Conference on System Science

and Engineering (ICSSE 2019) conference in Dong Hoi City, Quang Binh, Vietnam 19-21 July, 2019;

2. HODOs based Integral SMC with linear feedback for has been proposed for WECS with PMSG to maximize output power of the machine's side converter. Presented in Chapter 6 and the contents of which have been published in Wind Energy, vol. 23 (4), pp. 1026–1047, 2020.
3. SDRE based Integral SMC with nonlinear feedback and HODOs has been proposed for WECS with PMSG to maximize output power of the machine's side converter. Presented in Chapter 6 and the contents of which have been published in IEEE Access, vol. 8, pp. 51100–51113, 2020;
4. The integral servomechanism based SDRE nonlinear output feedback control WECS with PMSG to maximize output power of the machine's side converter has been proposed. Presented in Chapter 6 and the contents of which have been accepted in January 14, 2022 (published online February 9, 2022) for publication in Optimal Control Applications and Methods (OCAM), Wiley.
5. HODO based discrete-time PI-PI control system with back-calculation algorithm based anti-windup scheme has been and validated experimentally for improvement of the PMSM's angular shaft's speed tracking performance under speed variations and load torque disturbance. Presented in Chapter 7 and the contents of which have been published in IEEE Access, vol. 9, pp. 66323–66334, 2021.

The contributions to the knowledge have been summarized in Table 1.1.

1.6.List of publications arising from the thesis

The studies detailed in this thesis have resulted in several peer-reviewed publications as follows:

1. Sarsembayev, B., Kalganova, T., Zhetpissov, Y., Kaibaldiyev, A., & Do, T. D. (2019). Sliding mode control with High-order Disturbance Observer Design for Disturbance Estimation in SPMSM. 2019 International Conference on System Science and Engineering (ICSSE), 542–547, doi:10.1109/ICSSE.2019.8823109
2. Suleimenov, K., Sarsembayev, B., & Do, T. (2020). Disturbance observer-based integral sliding mode control for wind energy conversion systems. Wind Energy, 23(4), 1026–1047, doi:10.1002/we.2471

Table 1.1. The comparisons of the main features in proposed control systems

Control method	Application	External disturbance (Load/Wind)	Model uncertainty estimation	Noise (from sensors)	Modelling errors	Nonlinearity
1. HODO-based and SOFCL-based SMC has been proposed for improvement of the PMSM's angular shaft's speed tracking performance under speed variations and load torque disturbance	PMSM speed regulation	√			√	
2. HODOs-based Integral SMC with linear feedback has been proposed for WECS with PMSG to maximize the output power of the machine's side converter	PMSG based Wind energy conversion system	√	√	√	√	
3. SDRE based the nonlinear feedback based Integral SMC with HODOs has been proposed for WECS with PMSG to maximize the output power of the machine's side converter	PMSG based Wind energy conversion system	√	√	√	√	√
4. The integral servomechanism-based SDRE nonlinear output feedback control WECS with PMSG to maximize the output power of the machine's side converter without the use HODOs to compensate for model uncertainty	PMSG based Wind energy conversion system	√				√
5. HODO-based discrete-time PI-PI control system with a back-calculation algorithm-based anti-windup scheme has been validated experimentally for improvement of the PMSM's angular shaft's speed tracking performance under speed variations and load torque disturbance	PMSM speed regulation	√			√	

3. Sarsembayev, B., Suleimenov, K., Mirzagalikova, B., & Do, T. D. (2020). SDRE-based Integral Sliding Mode Control for Wind Energy Conversion Systems. IEEE Access, 8, 51100–51113, doi:10.1109/access.2020.2980239

4. Sarsembayev, B., Suleimenov, K., & Do, T. D. (2021). High Order Disturbance Observer Based PI-PI Control System with Tracking Anti-Windup Technique for Improvement of Transient Performance of PMSM. IEEE Access, 9, 66323–66334, doi:10.1109/ACCESS.2021.3074661
5. B. Sarsembayev, N. Zhakiyev, A. Akhmetbayev and K. Kayisli, "Servomechanism based Optimal Control System Design for Maximum Power Extraction from WECS with PMSG," 2022 10th International Conference on Smart Grid (icSmartGrid), 2022, pp. 309-313, doi: 10.1109/icSmartGrid55722.2022.9848769.
6. Sarsembayev, B., Zholtayev, D., & Do, T. D. (2022). Maximum Power Tracking of Variable-Speed Wind Energy Conversion Systems based on a Near-Optimal Servomechanism Control System. Optimal Control Applications and Methods, Accepted.

1.7.Organization of thesis

The rest of the thesis is organized in the following way. The second chapter reviewed the concept of DOBC and presents of the different approaches to improve the tracking performance under influence of the various sources of disturbance. The third chapter presents the mathematical modelling of PM synchronous AC machine in PMSM and WECS application. The disturbance observer design and its properties are presented in forth chapter. This follows with HODO-based control systems design for PM synchronous machine applications in the fifth chapter. In the sixth and seventh chapter, the simulation and experimental results of the HODO-based proposed control systems in servo PMSM and WECS applications respectively. Finally, the concluding remarks and further research are given in eighth chapter.

Chapter 2: Review of disturbance observer based control methods

2.1.Introduction to DOBC

Disturbances in the external environment and uncertainties associated with unmodelled dynamics, parameter variations, and nonlinear coupling of multivariable systems are widely presented in real-life engineering systems and harm the performance of the controlled system. Therefore, the design of a robust control system for PM AC machines is the mainstream of the research community for high-performance applications.

The task of controller design for PMSM system is rejecting various external disturbances and improve robustness in the presence of a wide range of uncertainties therefore; it has been widely recognized in research.

In the PM synchronous AC machine, the speed tracking performance is affected by different external disturbances such as load torque, friction torque, and other mechanical factors. The control performances of these systems are also subject to the effects of the models' mechanical and electrical parameter perturbations caused by the changes in operating conditions and external working environments [5], [11–13]. Furthermore, the unmodeled dynamics due to the motor's body structure induced torques, dead-time and measurement errors have effects on control system's performance [14].

In power converter control in WECS applications, the wind speed is considered an external disturbance whereas the parameter perturbations of the permanent magnet synchronous generator are usually caused by ambient temperature, as well as the wear of components of the wind turbine (WT), are considered as uncertainties [9], [15–17].

While the disturbances are presented in the systems with PM AC machines, they can not be measured by sensors but estimated mathematically via algorithms integrated into control systems. The problem of disturbance rejection is an everlasting research topic since the appearance of control theory. The traditional control methods, such as the proportional-integral-derivative (PID) controller and linear quadratic regulator (LQR) cannot handle disturbances and uncertainties in high-precision control applications [18-19]. The essential reason for this is that these traditional linear methods do not explicitly take into account disturbance or uncertainty attenuation performance in controllers' design.

The development of advanced control algorithms with the ability to reject disturbances is carried out by many researchers to handle the aforementioned issues in PM synchronous AC machine applications. Due to the significant impact of disturbances,

many elegant advanced control approaches have been proposed since the 1950s. While some approaches are designed to compensate for the disturbances in the feedforward scheme, others could suppress the internal disturbances via nonlinear feedback controllers [14].

2.2.Basic concept of DOBC and time-domain formulation

The general concept of DOBC is shown where the composite control system includes two parts, feedback control and disturbance observer-based feedforward control as shown in Figure 2.1. While the tracking and stabilization of the nominal dynamics of the controlled plant can be achieved by feedback control, the estimated disturbances can be compensated with the feedforward control part. The main idea of this design considers the separate adjustment of the control parts leading to the satisfactory tracking performance and disturbance rejection ability. The advantages of proposing this type of control are: faster responses to deal with disturbances; a so-called “patch” feature; and less conservativeness [2].

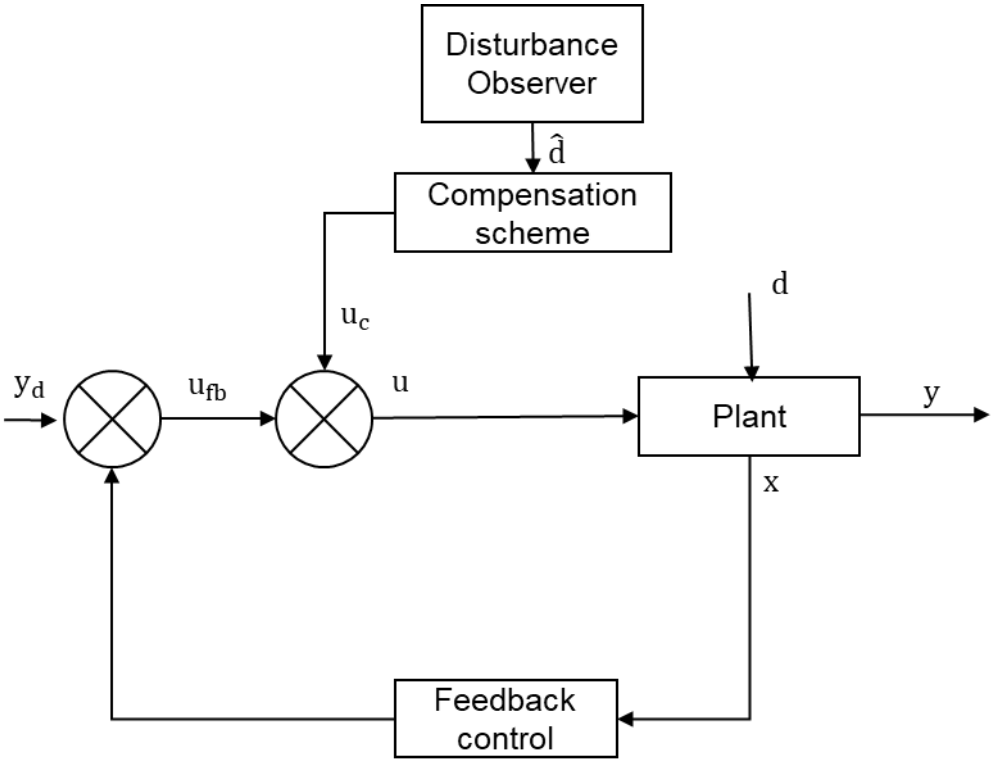

Figure 2.1. Disturbance observer-based control diagram courtesy of [2]

The time domain formulation of the DOBC to control the plant is depicted in Figure 2.2. Let us consider multi-input and multi-output (MIMO) linear systems with the presence of disturbance, equation (2.1)

$$\begin{cases} \dot{x} = Ax + B(u + d) \\ y = Cx \end{cases} \tag{2.1}$$

Let us suppose the disturbance and its derivatives are bounded and tent to some constants as time goes to infinity, so $\lim_{t\to\infty} \dot{d}(t) = 0$. The following linear disturbance observer, equation (2.2) can be used for the estimation of disturbance in the system (2.1).

$$\begin{cases} \dot{z} = -LB(z + Lx) - L(Ax + Bu) \\ \hat{d} = z + Lx \end{cases} \tag{2.2}$$

The control law consists feedback control and compensation scheme is

$$u = Kx - \hat{d} \tag{2.3}$$

The closed-loop system is governed by

$$\begin{cases} \dot{x} = (A + BK)x - Be_d \\ \dot{e}_d = -LBe_d - \hat{d} \end{cases} \tag{2.4}$$

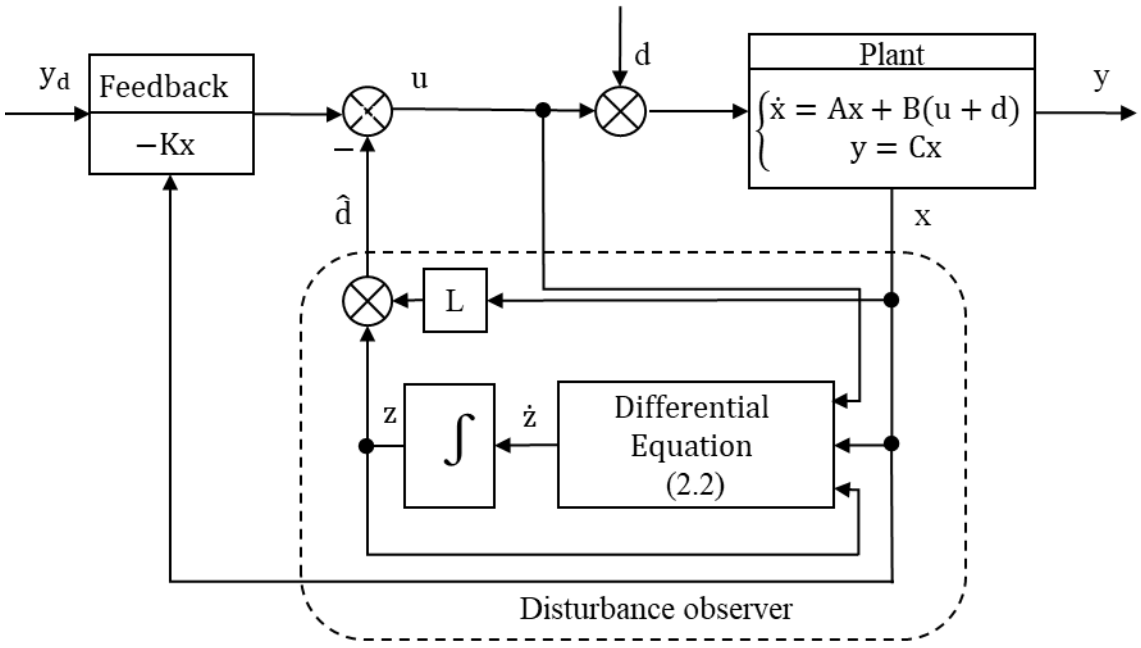

Figure 2.2. DOBC concept in time-domain formulation [2]

It can be proved that the closed-loop system (2.1) is bounded-input and bounded-output (BIBO) stable if the feedback control gain matrix, K is selected such $(A + BK)$ is

stable in sense of Routh-Hurwitz. Also, the observer gain matrix, L is selected such that $-LB$ is stable in sense of Routh-Hurwitz. Moreover, if the disturbance in the system is constant then the closed-loop system in equation (2.5) is asymptotically stable if the gains L and K are chosen such that $(A + BK)$ and $-LB$ are stable in sense of Routh-Hurwitz.

2.3.Review of disturbance estimation approaches

There are many disturbance estimation techniques have been designed such as unknown input observer (UIO)[20], perturbation observer (PO)[21], equivalent input disturbance observer (EIDO) [22-23], disturbance observer (DO) [24]–[26], extended state observer (ESO) [27]–[29]. The DO and ESO approaches are widely investigated among the other estimation techniques. ESO has been put forward in the 1990s ESO is directly linked with so-called active disturbance rejection control (ADRC) which is employed for the estimation of lumped disturbances associated with model uncertainties, external disturbances. The DO estimation technique on other hand is first introduced in 1960s to deal with sensitivity analysis of conventional state observers [30]. The design of nonlinear disturbance observer (NDO) and intelligent disturbance observer (IDO) was possible due to progress in conventional linear disturbance observer (LDO) associated with frequency domain.

The concept of linear disturbance observer design originates from linear system theory and its robust stability analysis, and it is still under the attention of the research community. In the [24], LDO was utilized to estimate load torque disturbance to compensate for the PMSM speed control application by proving stability via Lyapunov's theory. In the [31], LDO was used to estimate aerodynamic torque to facilitate maximum power point tracking (MPPT) in the WECS system. The wind speed was defined via the estimated torque to set the effective reference angular shaft speed of the PMSG.

2.4.Review of robust linear and nonlinear control systems

2.4.1.Review of linear control methods for PM synchronous AC machine applications

The PM synchronous AC machine has beneficial characteristics such as a compact structure, high air-gap flux density, high power density, and high torque to inertia ratio. Although these characteristics make them advantageous among AC machines,

controlling its nonlinear multivariable model in presence of external disturbances, noise, and parameter uncertainties is reported quite challenging [32].

Direct torque control (DTC) is one of the approaches to simplify the control system design in PMSM speed control applications. While field-oriented control (FOC) provides smooth starting, fast acceleration, and four-quadrant operation, DTC simplifies motor modelling and hence reduces the complexity of the control system [33]. In turn, the DTC method provides lower torque and inherits current ripples [34]. Several FOC-based sliding mode control (SMC) strategies have been proposed to optimize the performance of the speed controllers. While the first-order SMC-based composite control system has been designed with an extended sliding mode observer (ESMO), sliding mode speed controller with load torque disturbance compensation scheme has been synthesized with proportional-integral (PI-PI) current controllers in cascade structure [35].

The cascade PI-PI control structure is an effective closed-loop control system for PMSM speed regulation. This control architecture has direct access to limit armature currents via a simple saturation blocks. Typically, excessive currents come from a dramatic increase/decrease in motor speed and then armature voltages fluctuates. In this control, the current loops controls armature currents/torque whereas the speed loop regulates the speed of motors by providing the current/torque reference. The limited current/torque reference in the outer loop can facilitate current constraints. Therefore, it is essential to make sure that the inner loop response should be faster than the outer loop to guarantee quick limiting overcurrent and stability in the closed-loop scheme [36].

Due to the so-called windup phenomena in a traditional PI controller, its performance is not satisfactory for PMSM drive applications. This phenomenon is characterized by long periods of overshoot, which results in poor control performance and even makes the overall system unstable. Therefore, the cascade PI-PI control systems for motor drives are typically equipped with various anti-windup (AW) techniques to reduce the integral effect on control system performance. The effectiveness of back-calculation-based tracking gains AW scheme's performance has been experimentally demonstrated among other anti-windup techniques such as simple limited integration, limited output with dead zone element, and conditioned integration. These types of AW techniques were successfully tested for angular position control of a servo system [37] and PMSM control [38].

The PI speed controller equipped with an anti-windup scheme demonstrates good performance in both transient and steady-state times than the PI controller with

conventional forms [38]–[40]. However, tuning the gains of the PI controller is tedious and time-consuming work. The defining of optimal gains for PI-PI control system based on analysing plant dynamics with step response method is most common among others, which was first presented by Ziegler and Nichols in 1942. Detailed information about this method and other methods to determine optimal gains of PI controller can be found in [39].

Another problem of traditional PI controllers is their sensitivity to model uncertainties, external disturbances, and unmodeled dynamics in the system, which degrade its performance [36]. There are several approaches to tuning the gains of the controller to ensure the robustness of the control system. The model-based adaptive PID speed control scheme, which consists of decoupling, PID, and supervisory terms has been developed in [12]. The adjustment of control gains is based on the gradient descent method and calculated online. Because of the nonlinearities of the PMSM [19], [32], the decoupling terms have been introduced to compensate them in a feed-forward manner. However, this control gains tuning procedure highly depends on the knowledge of the model. Artificial neural network (ANN) based auto-tuning of the gains of PID is another way to improve its performance without prior knowledge of the system model. In [41], a training algorithm for PID controller gains based on the recursive least square method was developed to update the gains online.

The main advantage of using a PI-based control system is its ability to facilitate zero steady-state errors in finite time under low-frequency disturbances and model uncertainties and to guarantee the closed-loop system's stability. Moreover, the synthesized PI control system has practical importance because it is widely used in the industry. There are few studies devoted to the application of disturbance observer-based control synthesized with PI-PI controller for PMSM drives.

2.4.2.Review of the control systems with compensation of disturbances

Sliding-mode control (SMC) [41-42], H_∞ control [25], methods are considered robust to the model uncertainty and modelling errors. However, these methods are too complicated and based on the knowledge of the model of the PMSM [43]. Also, SMC-based control inherits the so-called chattering phenomenon and its full elimination is hard to achieve [7],[44]. On the other hand, intelligent and predictive control implementation requires processors with high-performance calculations in each time instance, so this makes these algorithms to be expensive [45]. Finally, an adaptive controller is difficult to

follow up all mathematical procedures because they are not straightforward [46].

Instead the disturbance observer-based control (DOBC) method can be used to compensate the disturbances effects in the system [14], [2]. The motion dynamics of PMSM are complex and intrinsically nonlinear. Therefore, the high precision control of PMSM is a rather challenging task. The sophisticated disturbance observer (DO) based control can improve the transient performance of the control system for PMSM regarding to the disturbances. In DO, the motion equation should be modified to include torque losses due to eddy currents [47]–[49], hysteresis, and friction [1], [50]. The various sources of disturbances reduce the produced torque and generate ripples in the system response, so they can be compensated with the use of disturbance observer-based control methods. Recently, a high-order disturbance observer (HODO), the nonlinear observer has been utilised to estimate fast-varying disturbances such as aerodynamic torque and synthesised with linear and nonlinear feedback controllers in renewable energy generation applications [15]–[17], [51]. This observer is free from the assumption that the disturbance varies slowly which was an obligatory condition for the traditional disturbance observers [2], [24].

The main sources of high-order disturbances in practical PMSM systems are cogging torque and high-frequency electromagnetic noise [8]. The cogging torque is produced due to the utilisation of different materials in PMSM and the uneven structure of windings of the motor, which induces various pulsating torques. The high-frequency electromagnetic noise associated with the PWM technique for voltage control also has high-order disturbance nature.

Motivated by HODO features in [38] and inspired by PI-PI based DOBC in [24], a discrete-time- PI controller with a back-calculation algorithm anti-windup scheme can be combined with a disturbance observer for the external disturbances compensation in the PMSM speed loop. The HODO can be used to compensate for the total disturbance to improve tracking performance and achieve asymptotic stability of the closed-loop system. In the motion equation in the HODO, the torque losses due to drag resulting from time-varying flux, the static moment of friction, and hysteresis should be taken into account. To handle windup phenomena in the transients, both loops controllers should be equipped with a back-calculation algorithm based anti-windup schemes. In the result chapter, the proposed HODO based discrete-time PI-PI control system’s performance will be demonstrated and compared with control system without HODO.

2.4.3.Review of nonlinear control systems for PMSM speed regulations

There have been different approaches to controlling PMSM to maintain its high performance. The conventional proportional-integral (PI) controller with a single-input and single-output (SISO) layout is one of the most well-known control schemes for PMSM speed regulation. The cascade structure is presented with one outer speed loop and two inner currents loops respectively. However, the main problem with using PI controller is its sensitivity to the inevitable presence of various sources of disturbances such as parametric variations, modeling errors, and external load torque disturbances [2].

The aforementioned methods are investigated for PMSM control applications with less considering the disturbances. However, disturbance widely exists in real applications; therefore, disturbance rejection ability is a key objective in the proposed control system design. The disturbances may come not only from external sources but also from controlled plant parameters uncertainties, unmodeled dynamics, and nonlinear couplings of multi-variables [14]. Therefore, it is an important task to handle the disturbances in the system on a short time basis.

Recently, to deal with disturbance/uncertainties in the PMSM speed control, the researchers have proposed the variety of control techniques based on methods as direct torque control (DTC) [34], [52], model predictive control (MPC) [45], [53], artificial neural network (ANN) based PID [41], SMC [7], [26], [35], [54], fuzzy control (FC) [55]–[57]. In these nonlinear control methods, the SMC method is more advantageous for its insensitive properties to parameter variations. It has been successfully applied in other types of applications, such as robot manipulator systems [58], piezoelectric actuation systems [59], and speed control of the DC motor [60]. While it can provide robust performance with matched disturbances, the external disturbances, such as load torque and friction can be measured and compensated in feedforward scheme. However, due to the high cost of torque transducer and its possible measurement errors, this option is less attractive.

The SMC based control systems with linear output feedback schemes have shown their effectiveness for uncertain dynamic systems [61]–[63]. The SMC can deal with matched disturbances whereas the external disturbance can be estimated by HODO to compensate for it in a feedforward manner. However, the robustness of SMC can only be guaranteed by the selection of large control gains, which lead to the so-called chattering phenomenon [44], [64]. The chattering is not preferable from a practical point of view because it results in low control accuracy, high heat losses in electrical power circuits,

and high wear of moving mechanical parts of the systems. Several approaches have been proposed to overcome chattering, such as continuous approximation [7], high-order sliding mode control (HOSMC) method [60],[65], smoothed sliding mode control (SSMC) [66], and twisting and super-twisting algorithms [35].

2.4.4.Review of nonlinear control systems for PM synchronous machine in WECS applications

The PM synchronous machines are utilised in wind energy conversion systems (WECS) application as better efficiency to generate the power than other renewables [67]. Permanent magnet synchronous generator (PMSG) has become popular due to their simple structure, higher reliability, lower maintenance, and higher efficiency [68]. In the industrial WECS, field-oriented control with proportional-integral (PI) controller [69] and linear quadratic regulator (LQR) [15]–[17], [70] have been widely utilised because of their simplicity. However, due to the their sensitivities to parameter uncertainties and external disturbances in WECSs, these control methods cannot guarantee good performance. Although the LQR control method is claimed to handle the chaotic nonlinear behaviour of electric machines [32], the nonlinear control methods have to be assessed thoroughly. Recently, to cope with the limitations of linear control methods, researchers have proposed various advanced linear and nonlinear control techniques to improve performance of WECS to maximise power extraction under effects of disturbances. To overcome these challenges in the systems, the SMC [71], [8], [72], [73], [74], DTC [75], optimal control [76], fault-tolerant control (FTC) [77], MPC [78], and hybrid control [4], [79], ANN based control [80] have attracted most attention of research groups in the field. Among nonlinear control methods, SMC algorithms present a suitable option for their robustness to parameter uncertainties. However, this method inherited undesirable chattering phenomena [44], [81] as it is stated about its negative effects on the mechanical parts of a system. One of the chattering reduction technique is introduction of the high-order sliding mode controller, for example, the second-order SMC control design has been proposed to eliminate chattering in the control system [82]. In addition, SMC invariance to parameter uncertainties is not guaranteed in the reaching phase [83]. Therefore, the sliding variable with integral term has been introduced in [74] which facilitated straight sliding mode. The study has proposed to improve limitations associated with conventional sliding surface (SS) in 5-phase PMSG. Moreover, to improve nominal transient performance the improved PI-type SS based ISMC has been designed to recover nominal transient performance of the control system [73].

The nominal performance of the control law can be recovered while model uncertainty is presented without asymptotic regulation. The ANN based nonlinear control method to track the reference angular shaft speed and electromagnetic torque of the PMSG has been proposed in [68]. This design suggests the modified Elman ANN - based controller, the recurrent weights, connective weights, translations, and dilations trained online via learning algorithm. However, this method should be confined to suggesting the mathematical rigor and the feasibility of the nonlinear control method [84]. The DTC has been proposed to control PMSG during overrated wind speed region via flux weakening technique. While in DTC electromagnetic torque is controlled directly via space vector modulation (SVM), it causes torque/flux ripples, high acoustic noise at low speed range which lead to poor control performance [33]. The MPC with revised prediction has been proposed to control direct driven PMSG with three level neutral-point-clamped back-to-back converter [78]. Although the control variable ripples are reduced, high computational requirement for longer prediction horizon cases is regarded as main its drawback [85]. Moreover, these methods are quite complicated and do not demonstrate detailed steps for implementations, their control techniques can be only verified individually.

The integral SMC has proven its feasibility to other classes of nonlinear systems, such as inverted pendulum [86], the attitude control of the spacecraft [87], and anthropomorphic industrial robot manipulators [88]. While the nominal control part of ISMC control law based on linear output feedback can provide stability and robust performance of the control for WECS as in [8],[54], it does not take into account the multivariables of the dynamic system. The mathematical model of PMSG-based WECS is a highly nonlinear system where nonlinear feedback control may provide better dynamic performance.

Among nonlinear optimal control approaches, state-dependent Riccati equation (SDRE) based control is quite popular to control the various nonlinear systems [5], [13], [19], [89], [90]. It can be generalized as LQR problem and requires solving the algebraic Riccati equation (ARE) to get optimal control gains for each set of weighting matrices. The SDRE-based method is considered as numerical approaches and can be approximated via Taylor's series expansion method [5]. The SDRE-based method has been validated in control of the PMSM [5], [13], a doubly fed induction generator (DFIG) [89], a free-floating space manipulator [91], a mobile robot for obstacle avoidance [92], a jet engine compensator, power converter-based DC microgrid, and Vander Pol's oscillator [90].

2.5.Summary of Chapter 2

In this chapter, the linear and nonlinear control systems for PM synchronous machine applications have been reviewed. The review has shown that the design of the robust control systems with disturbance rejection ability for PM synchronous machine applications is important research question. The analysis has revealed that performances of the electric machine's drives are degraded under presence of various source of disturbances and operational conditions. The reference tracking ability enables to improve precision of the PMSM system, and increases power extraction in variable-speed WECS application. This is why many studies have been devoted to develop the design of control systems with anti-disturbance feature. The linear control systems have simple structures but their performances are sensitive to parameter uncertainties and external disturbances. It has been found that traditional SMC, nonlinear control is insensitive to the parameters variations but the SMC insensitivity is not guaranteed in the reaching mode of this control. In addition, the convenience of DOBC approach is that any baseline controller can be combined with DOs. The use of DO is cost-effective solution rather the use of expensive sensors. The SDRE approach is suitable to take multivariable structure of the system into account. The PMSM and WECS models with emulation of realistic operational conditions in MATLAB/Simulink environment were built to test the performances of the proposed control systems as well as validated with wind turbine emulators.

Chapter 3: Mathematical modeling of PM synchronous AC machine in PMSM and WECS applications

3.1.Introduction

The mathematical models of PM synchronous machine's model is important to design and analyse of model-based control system's performance. While a model-free control system does not require the exact knowledge of the system parameters whereas DOBC synthesized with the high-order disturbance observer utilizes its nominal parameters. The space vector representation of the voltage, current, and flux of the machines in the stationary reference frames (ABC) are converted to (α-β) via Clark transformation, and then transformed to the rotational reference frame (d-q) via Park transformation matrix and visa versa. The proposed control laws are developed in the d-q coordinate system and then will be transformed back to ABC rotational reference frame where physically electric machines operate. In fact, the model of the machine can exist in all three coordinate systems. Moreover, the simulation results of the machine's model can be analysed in d-q coordinate system. The electrical speed and mechanical speed of the machine are related as the function of pole pairs in it. While the motion equation of the PMSG's model is affected by aerodynamic torque, the motion of the PMSM's model is influenced by load torque disturbance.

3.2.Space vector representation of PM synchronous AC machine

A three-phase AC machine can be described using the space vector method [3], [93], [94]. The AC motor variables $K_A(t), K_B(t), K_C(t)$ for symmetrical machine holds the condition [3]

$$\mathrm{K_A(t) + K_B(t) + K_C(t) = 0} \tag{3.1}$$

Where $\mathrm{K_A(t), K_B(t), K_C(t)}$ are voltages, currents, and fluxes of machines in ABC frame.

The summation of these variables gives the space vector [3]:

$$\mathrm{K = \frac{2}{3}[K_A(t) + a\,K_B(t) + a^2 K_C(t)]}, \tag{3.2}$$

where $a = e^{j\frac{2}{3}\pi}$, $a^2 = e^{j\frac{4}{3}\pi}$.

According to the space vector method, voltage, current, and flux can be represented through the vector K (Figure 3.1). In the vector control method, PMSM

electrical subsystem's variables are transformed from a stationary three-phase ABC system to α-β frame, or rotational frame d-q [3].

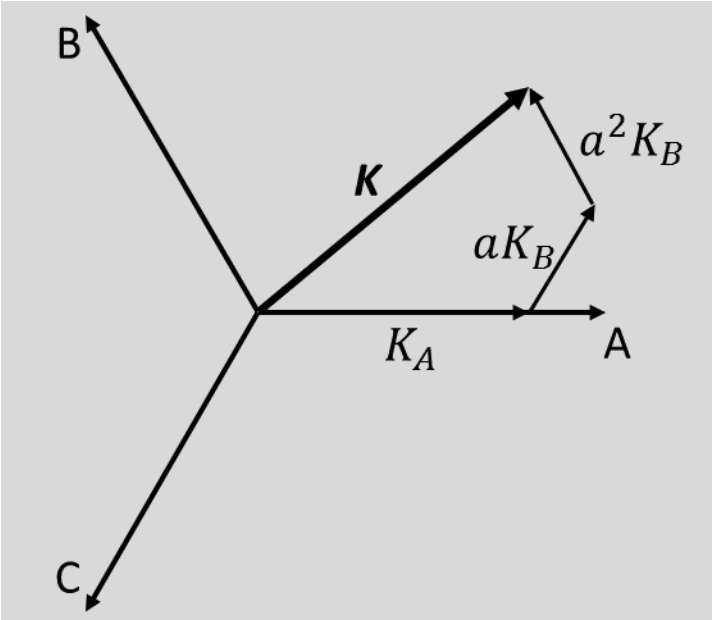

Figure 3.1. The space vector representation of the PMSM's variables courtesy of [3]

Three-phase PMSM may be described using the space vector method.

3.3.Per unit PMSM mathematical model

A simplified mathematical model of PMSM per unit in an arbitrary reference frame rotating with electrical speed, ω is [3]

$$u_s = \mathrm{R_s i_s} + \frac{\mathrm{d\Psi_s}}{\mathrm{dt}} + \mathrm{j\omega\Psi_s} \tag{3.3}$$

Where $\mathrm{R_s}$ is stator resistance, $\mathrm{i_s}$ armature current, Ψ_s is magnetic flux respectively.

The stator magnetic flux will be

$$\Psi_s = \mathrm{L_s i_s} + \lambda_m, \tag{3.4}$$

Where $\mathrm{L_s}$ is stator winding inductance and λ_m is PM flux linkage respectively.

The produced mechanical speed will be as

$$\frac{\mathrm{d\omega_m}}{\mathrm{dt}} = \frac{1}{\mathrm{J_{ri}}}(\mathrm{T_e} - \mathrm{T_L}), \tag{3.5}$$

Where $\mathrm{J_{ri}}$ is the rotor inertia, $\mathrm{T_e}$ is the electromagnetic torque, and $\mathrm{T_L}$ is the load torque respectively.

The derivative of the mechanical angle is the mechanical speed

$$\frac{d\theta_m}{dt} = \omega_m \quad (3.6)$$

3.4.Mathematical model of PMSM in the d-q rotating frame

The transformation of the PMSM model from three-phase ABC and stationary α-β to the rotating frame d-q is quite convenient for designing a high-performance control system. This is realized according to space vector theory and using transformation matrices. The decoupled schematic of the PMSM model is shown in the d-q axis (Figure 3.2. (a) and (b) [3].

The dynamic equations in terms of phases are

$$V_A = R_S I_A + \frac{d\Psi_A}{dt} \quad (3.7)$$

$$V_B = R_S I_B + \frac{d\Psi_B}{dt} \quad (3.8)$$

$$V_C = R_S I_C + \frac{d\Psi_C}{dt} \quad (3.9)$$

Where $V_A, V_B, V_C, I_A, I_B, I_C, \Psi_A, \Psi_B, \Psi_C$ are voltages, currents and fluxes per ABC phases respectively,

The flux linkages in ABC phases are defined as in [6]

$$\Psi_A = L_{AA} I_A + L_{AB} I_B + L_{AC} I_C + \lambda_{mA} \quad (3.10)$$

$$\Psi_B = L_{BA} I_A + L_{BB} I_B + L_{CC} I_C + \lambda_{mB} \quad (3.11)$$

$$\Psi_C = L_{CA} I_A + L_{CB} I_B + L_{CC} I_C + \lambda_{mC} \quad (3.12)$$

where $\lambda_{mA}, \lambda_{mB}, \lambda_{mC}$ are flux linkages provided by permanent magnets per ABC phases. The inductances are functions of the angle θ. While mutual inductances are maximum when the rotor q-axis is midway between the two phases, the stator self-inductances are maximum when the rotor q-axis is aligned with the phase axis. The saliency in the stator windings' self and mutual inductances of interior-type PM machines is expressed via 2θ. However, surface-mount PM machines are considered non-salient machines, their winding inductance are such that $L_d = L_q$ due to uniform airgap or constant reluctance path. The permanent magnet flux linkages at the stator windings per phase are expressed as [6]

$$\lambda_{mA} = \lambda_m \cos\theta \quad (3.13)$$

$$\lambda_{mB} = \lambda_m \cos(\theta - \frac{2\pi}{3}) \quad (3.14)$$

$$\lambda_{mC} = \lambda_m \cos(\theta + \frac{2\pi}{3}) \quad (3.15)$$

The input power for PMSM is

$$P_{in} = \vec{V}_A\vec{I}_A + \vec{V}_B\vec{I}_B + \vec{V}_C\vec{I}_C \tag{3.16}$$

For transformation of the voltages equations in the system from stationary ABC to rotating d-q reference frame, the following Park's transformation can be utilized via knowledge of position angle

$$\begin{bmatrix} V_q \\ V_d \\ V_0 \end{bmatrix} = \begin{bmatrix} \cos(\theta) & \cos(\theta - \frac{2\pi}{3}) & \cos(\theta + \frac{2\pi}{3}) \\ \sin(\theta) & \sin(\theta - \frac{2\pi}{3}) & \sin(\theta + \frac{2\pi}{3}) \\ \frac{1}{2} & \frac{1}{2} & \frac{1}{2} \end{bmatrix} \begin{bmatrix} V_A \\ V_B \\ V_C \end{bmatrix} \tag{3.17}$$

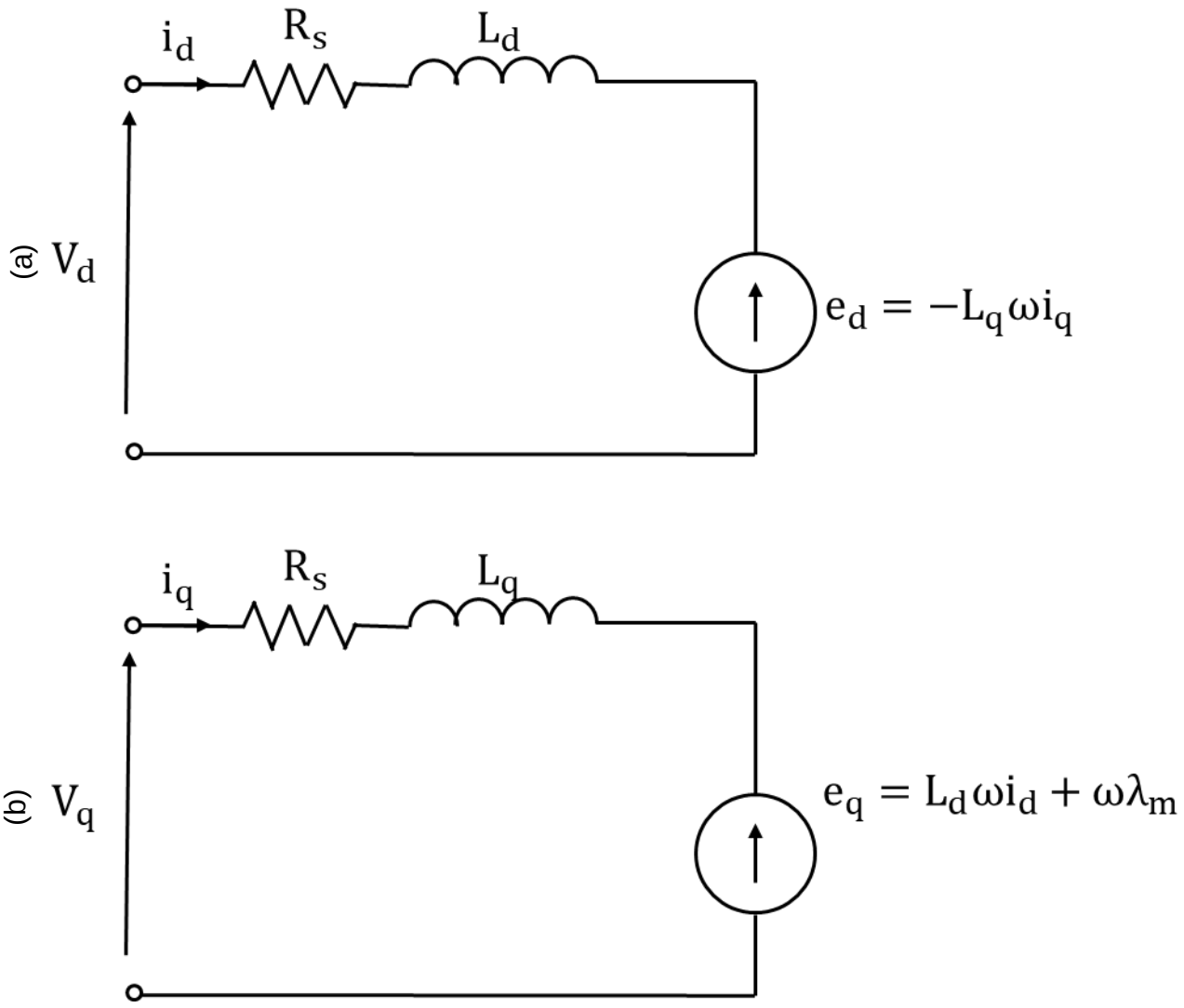

Figure 3.2. PMSM's equivalent circuits in d-q frame (a) d-axis and (b) q-axis courtesy of [3]

With this transformation the stator voltage equations of the PM synchronous machine are

$$V_q = R_s i_q + \frac{d\Psi_q}{dx} + \omega\Psi_d \quad (3.18)$$

$$V_d = R_s i_d + \frac{d\Psi_d}{dx} - \omega\Psi_q \quad (3.19)$$

Then with $L_d = L_q = L_s$

$$\Psi_q = L_s i_q \quad (3.20)$$

$$\Psi_d = L_s i_d + \lambda_m \quad (3.21)$$

λ_m is the magnetic flux linkage. The dynamic equivalent circuits of PM synchronous machine in the rotating reference frame are depicted in Figure 3.4.

The distortion of the magnetic field depends on the stator's current position and magnitude. At no load operation conditions, the armature reaction is assumed to be zero due to the insignificant value of the stator current (Figure 3.3).

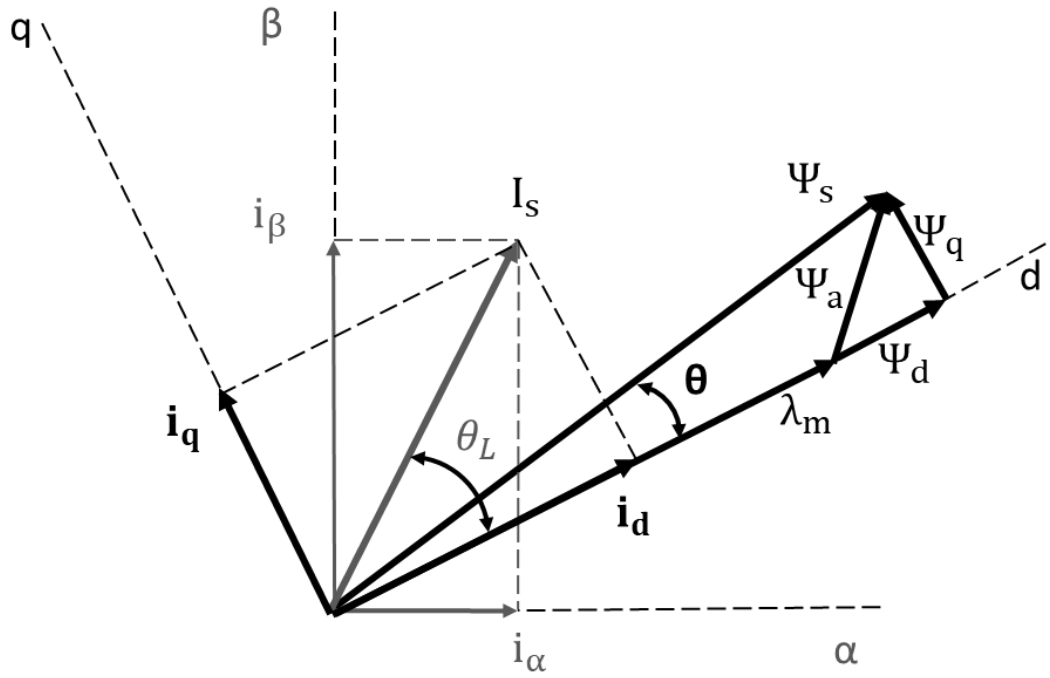

Figure 3.3. Phasor diagram of stator flux and stator current courtesy of [3]

Back electro-motive force (EMF), e induced in the PMSM coils in the d-q frame is

$$e_d = -L_q \omega i_q, \quad (3.22)$$

$$e_q = L_d \omega i_d + \omega\lambda_m, \quad (3.23)$$

The produced torque of PMSM can be expressed as a function of back EMF in the α-β frame as following

$$T_p = \frac{(e_\alpha i_\alpha + e_\beta i_\beta)}{\omega}, \tag{3.24}$$

The maximum electrical speed of PMSM can be found

$$\omega_{max} = \frac{E_{s\,max}}{\Psi_s}, \tag{3.25}$$

where $E_{s\,max}$ is maximum induced phase voltage in PMSM and ω_{max} is the maximum motor speed for the rated flux. Higher speed can be obtained by weakening the flux.

The dynamic equations of a three-phase surface mount PMSM in d-q reference frame is [5]

$$\begin{cases} \dot{\omega} = \frac{3}{2}\frac{1}{J_{ri}}\frac{P^2}{4}\lambda_m i_q - \frac{B_{vf}}{J_{ri}}\omega - \frac{P}{2J_{ri}}T_L \\ \dot{i_q} = -\frac{R_s}{L}i_q - \frac{\lambda_m}{L_s}\omega + \frac{1}{L}V_q - \omega i_d \\ \dot{i_d} = -\frac{R_s}{L}i_d + \frac{1}{L}V_d + \omega i_q \end{cases} \tag{3.26}$$

where $(\dot{..})$ denotes derivatives of the argument function; i_d and i_q are the d-axis and q-axis currents, respectively; V_d and V_q are the d-axis and q-axis voltages, respectively; P is the number of poles; B_{vf} is the viscous friction coefficient

Also, the following coefficients will be used in the next chapters to design a control system.

$$k_1 = \frac{3}{2}\frac{1}{J_{ri}}\frac{P^2}{4}\lambda_m;\ k_2 = \frac{B_{vf}}{J_{ri}};\ k_3 = \frac{P}{2J_{ri}};$$

$$k_4 = \frac{R_s}{L_s};\ k_5 = \frac{\lambda_m}{L_s};\ k_6 = \frac{1}{L_s}.$$

In the system model in equation (3.26), it is noted that ω, i_d and i_q are the state variables; V_d and V_q are the control inputs, and T_L is defined as an external disturbance.

3.5.Wind energy conversion system

3.5.1.Wind turbine modelling

A wind turbine transforms wind kinetic energy into turbine mechanical energy, which, in turn, is converted into electric energy using a generator. Recently, the configuration with a PMSG and full-scale back-to-back (B2B) power converters has been taken over the wind-turbine market to be the dominant solution [95]. The full-scale B2B power converter include two sets of two-level (2L) power converters (PC) named generator-side and grid-side power converters as shown in Figure 3.4. In this study, the *generator-side* PC control system is going to be improved separately from the grid-side one.

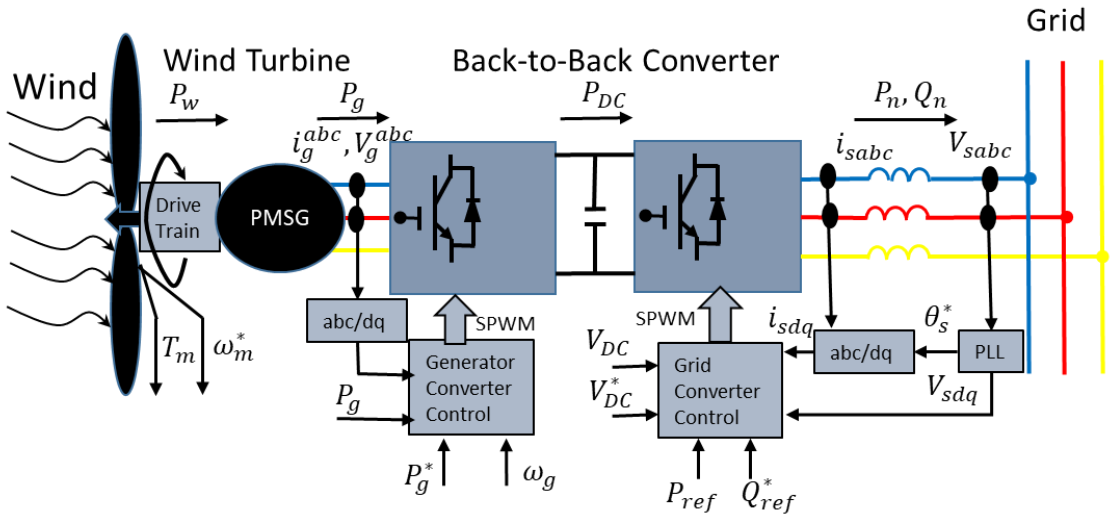

Figure 3.4. A back-to-back power converter for WECS

The aerodynamic power extracted by wind turbines (WT) is quantified using the flowing equation [96]

$$\mathrm{P_a} = \frac{1}{2}\rho\pi\mathrm{R}^2\mathrm{C_p}(\lambda,\beta)\mathrm{v}^3 \tag{3.27}$$

where ρ is the air density, R is the WT rotor radius, v is the wind speed, $\mathrm{C_p}(\lambda,\beta)$ is the power coefficient of the wind turbine, which describes the capacity of the turbine to transform the wind kinetic power into mechanical power.

In present study C_p is defined as in [97]

$$\begin{cases} \mathrm{C_p}(\beta,\lambda) = 0.5(116\frac{1}{\lambda_i} - 0.4\beta - 5)\mathrm{e}^{(-21/\lambda_i)} \\ \frac{1}{\lambda_i} = \frac{1}{\lambda+0.08\beta} - \frac{0.035}{1+\beta^3} \end{cases} \tag{3.28}$$

The coefficient $\mathrm{C_p}$ is a nonlinear function of the tip-speed ratio λ and blade pitch angle β, and it is typically determined experimentally and provided by the manufacturer. The optimal tip-speed ratio is defined as [15]

$$\lambda = \frac{\omega_t \mathrm{R}}{\mathrm{v}} \tag{3.29}$$

where ω_t is the angular shaft speed of the turbine.

According to (3.29), WT produces maximum power when $\mathrm{C_p}$ is at its maximum with pitch angle $\beta = 0$ (Figure 3.5). An operation of WECS at λ_{opt} facilitates maximum power extraction from wind energy during its partial load operation, $\mathrm{C_p^{max}}$. In full-load operation of WECS, it requires reducing stresses on its mechanical elements by regulating the pitch angles of the blades. For sake of assessment of the performance of the proposed control

system, the ability to extract maximum power via used MPPT algorithm is evaluated in the results section. Based on that, the optimal reference angular shaft speed of WT is defined as follows [16]:

$$\omega_{t,d} = \frac{\lambda_{opt} v}{R} \tag{3.30}$$

where ω_t is the angular shaft speed of the WT.

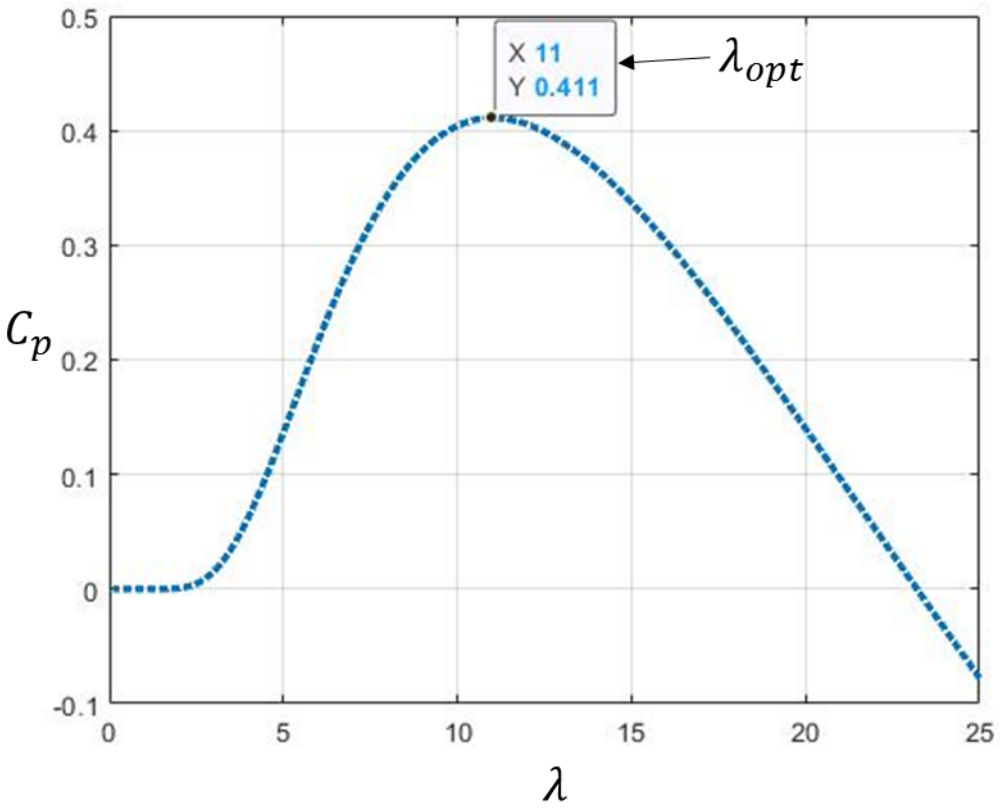

Figure 3.5. Relation of C_p and tip speed ratio λ [4]

The gearbox ratio, reflecting the relation between angular speed and torque of the turbine's side and the generator side is given as follows [15]

$$n_{gb} = \frac{\omega_m}{\omega_t} = \frac{T_a}{T_{gs}}. \tag{3.31}$$

where T_a is the aerodynamic torque from WT-side and T_{gs} is the generator-side torque respectively.

It should be noted in this study the gearbox ratio is equal to one due to the fact that gearbox in direct-driven PMSG can be omitted. The increase of number of poles in the PMSG design allows to the grid requirement without use of gearbox.

The following equation shows the aerodynamic torque obtained from the wind is [54]

$$T_a = \frac{P_a}{\omega_t} = \frac{1}{2}\rho\pi R^3 C_q(\lambda,\beta)v^2 \quad (3.32)$$

where the torque coefficient is $C_q(\lambda,\beta) = C_p(\lambda,\beta)/\lambda$,

3.5.2. Permanent magnet synchronous generator's model

For this work, the PMSG was modelled in the *d-q* reference frame. This allows us to simplify the generator model. The dynamic model of PMSG is expressed as follows [15]

$$\begin{cases} J\frac{d\omega}{dt} = T_{gs} - B_{vf}\omega - T_e \\ \frac{di_q}{dt} = -\frac{R_s}{L}i_q - P\omega i_d - \frac{\psi_m P}{L}\omega + \frac{1}{L}v_q \\ \frac{di_d}{dt} = -\frac{R_s}{L}i_d + P\omega i_q + \frac{1}{L}v_d \end{cases} \quad (3.33)$$

The electromagnetic torque is then calculated as

$$T_e = Ki_q \quad (3.34)$$

where $K = 3/2\,\lambda_m P$.

The PMSG in the WECS is connected to the wind turbine all the time. This makes the mechanical parameters in the WT very stable and robust to changes. However, the generator's electrical parameters can change with the environment temperature or due to friction of the mechanical parts. Considering all uncertainties of stator resistance and inductance, as well as noise, and modeling errors, and combining equations (3.31), (3.33), (3.34), the PMSG dynamic model can be expressed as follows

$$\begin{cases} \frac{d\omega}{dt} = \frac{1}{J_{ri}n_{gb}}T_a - \frac{B}{J_{ri}}\omega - \frac{1}{J_{ri}}T_e \\ \frac{dT_e}{dt} = -PK\omega i_d - \frac{R_s}{L}T_e - \frac{\psi_m PK}{L}\omega + \frac{K}{L}v_q + d_q \\ \frac{di_d}{dt} = \frac{1}{L}v_d - \frac{R_s}{L}i_d + \frac{P}{K}\omega T_e + d_d \end{cases} \quad (3.35)$$

As ambient temperature causes the variations of the electrical parameters such as stator resistance R_s and inductance, L of the PMSG model which have impacts on its accuracy.

3.5.3.Model uncertainty and unmodelling dynamics in PM synchronous machine

In the system of equations (3.45) the terms d_q and d_d are included to signify modeling errors, parameter uncertainties, and noise. The model uncertainty are affected by the varied parameters which in the case are R_s, L and defined in both control channels as

$$d_q = \left(\frac{R_s}{L} - \frac{R_s+\Delta R_s}{L+\Delta L}\right)T_e + \left(\frac{1}{L} - \frac{1}{L+\Delta L}\right)\lambda_m PK\omega + \left(\frac{1}{L} - \frac{1}{L+\Delta L}\right)Kv_q + d_{qn} \quad (3.36)$$

and

$$d_d = \left(\frac{R_s}{L} - \frac{R_s+\Delta R_s}{L+\Delta L}\right) i_d + \left(\frac{1}{L} - \frac{1}{L+\Delta L}\right) v_d + d_{dn} \quad (3.37)$$

where ΔR_s and ΔL are the variations of stator resistance and inductance, and d_{qn} and d_{dn} are the noise and modeling errors.

The model-based control techniques are an effective way to handle complex systems, in which the models are known or partially known. However, in some systems such as a PMSM system, there are various sources of disturbance, coming from cogging torque, and flux harmonics [14]. These types of disturbances with high-order nature are difficult to model and hence should be estimated by sophisticated disturbance observers separately.

In PM synchronous machime, the utilization of different materials for the rotor, and the structure of windings of the motor may induce various pulsating torques, which are also called cogging torques. This happens due to the interaction of the rotor magnetic flux and angular variations in the stator magnetic reluctance. It should be noted that cogging torque is presented even if the power source is disconnected and defined as [14]

$$d_T^{cog} = \sum_{i=1}^{\infty} d_T^{cogi} \sin(iN_c\theta_e) \quad (3.38)$$

where N_c is the least common multiple between the number of slots and pole pairs, θ_e is the electrical angle expressed as $\theta_e(t) = \theta_e(t_0) + \int_{t_0}^{t} z_p\omega(\tau)d\tau$ and d_T^{cogi} is the amplitude of the i^{th}-order harmonic cogging torque.

The flux density of the materials used for the magnet in PMSM is mostly changed by the temperature variation. The resultant demagnetization phenomenon of permanent magnets due to the rise of temperature has a significant impact on the maximum torque capability and the efficiency of PMSM. The flux linkage between the rotor and stator magnets can be expressed as [14]

$$\lambda_m = \sum_{i=0}^{\infty} \lambda_{mi} \cos(6i\theta_e) \quad (3.39)$$

where λ_{mi} is the amplitude of the 6^{th}-order harmonic flux. According to the definition of electromagnetic torque, $T_e = \frac{3}{2} z_p \lambda_m i_q$, it is indicated that the effect of flux harmonics can be represented as follows [14]

$$d_T^{flux} = \frac{3}{2} z_p i_q \sum_{i=0}^{\infty} \lambda_m \cos(6i\theta_e)\,, \quad (3.40)$$

As just discussed, the main fluctuating disturbances in the PMSM system are cogging torque and flux harmonics. These disturbances cause ripples and hence errors in the speed response during the steady state and bigger errors during transient times. These internal disturbances along with external ones such as friction and load torque are

always presented in the system; therefore, they should be compenated with a comprehensive disturbance observer, which will be presented in the next subsection. Note that there is another source of high-order disturbance of PMSM drives, it comes from the PWM inverter.

3.8 Summary of Chapter 3

The PM synchronous machines such as the surface-type PMSM's model and PMSG's model can be presented not only in ABC stationary reference frame but also in d-q rotational reference frame via transformation matrices used in FOC. These models enable to develop the comprehensive control laws. The motion equations in the models are defined differently as PMSM converts electrical energy to mechanical one whereas in WECS the aerodynamic torque created by wind converted to mechanical rotational energy and to electrical energy ejected to the grid or consumed by load. The disturbance due to electrical parameter variations, noise as well as external disturbances are defined in the example of PMSG's model. Also, unmodelled dynamics These disturbances will be estimated with HODO which will be subsect of consideration in the next chapter.

Chapter 4: Disturbance Observer Design

4.1.Introduction

In this chapter, the linear and nonlinear disturbance observer designs are presented. First, the linear disturbance observer design is presented in the time-domain. Then, the nonlinear high-order disturbance observer design is given and followed by analysis of its capability to estimate a constant, ramp, and high-order disturbance types of disturbances. The HODOs are adopted to estimate in the practical examples of the estimation of aerodynamic torque, model uncertainty for the WECS application. Also, the HODO design are used to estimate the load torque disturbance for PMSM speed regulation application.

4.2.Time-domain linear disturbance observer design

Let's take MIMO linear system is described as follows

$$\begin{cases} \dot{x} = Ax + Bu + Dd \\ y = Cx \end{cases} \tag{4.1}$$

Where $x \in R^n, u \in R^m, d \in R^r, y \in R^l$ represent the state, control, disturbance, and output vectors. A, B, C, and D denote coefficient matrices of the system with dimensions of $n \times n,\ n \times m,\ n \times r,\ l \times n$.

When the disturbance slowly varies, it satisfies to the condition

$$\dot{d} = 0 \tag{4.2}$$

The estimation error will be as

$$e_d = \hat{d} - d \tag{4.3}$$

Where ($\hat{\cdot}$) denotes the estimated value.

Rearranging the equation (4.1)

$$Dd = \dot{x} - Ax - Bu \tag{4.4}$$

The initial linear disturbance observer's structure is

$$\dot{\hat{d}} = -L\left(D\hat{d} - Dd\right) = -LD\hat{d} + L(\dot{x} - Ax - Bu) \tag{4.5}$$

However, the state vector can not be directly measured in practical applications, therefore it should rearranged as

$$\dot{\hat{d}} - L\dot{x} = -LD\hat{d} - L(Ax + Bu) \tag{4.6}$$

By defining the intermediate variable $z = \hat{d} + Lx$, the linear disturbance observer (LDO) is formed as in equation (4.7) [2]

$$\begin{cases} \dot{z} = -LD(z + Lx) - L(Ax + Bu) \\ \hat{d} = z + Lx \end{cases} \tag{4.7}$$

where $\hat{d}$ estimated disturbance, z is the internal variable of the observer, and L is the observer gain matrix to be designed respectively.

The time-domain linear disturbance observer design block diagram for the linear system in equation (4.1) is depicted in Figure 4.1.

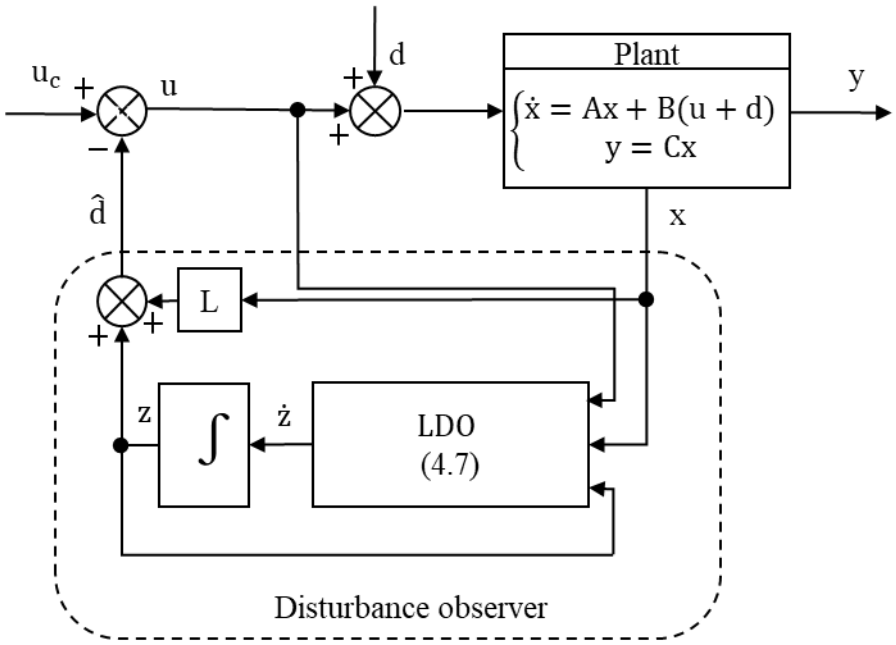

Figure 4.1. Time-domain of disturbance observer formulation for linear systems

4.3.High-order disturbance observer design for disturbance estimation

4.3.1.Constant disturbance case.

Let the nonlinear systems defined by

$$\dot{x} = f(x, u; t) + Fd(t) \tag{4.8}$$

Where $f(x, u; t)$ and matrix F with $\text{rank}(R) = r$ are known. The disturbance $d(t)$ is constant. The state variables x are measurable and their initial values are known.

The reduced order system of equation (4.8) can be shown as

$$F^{+}\dot{x} = F^{+}f(x, u; t) + d(t) \tag{4.9}$$

Where F^{+} is pseudo inverse matrix of F.

The constant disturbance presented in the system is given in [51] as

$$\begin{cases} \dot{z} = F^{+}f(x, u; t) + \Gamma_0(F^{+}x - z) \\ \hat{d} = \Gamma_0(F^{+}x - z) \end{cases} \tag{4.10}$$

Where $\Gamma_0 = diag(\xi_{01} \dots \xi_{0r})$ is a positive disturbance observer gain matrix to be designed for constant disturbance.

The estimated disturbance errors are as in the equation (4.3), then its derivative will be

$$\dot{e}_d = -\Gamma_0 e_d \tag{4.11}$$

which implies that the disturbance estimation errors converge to zero as time goes to infinity if the observer gains the matrix $-\Gamma_0$ are chosen such that polynomials $p_j(s) = s^r + \xi_{0j}s + \cdots \xi_{0j}$ with $j = 1,2,3,r$ are stable.

4.3.2.Ramp disturbance case

Let's consider ramp disturbances $\mathrm{d(t)}$ as;

$$\mathrm{d(t)} = \mathrm{d_0} + \mathrm{d_1 t}, \tag{4.12}$$

where $\mathrm{d_0}$ and $\mathrm{d_1}$ are constant but unknown. A ramp disturbance observer proposed in [51] is given by equation (4.13)

$$\begin{cases} \dot{\mathrm{z}} = \mathrm{F^+ f(x,u;t)} + \Gamma_0(\mathrm{F^+ x - z}) + \Gamma_1 \int_0^{\mathrm{t}} (\mathrm{F^+ x - z})\mathrm{dt}, \\ \hat{\mathrm{d}} = \Gamma_0(\mathrm{F^+ x - z}) + \Gamma_1 \int_0^{\mathrm{t}} (\mathrm{F^+ x - z})\mathrm{dt}, \end{cases} \tag{4.13}$$

where $\Gamma_1 = \mathrm{diag}(\xi_{11} \dots . \xi_{1\mathrm{r}})$ is positive disturbance observer gain matrix should be chosen such that polynomials in the equation (4.14) are Hurwitz stable.

$$p_j(s) = s^r + \xi_{1j}s + \cdots \xi_{1j} \text{ with } j = 1,2,3,r \tag{4.14}$$

Combination of (4.9), (4.12), and (4.13) the dynamics of the disturbance estimation errors will become as;

$$\begin{aligned} e_d = \dot{\hat{d}} - \dot{d} &= \Gamma_0(\mathrm{F^+ \dot{x} - \dot{z}}) + \Gamma_1(\mathrm{F^+ x - z}) - \dot{d} \\ &= -\Gamma_0 e_d + \Gamma_1(\mathrm{F^+ x - z}) - \dot{d}, \end{aligned} \tag{4.15}$$

After taking the derivatives of both sides of the equation (4.12) in terms of time along the system trajectory (4.9) and observer dynamics (4.13) it becomes as;

$$\ddot{e}_d = -\Gamma_0 \dot{e}_d + \Gamma_1(\mathrm{F^+ x - z}) - \ddot{d} = -\Gamma_0 \dot{e}_d - \Gamma_1 e_d - \ddot{d} \tag{4.16}$$

while Γ_0 and Γ_1 are diagonal form matrices, the observer error dynamics become decoupled. In the case of ramp disturbance, it has been shown in equation (4.16) that $\ddot{d}(t) = 0$ and error dynamics of j-th order observer governed by following

$$e_{dj} + \xi_{0j} e_{dj} + \xi_{1j} e_{dj} = 0 \tag{4.17}$$

The convergent dynamics of the observer error system in equation (4.17) can be separately tuned by assigning the poles of the polynomial equation (4.14).

4.3.3. High-order disturbance case

Let us consider the high-order disturbance $\mathrm{d}(\mathrm{t})$ in equation (4.1) as

$$d(t) = d_0 + d_1 t + d_2 t \ \ldots + d_q t^q \tag{4.18}$$

where d_0, d_1, d_p are constant coefficients but unknown.

The high-order disturbance observer design for the estimation of wind speed which is cubic of the aerodynamic torque in sensorless WECS application has been proposed in [15]–[17] and can be generalized as

$$\begin{cases} \dot{z} = \mathrm{F}^{+}\mathrm{f}(\mathrm{x},\mathrm{u};\mathrm{t}) + \Gamma_0 \mathrm{g}_0(\mathrm{t}) + \Gamma_1 \mathrm{g}_1(\mathrm{t}) + \cdots + \Gamma_\mathrm{q} \mathrm{g}_\mathrm{q}(\mathrm{t}) \\ \hat{\mathrm{d}} = \Gamma_0 \mathrm{g}_0(\mathrm{t}) + \Gamma_\mathrm{q} \mathrm{g}_\mathrm{q}(\mathrm{t}) \end{cases} \tag{4.19}$$

With

$$\mathrm{g}_\mathrm{k}(\mathrm{t}) = \begin{cases} \mathrm{F}^{+}\mathrm{x} - \mathrm{z}, \ (\mathrm{k} = 0) \\ \int_0^{\mathrm{t}} \mathrm{g}_{\mathrm{k}-1}(\mathrm{t})\mathrm{dt}, (\mathrm{k} \geq 1) \end{cases} \tag{4.20}$$

For $k \in [0, q]$, where $\Gamma_\mathrm{k} = \mathrm{diag}(\xi_{\mathrm{k}1} \ldots . \xi_{\mathrm{kr}})$ with $\mathrm{j} = 0, \ldots \mathrm{q}$ is positive diagonal gain matrices to be designed such that polynomial equation (4.21) is Hurwitz stable.

$$\mathrm{p}_\mathrm{j}(\mathrm{s}) = \mathrm{s}^{\mathrm{q}+1} + \xi_{0\mathrm{j}}\mathrm{s}^{\mathrm{q}} + \cdots \xi_{(\mathrm{q}-1)\mathrm{j}}\mathrm{s} + \xi_{\mathrm{qj}} \tag{4.21}$$

High-order disturbance observer design can be generalized by the block diagram shown in Figure 4.2.

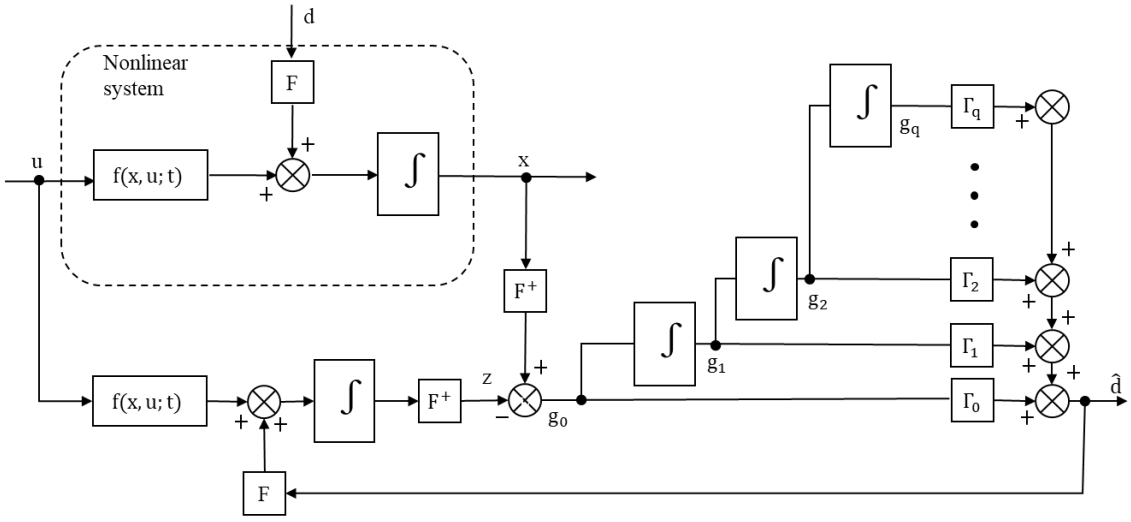

Figure 4.2. High-order disturbance observer block diagram

After combining (4.3), (4.10), and (4.18)-(4.20), the disturbance dynamics estimation error becomes

$$\dot{e}_\mathrm{d} = \dot{\hat{\mathrm{d}}} - \dot{\mathrm{d}} = \Gamma_0 \dot{\mathrm{g}}_0(\mathrm{t}) + \Gamma_1 \dot{\mathrm{g}}_1(\mathrm{t}) + \cdots + \Gamma_\mathrm{q} \dot{\mathrm{g}}_\mathrm{q}(\mathrm{t}) - \dot{\mathrm{d}}$$

$$= -\Gamma_0 e_d + \Gamma_1 g_1(t) + \cdots + \Gamma_q g_{q-1}(t) - \dot{d}, \quad (4.22)$$

After taking the derivatives of both sides of the equation (4.22) in terms of time along the system trajectory (4.10), the observer dynamics (4.19) and (4.20) it becomes as

$$\ddot{e}_d = -\Gamma_0 \dot{e}_d + \Gamma_0 \dot{g}_0(t) + \Gamma_1 \dot{g}_1(t) + \cdots + \Gamma_q \dot{g}_q(t) - \ddot{d}$$
$$= -\Gamma_0 \dot{e}_d - \Gamma_1 e_d + \cdots + \Gamma_q g_{q-2}(t) - \ddot{d} \quad (4.23)$$

The calculation of the q-th order disturbance estimation errors will take the form

$$e_d^q = -\Gamma_0 e_d^{q-1} - \Gamma_1 e_d^{q-2} - \cdots - \Gamma_q e_d - d^q \quad (4.24)$$

Let us consider the case when the disturbances in equation (4.17) satisfying $d^q(t) = 0$, it can be found that error dynamics of q-th order disturbance observer governed by

$$e_{dj}^q = -\xi_0 e_{dj}^{q-1} - \xi_{1j} e_{dj}^{q-2} - \cdots - \xi_{qj} e_{dj} = 0 \quad (4.25)$$

The tuning by assigning poles of the polynomial equation (4.21) provides the convergent dynamics of the observer's estimated errors in equation (4.25).

4.4.HODO design for aerodynamic torque estimation

In design of observers, it is common to assume that the disturbances have slow-changing behavior. However, in real systems, such kind of assumption leads to poor performance and less accuracy of system output. Although in many research publications, it is stated that this assumption is applicable for even fast-changing uncertainties, it has not been observed zero errors at the steady-state [15].

Assumption 4.1: The aerodynamic torque (T_a) and uncertainties (d_q and d_d) are not necessarily constant but are smooth enough. In other words, there exist positive integers ki such that T_a, d_q, $d_d \in C^{k_i+1}(i = 1,2,3)$. Furthermore, $(k_i + 1)$-order derivatives of the aerodynamic torque and disturbances are ignorable, $\frac{d^{k_i+1}}{dt^{k_i+1}} \approx 0$ $(i = 1,2,3;\ M = T_a, d_q, d_d)$.

To estimate aerodynamic torque for estimation wind speed the PMSG rotor's speed dynamic equation (4.45) has to be recalled

$$\frac{d\omega}{dt} = \frac{1}{Jn_{gb}} T_a - \frac{B}{J}\omega - \frac{1}{J} T_e \quad (4.26)$$

Then, the generalized high-order aerodynamic torque observer is designed as [15]

$$\begin{cases} \dot{Z}_{\omega} = -n_{gb}(B\omega + T_e) + \hat{T}_a \\ \hat{T}_a = L_{01}g_{01} + L_{11}g_{11} + \cdots + L_{k_1 1}g_{k_1 1} \\ \dot{g}_{01} = Jn_{gb}\omega - Z_{\omega} \\ \dot{g}_{11} = g_{01} \\ \dot{g}_{21} = g_{11} \\ \vdots \\ g_{k_1 1} = g_{(k_1-1)1} \end{cases} \tag{4.27}$$

where $(\hat{\cdot})$ and $(\dot{\cdot})$ denotes the estimation and 1st order derivative of the argument functions, respectively, $L_{01}, L_{11}, L_{k_1 1}$ are aerodynamic observer gains.

From this using (3.40) and (3.42) the estimation of angular shaft speed reference can be defined as following

$$\hat{\omega}_d = \sqrt{\frac{\hat{T}_a}{k_{opt}}}, \tag{4.28}$$

With

$$k_{opt} = \frac{\rho \pi R^5 C_{pmax}}{2\lambda_{opt}^3 n_{gb}^2} \tag{4.29}$$

4.5.HODO design for model uncertainty estimation

To estimate disturbances associated with model uncertainties, modeling errors and noise the PMSG T_e and i_d dynamic equations from (4.45) have to be recalled

$$\begin{cases} \frac{dT_e}{dt} = -PK\omega i_d - \frac{R_s}{L}T_e - \frac{\psi_m PK}{L}\omega + \frac{K}{L}v_q + d_q \\ \frac{di_d}{dt} = \frac{1}{L}v_d - \frac{R_s}{L}i_d + \frac{P}{K}\omega T_e + d_d \end{cases} \tag{4.30}$$

From above the following generalized high-order disturbance observers can be deduced. For estimation of the disturbance in q-axis:

$$\begin{cases} \dot{Z}_{T_e} = -PK\omega i_d - \frac{R_s}{L}T_e - \frac{\psi_m PK}{L}\omega + \frac{K}{L}v_q + \hat{d}_q \\ \hat{d}_q = L_{02}g_{02} + L_{12}g_{12} + \cdots + L_{k_2 2}g_{k_2 2} \\ \dot{g}_{02} = T_e - Z_{T_e} \\ \dot{g}_{12} = g_{02} \\ \dot{g}_{22} = g_{12} \\ \vdots \\ g_{k_2 2} = g_{(k_2-1)2} \end{cases} \tag{4.31}$$

where $L_{02}, L_{12}, L_{k_2 2}$ are q-disturbance observer gains.

For estimation of the disturbance in d-axis:

$$\begin{cases} \dot{Z}_{i_d} = \frac{1}{L} v_d - \frac{R_s}{L} i_d + \frac{P}{K} \omega T_e + \hat{d}_d \\ \hat{d}_d = L_{03} g_{03} + L_{13} g_{13} + \cdots + L_{k_3 3} g_{k_3 3} \\ \dot{g}_{03} = i_d - Z_{i_d} \\ \dot{g}_{13} = g_{03} \\ \dot{g}_{23} = g_{13} \\ \vdots \\ g_{k_3 3} = g_{(k_3-1)3} \end{cases} \tag{4.32}$$

where $L_{03}, L_{13}, L_{k_3 3}$ are d-disturbance observer gains.

The detailed explanation to how choose the gains for stability and improve the accuracy in steady-state for HODO are given in [15].

4.6.HODO observer design for load torque estimation

The applied load torque disturbance in PMSM system is usually constant and its derivatives is zero. However, the performance of the speed controller deteriorates with the presence of the unmodeled dynamics, model uncertainty, and external disturbances. These disturbances fluctuate torque ripples in the response causing the steady state errors between desired and actual the angular shaft speed of the PMSM. Therefore, to improve the tracking performance of the control system, the speed controller can be synthesized with HODO for compensation in feedforward manner.

To estimate the total disturbance d including load torque disturbance, T_L in the continuous-time domain, the first equation of (3.36) should be recalled,

$$\dot{\omega} = k_1 i_q - k_2 \omega - k_3 d \tag{4.33}$$

Then high-order disturbance observer is designed as

$$\begin{cases} \dot{\hat{\omega}} = k_1 i_q - k_2 \omega - k_3 \hat{d} \\ \hat{d} = L_{11} g_1 + L_{12} g_2 + L_{13} g_3 \\ g_1 = -\frac{(\omega - \hat{\omega})}{k_7} \\ \dot{g_2} = g_1 \\ \dot{g_3} = g_2 \end{cases} \tag{4.34}$$

where $k_7 = \frac{1}{J}, L_{11}, L_{12}, L_{13}$ are observer gains for estimation the total disturbance.

Theorem 4.1: Let observer gains L_{1k}, L_{2k}, L_{3k} (k = 1, 2, 3) are chosen such that the following polynomial is stable by the Hurwitz Routh criterion;

$$r(s) = s^{k_1+1} + L_1 s^{k_1} + L_2 s^{k_1-1} + \cdots + L_{k_1} \tag{4.35}$$

Then the estimated disturbance asymptotically converges to the true value.

Proof: This is straightforward to see that if $(k+1)^{th}$ time derivative of disturbance is zero, $d^{(k+1)} = 0$, then the Theorem 4.1 is hold. More details on how to choose the gains to achieve stability and less steady-state errors in estimation with HODO observer is given in [35]–[38].

4.7. Summary of Chapter 4

In this chapter, the linear and nonlinear disturbance observers design have been reviewed for the PM synchronous machine applications. First, the concept of linear disturbance observer design has been introduced for the estimation of the disturbances in the linear system. Second, the high-order disturbance observer design has been demonstrated for the estimation of the nonlinear dynamics of the disturbances in the PM synchronous machine applications. system with. Third, it has been shown that the disturbance estimation errors converge to zero for constant, rump, and high-order disturbance cases. Finally, the HODO designs for estimation of the aerodynamic torque and model uncertainty in the WECS, and total external disturbance in the PMSM system have been presented. In the next chapters, the performance of the HODO for the given applications will be demonstrated.

Chapter 5: HODO-based control systems design for PM synchronous machine applications

5.1.Introduction

In this chapter, linear and nonlinear controllers have been developed for PM synchronous machine applications. Firstly, switching output feedback-based SMC along with HODO for load torque compensation in feedforward scheme has been proposed to improve the tracking performance of the PMSM system. Secondly, HODO based discrete-time PI-PI control system with an anti-windup scheme has been proposed for the PMSM system. Thirdly, the SDRE control-based ISMC control system has been proposed for maximizing power extraction in the WECS application. This controller is synthesised with HODOs for compensations of the model uncertainty, noise and estimation of aerodynamic torque which acts as external disturbance to define reference angular shaft speed of the variable speed WECS. Finally, SDRE control system with servomechanism technique has been proposed for the maximum power extraction in the variable-speed WECS. The aforementioned proposed HODO-based controls' performance will be tested under presence of the model uncertainty, noise and external disturbances.

5.2.Switching output feedback control law design

To develop a model-based switching output feedback control law for the control system of the SPMSM, the nonlinear model of the SPMSM in (3.27) first needs to be transformed to the appropriate error dynamics. By introducing the error vector $x = [x_1 \quad x_2 \quad x_3]^T$.

Then,

$$x_1 = \omega - \omega_d,\ x_2 = \dot{\omega} = k_1 i_{qs} - k_2\omega - k_3\hat{T}_L,\ x_3 = i_{ds} \tag{5.1}$$

The following error dynamics can be obtained

$$\begin{cases} \dot{x}_1 = x_2 \\ \dot{x}_2 = -k_1k_5x_1 - k_2x_2 + k_1k_6V_q - k_1i_d\omega - k_1k_5\omega_d - k_1k_4i_q \\ \dot{x}_3 = -k_4x_3 + k_6V_d + i_q\omega \end{cases} \tag{5.2}$$

Taking into account the disturbance the equation (5.2) can be considered as the multi-input-multi-output (MIMO) system with disturbance

$$\dot{x}(t) = Ax + B[u + u_d] \tag{5.3}$$

Where the disturbance is $u_d = T_L$.

The control input u is decomposed as $u_1 = V_q, u_2 = V_d$.

The (5.2) can be cast as following matrices

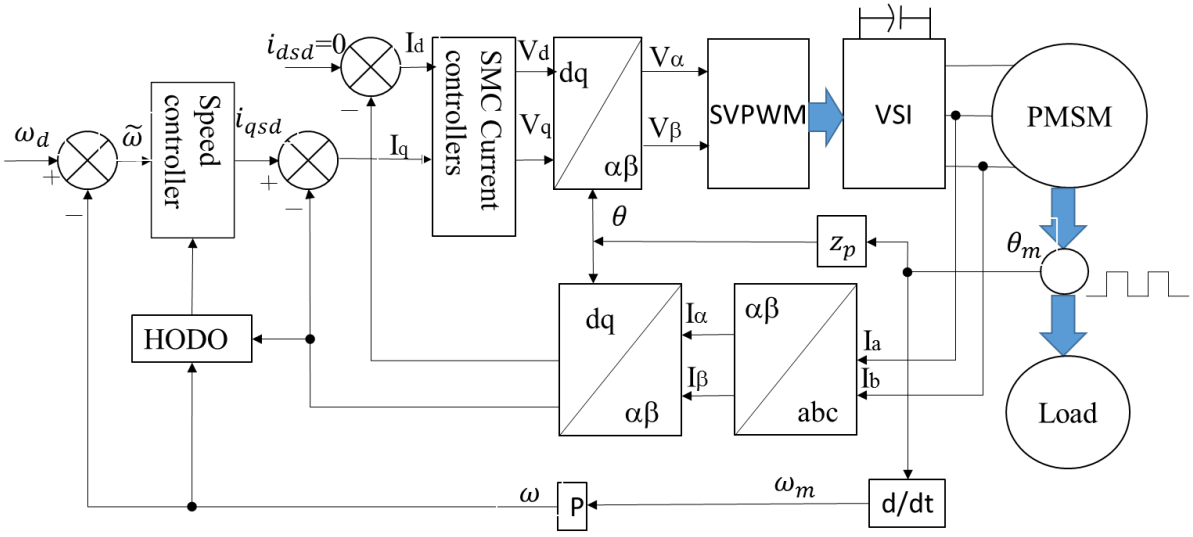

Figure 5.1. The proposed switching output feedback-based SMC synthesized with HODO

$$A = \begin{bmatrix} -k_2 & k_1 & 0 \\ -k_1 k_5 & -k_2 & 0 \\ 0 & 0 & -k_4 \end{bmatrix}, B = \begin{bmatrix} 0 & 0 \\ k_1 k_6 & 0 \\ 0 & k_6 \end{bmatrix}, \; u = \begin{bmatrix} u_1 \\ u_2 \end{bmatrix}, \tag{5.4}$$

In (5.4), A is a constant matrix for all $x(t)$'s, and B is a constant matrix.

For designing the switching output feedback control law, the sliding surface has to be chosen appropriately.

The sliding surface is governed by

$$\dot{\sigma} = Sx = (B^T P B)^{-1} B^T P x(t) = 0 \tag{5.5}$$

where $P \in R^{n \times n}$ is a positive-definite matrix such that the following Algebraic Riccati Equation (ARE) holds for some $Q \geq 0, R > 0$.

$$PA + A^T P - PBR^{-1}B^T P + Q = 0 \tag{5.6}$$

It should be noted that with different Q, R tuning matrices, the various σ sliding surfaces can also be obtained.

Remark 5.1: The procedure of the selection of the values of the tuning matrix is shown in this remark. As it can be observed, the performance is depends on Q and R tuning matrices which affect on the response time and steady-state error between the reference and actual speed commands. Generally, if a precise tracking is required, Q is needed to be large, whereas if energy minimization, i.e., small control inputs, is required, R needs to be large. Therefore, there is a tradeoff between control performance and control effort, or in other words, between Q and R.

Typically, Q and R are selected to be diagonal matrices as:

$$\mathrm{Q} = \begin{bmatrix} q_1 & \cdots & 0 \\ \vdots & \ddots & \vdots \\ 0 & \cdots & q_n \end{bmatrix}, \mathrm{R} = \rho \begin{bmatrix} r_1 & \cdots & 0 \\ \vdots & \ddots & \vdots \\ 0 & \cdots & r_m \end{bmatrix} \tag{5.7}$$

Where

$$q_i = \frac{1}{t_{si}(x_{imax})^2}, r_i = \frac{1}{(u_{imax})^2}, \rho > 0 \tag{5.8}$$

Where t_{si} is the desired settling time of x_i, $x_{max}$is a constraint on $|x_i|, u_{imax}$ is a constraint on $|u_i|, \rho$ is chosen to tradeoff regulation versus control effort. Starting with an initial guessed value, the weighting matrices Q and R can be adjusted via a trial-and-error method until the results is satisfied. In fact identity matrices are a good choice for initial values of weighting matrices.

Finally, the switching output feedback control law is given by

$$\mathrm{u} = -\mathrm{SA} - \mathrm{k}\frac{\sigma}{||\sigma||} \tag{5.9}$$

where k is the positive scalar.

For the reduction of the chattering phenomenon, the continuous approximation such as $\frac{\sigma}{||\sigma||+\delta}$ can be used, where δ is a small positive number. The approximation methods may affect to the performance degradation and oscillatory behaviour of unpredictable frequency. As δ tends to zero, the performance of the approximated solution is close to the exact one. However, computational time to run simulation with such control system may take longer time.

The design of baseline MIMO controller has been built. Next, HODO demonstrated in Chapter 4 should be synthesised with speed controller where estimated load torque disturbance is compensated. While this load torque disturbance is constant, other fast-varying disturbances such as pulsating torque due to body structure causing eddy currents, and flux harmonics also are presented in the PMSM system. To compensate these disturbances, the improved disturbance rejecting speed controller of the servo PMSM with HODO will be presented in the next section.

5.3.HODO-based discrete-time PI-PI control system design

5.3.1.Updated model of PMSM system

The available electromagnetic torque of the PMSM is reduced by various source disturbances and the motion equation of the mathematical model in equation (3.26) is detailed. These disturbances can be notated as the total disturbance associated with

friction, viscosity, and drag resulting from time-varying flux. As disturbance estimation based on the angular shaft speed, the mechanical speed equation is defined as

$$\dot{\omega}_m J_{ri} = \frac{3}{2} z_p \lambda_m i_q - (c_{ed} + b) - d \tag{5.10}$$

where z_p is number of poles, c_{ed} is eddy currents coefficient, $\frac{N \cdot m}{\left(\frac{rad}{s}\right)}$,

It should be noted that electrical speed is equal to the mechanical speed multiplied to half of the number of poles.

In this control system, the load torque disturbance, the time-varying magnetic flux due to eddy currents, the friction, and the hysteresis causing torque losses are considered as the total external disturbances. These disturbances affects to the motion equation of the PMSM, hence reduce produced torque and associated with fluctuations in the speed response. Equation (5.11) presents the total disturbance d in the mechanical motion equation which will be estimated by HODO for its compensation in the speed controller

$$d = \left(C_{hy} + C_f\right) \text{sign}(\omega_m) + d_{ed} \frac{\Psi_{dq} \Psi_{dq}}{|\Psi_{dq}|^2} + T_L \tag{5.11}$$

where d_{ed} is eddy currents damping coefficient, $\frac{N \cdot m}{(rad/s)}$, C_{hy} is hysteresis losses coefficient, $N \cdot m$, C_f is a static moment of friction, $N \cdot m$, Ψ_{dq} – d-q frame magnetic flux linkage, Wb.

To design a DOBC with HODO, the following assumptions are established.

***Assumption 5.1*:** ω, i_q, and i_d are measurable.

Assumption 5.2: $\dot{d} \neq 0$

In the linear disturbance observer for example, the disturbance is assumed to be slowly varying, i.e., its time derivative is zero. In the proposed disturbance observer-based control, this constraint is released.

5.3.2.Discrete-time PI controller design with anti-windup scheme

The digital controller design is important for the practical PM synchronous machine control applications. The converting the continuous plant to discrete-time equivalent and designing the controller in discrete domain is one way to control the plant. Alternatively, the discrete-time controller can be applied for controlling continuous plant via discrete filters which closely approximate behavior continuous plant. The digital controller implementation on the integrated system such as MATLAB.

The proportional integral – proportional integral (PI-PI) stands for cascade closed-loop control where inner loops are regulated by two PI current controllers and outer loop

is controlled by the PI speed controller. The baseline scenario with PI-PI control system without DO is considered as sufficient to achieve satisfactory performance for speed regulation. The control objective, in this case, is to achieve a specified tracking performance employing the PI controller and facilitate zero errors in a finite time. The discrete-time PI speed controller is presented in Figure 5.2.

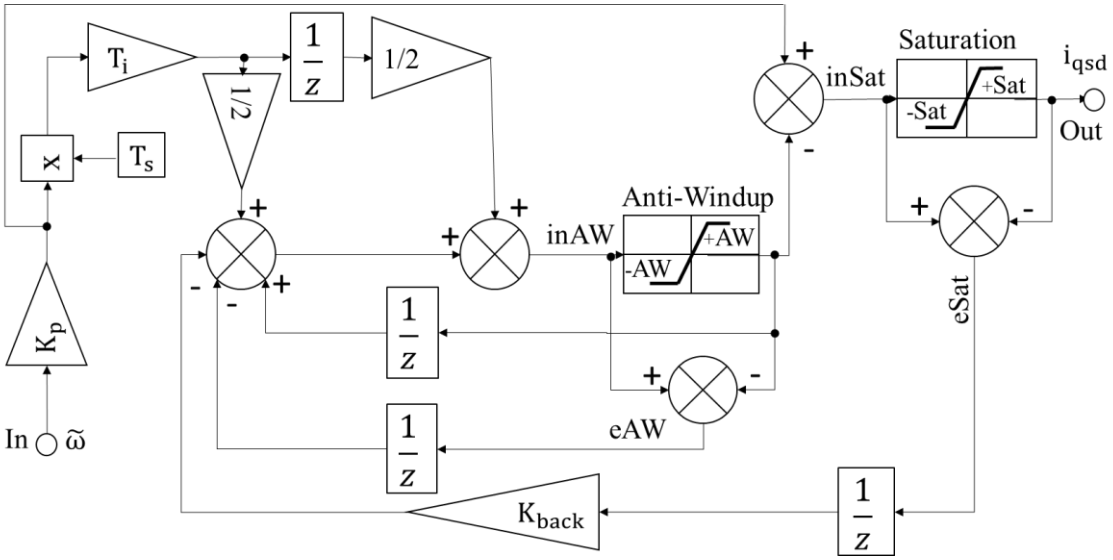

Figure 5.2. Discrete-time PI speed and current controller with the back-calculation anti-windup scheme

where

inSat – input of saturation block

$\mp\mathrm{Sat}$ – output of saturation block

out – output of PI controller

inAW – input of anti-windup block

$\mp\mathrm{AW}$ – output of anti-windup block

eSat – error of saturation block

eAW – error of anti-windup block

$\tilde{\omega}$ – speed error, rad/s

K_p – proportional gain

T_i – integrator time

T_s – sampling time

$\frac{1}{z}$ – unit delay

K_{back} – back-calculation gain

5.3.3.HODO design for total disturbance estimation

While the speed controller in the conventional PI-PI control is easy to implement with fixed gains, the tracking accuracy can be degraded under various operational conditions. Previously, the fast varying total disturbances including load torque T_L were assumed to be slowly varying. Consequently, these varying terms may not be estimated and compensated correctly with the DOBC using this assumption. Therefore, to improve the performance of the PI speed controller with a tracking back-calculation anti-windup scheme, a HODO observer can be integrated to compensate for these disturbances.

The original concept of a HODO design is presented for wind speed as well as model uncertainty estimations in renewable energy generation applications even for the case of fast-varying disturbances [15], [16]. HODO is considered a cost-efficient solution with an acceptable range of accuracy in estimating aerodynamic torque. Using inappropriate observers leads to poor performance of the whole control system. The high-quality observer along with the robust controller can provide better performance in speed control of PMSM under various disturbances.

To estimate the total disturbance d including load torque disturbance, T_L, the first detailed motion equation of mechanical speed of the PMSM converted to electrical speed (5.10) should be recalled,

$$\dot{\omega}_m = \frac{1}{J_{ri}}\left[\frac{3}{2} z_p \lambda_m i_q - (c_{ed} + b) - d\right], RPM \tag{5.12}$$

Then high-order disturbance observer is designed as:

$$\begin{cases} \dot{\hat{\omega}}_m = \frac{1}{J_{ri}}\left[\frac{3}{2} z_p \lambda_m i_q - (c_{ed} + b) - \hat{d}\right] \\ \hat{d} = L_{11} g_1 + L_{12} g_2 + L_{13} g_3 \\ g_1 = -\frac{(\omega - \hat{\omega})}{J_{ri}} \\ \dot{g_2} = g_1 \\ \dot{g_3} = g_2 \end{cases} \tag{5.13}$$

where the difference between actual and estimated angular shaft speed is proportional to $J_{ri}, \text{and } L_{11}, L_{12}, L_{13}$ are observer gains for estimating of the total disturbance. In order to integrate with discrete-time PI controller resulting internal variables should be multiplied with delay block, z^{-1}.

5.3.4.HODO-based discrete-time PI-PI control system

The cascade discrete-time PI-PI control system is synthesised with HODO to compensate the estimated total disturbance in the feedforward manner. In Figure 5.3, the block diagram of the proposed DOBC to compensate for the total disturbance is shown for the PMSM speed regulation.

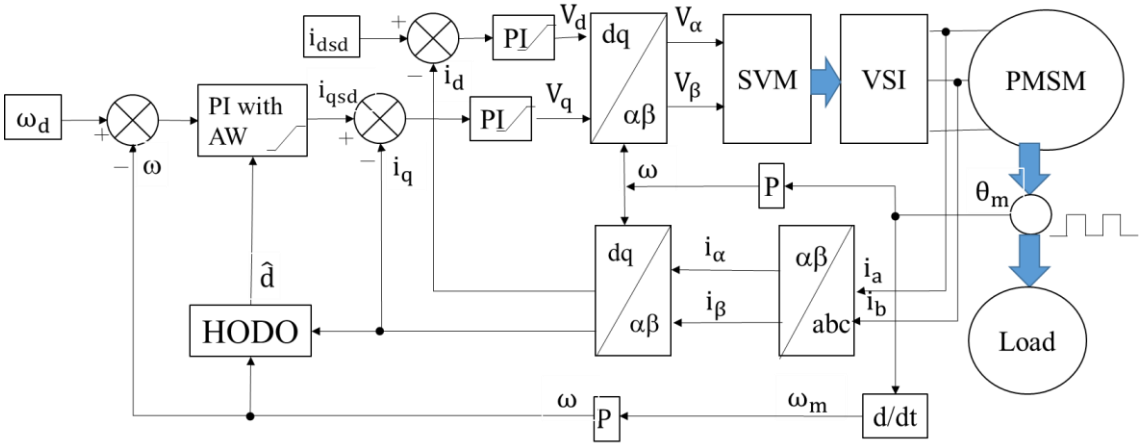

Figure 5.3. Proposed DOBC method block-diagram

The estimated total disturbance is compensated in the PI speed controller of the proposed control design as shown in Figure 5.4. While the inputs of the saturation (inSat) block are between its control system. Otherwise, the outputs of the speed controller are equal to ∓Sat and the estimated value does not affect to reference q-axis current in a steady state.

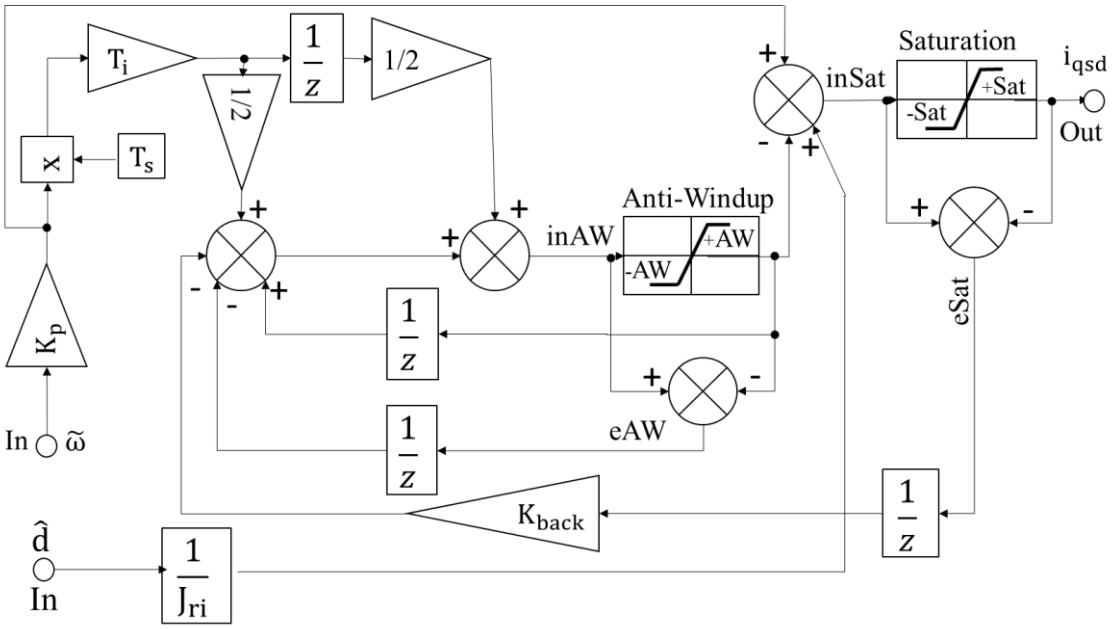

Figure 5.4. The total disturbance compensation in the PI speed controller of the proposed

control design

The logic of the proposed speed controller is explained briefly below. When the posed conditions given in equations (5.14) and (5.15) are true, the proposed speed controller's outputs will be equal to zero or equal to the limits of the saturation block.

$$|\mathrm{inSat} = 0| \text{ and } |\mathrm{inAW} = 0| \ \{\mathrm{out} = 0\} \tag{5.14}$$

$$|\mathrm{inSat} \geq \mp \mathrm{Sat}| \text{ and } |\mathrm{inAW} \geq \mp \mathrm{AW}| \ \{\mathrm{out} = \mp \mathrm{Sat}\} \tag{5.15}$$

When the posed conditions given in equations (5.16) and (5.17) are true the proposed speed controller will be completed with the compensating term $\frac{1}{\mathrm{J_{ri}}}\hat{\mathrm{d}}$.

$$|\mathrm{inSat} < \mp \mathrm{Sat}| \text{ and } |\mathrm{inAW} \geq \mp \mathrm{AW}|, \ \left\{\mathrm{out} = \mathrm{eK_p} - (\mp \mathrm{AW}) + \frac{1}{\mathrm{J_{ri}}}\hat{\mathrm{d}}\right\} \tag{5.16}$$

$$|\mathrm{inSat} < \mp \mathrm{Sat}| \text{ and } |\mathrm{inAW} < \mathrm{AW}| \ , \ \left\{\begin{matrix} \mathrm{out} = \mathrm{eK_p} - (\frac{1}{2}\frac{1}{\mathrm{z}}\mathrm{K_{pi}eK_pT_s} + (\frac{1}{2}\mathrm{K_{pi}eK_pT_s} + \\ \frac{1}{\mathrm{z}}\mathrm{inAW} - \frac{1}{\mathrm{z}}\mathrm{eSatK_{back}} - \frac{1}{\mathrm{z}}\mathrm{eAW})) + \frac{1}{\mathrm{J}_{ri}}\hat{\mathrm{d}} \end{matrix}\right\} \tag{5.17}$$

The proposed discrete-time PI speed controller has back-calculation algorithm based anti-windup scheme synthesized with HODO which allows to achieve to the desired control performances under given operational conditions. While the HODO based control laws have been designed for servo PMSM system, the HODO-based control system with nonlinear feedbacks are going to be presented in the next sections for WECS application.

5.4.SDRE-based ISMC control design with HODO

5.4.1. SDRE-based nominal part of ISMC control law

In this subsection, the nonlinear dynamic model (3.35) of PMSG-based WECS is transformed into the error dynamics, and then the proposed ISMC with SDRE control law will be developed. The proposed SDRE-based ISMC diagram for maximum power extraction in the WECS is depicted in Figure 5.5.

To make the system less susceptible to the disturbances, the ISMC is going to be designed for improve tracking performance of the wind speed based the variable speed WECS.

Introducing the following error dynamics

$$\begin{aligned} &\tilde{\omega} = \omega - \omega_{\mathrm{d}}, \omega_{\mathrm{d}} = \omega_{\mathrm{t,d}} \cdot \mathrm{n_{gb}} = \frac{\lambda_{\mathrm{opt}}}{\mathrm{R}}\vartheta \cdot \mathrm{n_{gb}}, \\ &\tilde{\mathrm{T}_{\mathrm{e}}} = \mathrm{T_e} - \mathrm{T_{ed}}, \ \mathrm{T_{ed}} = \frac{1}{\mathrm{n_{gb}}}\mathrm{T_a} - \mathrm{B_{vf}}\omega_{\mathrm{d}} - \mathrm{J_{ri}}\dot{\omega}_{\mathrm{d}} \end{aligned} \tag{5.18}$$

Where T_{ed} is reference of electromagnetic torque. The wind speed acts as external disturbance, and it will be estimated via aerodynamic torque which is not known for WECS.

The control inputs, V_q and V_d are consist of feedback and compensating terms. While feedback terms of the control law are based on the SDRE control and ISMC, the compensating terms for both control channels are based on the estimations of the model uncertainty, noise and modelling errors found during the defined the error dynamics.

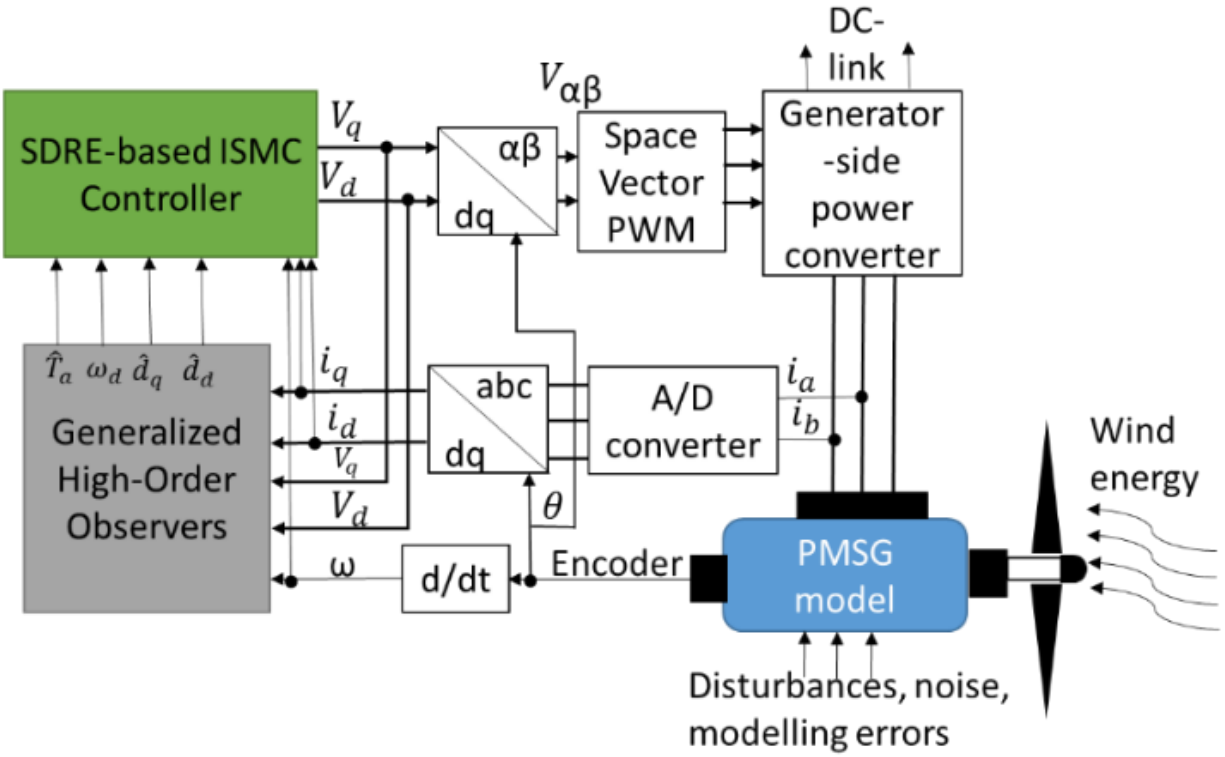

Figure 5.5.The proposed SDRE -based ISMC diagram for the WECS

$$V_q = u_{ffq} + u_{fbq}, \quad V_d = u_{ffd} + u_{fbd} \tag{5.19}$$

where u_{ffq}, u_{fbq} - q-axis feedforward and feedback control laws, respectively; u_{ffd}, u_{fbd} - d-axis feed-forward and feedback control laws, respectively.

The feedforward part of the control laws u_{ffq}, u_{ffd} includes the remaining terms after forming state-space equations. Note, the estimating model uncertainty for both control channels are included

$$u_{ffq} = \frac{R_s}{K} T_{ed} + LP\omega i_d + \lambda_m P\omega_d - \frac{L}{K}\hat{d}_q \tag{5.20}$$

$$u_{ffd} = -\frac{R_s}{K}\omega T_e - L\hat{d}_d \tag{5.21}$$

The WECS nonlinear state space model will be as follows

$$\begin{cases} \frac{d\tilde{\omega}}{dt} = -\frac{B_{vf}}{J_{ri}}\tilde{\omega} - \frac{1}{J_{ri}}\tilde{T}_e \\ \frac{d\tilde{T}_e}{dt} = -PK\tilde{\omega}i_d - \frac{R_s}{L}\tilde{T}_e - \frac{\lambda_m PK}{L}\tilde{\omega} + \frac{K}{L}v_q + \hat{d}_q \\ \frac{di_d}{dt} = \frac{1}{L}v_d - \frac{R_s}{L}i_d + \frac{P}{K}\tilde{\omega}\,\tilde{T}_e + \hat{d}_d \end{cases} \quad (5.22)$$

By using the above equations the state-space model can be formed as follows

$$\dot{x} = A(x)x + B(u - u_c) \quad (5.23)$$

where $x = [\tilde{\omega}\ \tilde{T}_e\ i_d]^T$ the system state vector; $A(x)$ is the continuous matrix for all x's and B is the constant control matrix; $u = [u_q\ u_d]^T$ - control input; u_c – compensating term. The nonlinear terms are associated with the state variables which are product of $\tilde{\omega}$.

$$A(x) = \begin{bmatrix} -\frac{B_{vf}}{J_{ri}} & -\frac{1}{J_{ri}} & 0 \\ -\frac{\lambda_m PK}{L} & -\frac{R_s}{L} & -PK\tilde{\omega} \\ 0 & \frac{P}{K}\tilde{\omega} & -\frac{R_s}{L} \end{bmatrix},\ B = \begin{bmatrix} 0 & 0 \\ \frac{K}{L} & 0 \\ 0 & \frac{1}{L} \end{bmatrix} \quad (5.24)$$

The matrix A(x) in the equation (5.21) can be cast as follows

$$A(x) = A_0 + \Delta A(x). \quad (5.25)$$

To have the state matrix A(x), which can be split into two parts: constant matrix A_0 and state-dependent incremental matrix $\Delta A(x)$.

$$A_0 = \begin{bmatrix} -\frac{B_{vf}}{J_{ri}} & -\frac{1}{J_{ri}} & 0 \\ -\frac{\psi_m PK}{L} & -\frac{R_s}{L} & 0 \\ 0 & 0 & -\frac{R_s}{L} \end{bmatrix},$$

$$\Delta A(x) = \begin{bmatrix} 0 & 0 & 0 \\ 0 & 0 & -PL\tilde{\omega} \\ 0 & \frac{PL}{K}\tilde{\omega} & 0 \end{bmatrix},\quad B = \begin{bmatrix} 0 & 0 \\ \frac{K}{L} & 0 \\ 0 & \frac{1}{L} \end{bmatrix}$$

For the system (5.23) the control input has to be designed such that

$$u_{fb}(t) = u_{SDRE}(t) + u_1(t) \quad (5.26)$$

where $u_{SDRE}(t)$ is SDRE-based the nominal control part, and $u_1(t)$ is integrally based discontinuous part to eliminate the reaching phase and to facilitate robust control of unmeasured matched disturbance.

Allowing the nonlinearities in the system, SDRE creates the nonlinear output feedback control in the system. Its flexibility is defined by the use of a state-dependent weighting matrix. The Taylor series expansion can be used to obtain the approximated

solution. The coefficients of the Riccati equations vary with varying points in the state space.

As the state and input weighting matrix of equation (5.25) are assumed to be state-dependent, ***care*** and ***lyap*** Matlab's solvers are applied to design the nominal part of the proposed control law. It is applied in a point-wise manner and tends to minimize performance index (5.27) and drive the control system to the origin.

Let us define the performance index

$$J = \frac{1}{2}\int_0^\infty x^T Q(x)x + u^T R(x)u\, dt \tag{5.27}$$

Where $Q \in R^{3\times3}$ is constant symmetric positive semidefinite weighting matrix, and $R \in R^{2\times2}$ is a constant symmetric positive definite weighting matrix. The suboptimal control law of the system with nonlinear dynamics given in equation (5.24).

Thus, the feedback control term can take the form

$$u = -K(x)x = R^{-1}B^T P(x)x, \;\; K: \mathcal{R}^n \to \mathcal{R}^{p\times n} \tag{5.28}$$

where $P: \mathcal{R}^n \to \mathcal{R}^{n\times n}$ satisfies ARE and for the given system the control function (5.28) $P(x)$ is a unique symmetric and positive definite solution of the following SDRE

$$P(x)A(x) + A(x)^T P(x) - P(x)BR^{-1}B^T P(x) + Q = 0 \tag{5.29}$$

As a result, the state-dependent optimal gain matrix K can also be expressed as the sum of constant and state-dependent matrices

$$u_{SDRE}(t) = -(K_0 + \Delta K(x))x \tag{5.30}$$

where

$$K_0 = -R^{-1}B^T P_0 \qquad \Delta K(x) = R^{-1}B^T \Delta P(x) \tag{5.31}$$

The detailed stability analysis for the state-dependent Riccati equation can be found in [5].

5.4.2.Solving of SDRE-based ISMC controller by Taylor series method

The approximated solution of the SDRE-based nominal part of ISMC of the proposed control law by Taylor series method can be expressed as [5], [13]:

$$u^N(x) = -R^{-1}B^T\left(\sum_{n=0}^{N}\left(g(x)\right)^n (P_n)_C\right)x = -\left(\sum_{n=0}^{N}\left(g(x)\right)^n K_n\right)x, \tag{5.32}$$

where $K_n = R^{-1}B^T(P_n)_C$, N is the number of members in the series computed offline, and $(P_n)_C$ is a constant matrix, achieved by solving the following algebraic Riccati and Lyapunov equations [5]:

$$P_0^C A + A^T P_0 - P_0 B R^{-1} B^T P_0 + Q = 0 \quad (5.33)$$

$$(P_1)_C (A - BR^{-1}B^T P_0) + (A^T - BR^{-1}B^T P_0)(P_1)_C + P_0 \Delta A_C + \Delta A_C P_0 = 0 \quad (5.34)$$

$$(P_n)_C (A - BR^{-1}B^T P_0) + (A^T - BR^{-1}B^T P_0)(P_n)_C + \\ +(P_{n-1})_C \Delta A_C + \Delta A_C^T (P_{n-1})_C - \sum_{k-1}^{n-1} P_k B R^{-1} B^T (P_{n-1})_C = 0 \quad (5.35)$$

with $A_1 = A_0 - BR^{-1}B^T P_0$, and

The state-dependent incremental matrix can be extracted from equation (5.24)

$$\Delta A_C = \begin{bmatrix} 0 & 0 & 0 \\ 0 & 0 & -PL \\ 0 & \frac{PL}{K} & 0 \end{bmatrix} \quad (5.36)$$

5.4.3. Design of switching function of ISMC with SDRE control technique

In this subsection, the discontinuous function of the proposed SDRE-based ISMC will be presented. The task is to design the integral-based discontinues controlling part which will drive the sliding variable to zero to guarantee sliding mode in finite time and eliminate reaching phase.

Shall the equation (5.23) be formed as;

$$\dot{x}(t) = A(x)x + B(u - u_c) + L\epsilon(t,x) + d_u(t,x) \quad (5.37)$$

where $\epsilon(t)$ and $d_u(t,x)$ are matched and mismatched disturbances, respectively. $L = BD$ for $D \in R$.

By substituting (5.26) into (5.37), the following is obtained;

$$\dot{x}(t) = A(x)x + Bu_{SDRE}(t) - Bu_C(t) + Bu_1(t) + BD\epsilon(t,x) + d_u(t,x) \quad (5.38)$$

The sliding variable includes an integral term as;

$$\sigma(x) = Gx(t) + w(t) \quad (5.39)$$

where G is the design matrix ($G = (B^T B)^{-1} B^T$), $w(t)$ is an integral term.

During sliding mode, the sliding variable and its derivatives must be zero as:

$$\dot{\sigma}(x) = G\dot{x}(t) + \dot{w}(t) = 0 \quad (5.40)$$

By substituting (5.38) into (5.40) the following is obtained;

$$\dot{\sigma}(t) = G\big(A(x)x + Bu_{SDRE}(t)\big) + GBu_1(t) + \\ +GBD\epsilon(t,x) + Gd_u(t,x) + \dot{w}(t) \quad (5.41)$$

During sliding mode discontinuous part of the control law is;

$$u_1(t) = -D\epsilon(t,x) - (GB)^{-1}Gd_u(t,x) \tag{5.42}$$

The derivative of the integral term of the sliding variable should be selected as;

$$\dot{w}(t) = -G(Ax(t) + Bu_{SDRE}(t)) \tag{5.43}$$

Finally, the integral sliding variable will be as;

$$\sigma(x) = G\big(x(t) - x(0)\big) - G\int_0^t (Ax(t) + Bu_{SDRE}(t))dt \tag{5.44}$$

To reduce chattering presented in ISMC, continuous approximation using Euclidian norms is utilized like in [7];

$$u_1(t) = -k\frac{\sigma(t)}{\|\sigma(t)\|+\delta}\,. \tag{5.45}$$

To justify, the designed ISMC controller in (5.42) satisfies the η-reachability condition that ensures the existence of an ideal sliding motion [98].

Let's take Lyapunov's candidate function as;

$$V(t) = \frac{1}{2}\sigma^2(t) \tag{5.46}$$

Then

$$\dot{V}(t) = \sigma^T(t)\dot{\sigma}(t) \tag{5.47}$$

And

$$\dot{\sigma}(t) = G(Ax(t) + Bu(t) + BD\xi(t,x) + f_u(t,x)) - GAx(t) + GBFx(t) \tag{5.48}$$

After reforming and substituting (5.45) into (5.48) is obtained;

$$\dot{\sigma}(t) = GAx(t) + GB\big(-Fx(t) + u_c(t)\big) + GBD\xi(\cdot) + Gd(\cdot) - GAx(t) +$$

$$+GBFx(t) = -\rho(t,x)\frac{\sigma(t)}{\|\sigma(t)\|} + GBD\xi(t,x) + Gf_u(t,x) \tag{5.49}$$

where F is gain matrix which is responsible for the performance of the system after reaching the sliding phase and $\rho(t,x)$ is the gain of discontinuous function to enforce the sliding mode. Then;

$$\sigma^T(t)\dot{\sigma}(t) = -\rho(t,x)\big||\sigma(t)||\big| + \sigma^T(t)D\xi(t,x) + \sigma^T(t)Gf_u(t,x)$$

$$\leq ||\sigma(t)||(-\rho(t,x) + ||D\xi(t,x)|| + ||Gfu(t,x)||) \tag{5.50}$$

where the fact that $GB = I_m$, has been used. To enforce a sliding mode the value of the modulation gain ρ(t,x) should be greater than any disturbance or uncertainty in the system, and therefore for any choice of ρ(t,x) which satisfies

$$\rho(t,x) \geq \big||D|\big|||\xi(t,x)|| + ||G||||f_u(t,x)|| + \eta \tag{5.51}$$

where η is some positive scalar,

$$\sigma^T(t)\dot{\sigma}(t) \leq -\eta||\sigma(t)|| \tag{5.52}$$

the η-reachability condition is satisfied.

Remark 5.1. Inequality (5.49) can also be interpreted from a Lyapunov perspective. Define $V(t) = \frac{1}{2}\sigma^2(t)$, then $\dot{V}(t) = \sigma^T(t)\dot{\sigma}(t)$ and from the inequalities in (5.50)-(5.52), it follows;

$$\dot{\mathrm{V}}(\mathrm{t}) \leq -\eta\|\sigma(\mathrm{t})\| = -\eta\sqrt{2\mathrm{V}(\mathrm{t})} \tag{5.53}$$

Integrating both sides of (5.75) yields;

$$\sqrt{2\mathrm{V}(\mathrm{t})} - \sqrt{2\mathrm{V}(0)} \leq -\eta\mathrm{t} \tag{5.54}$$

which implies $V(t) \equiv 0$ in less than $\frac{\eta}{\sqrt{2V(0)}}$ units of time.

The designed the SDRE-based nominal part and switching part of the control law of the proposed ISMC provides the nominal performance of the WECS. However, the proposed ISMC control can be complemented with HODOs for compensation the disturbances due to model uncertainty, noise and unmodelled dynamics in the system which has been discussed in Chapter 4. Moreover, the use of HODO for estimation wind speed instead of using anemometer can enhance the reliability of the whole WECS. The performance of this control system will be demonstrated in the simulation results section and compared with linear such as LQR method as well as the nonlinear methods such quasi-SMC and LQR based ISMC.

5.5.Servomechanism-based SDRE control design

5.5.1.Servomechanism-based SDRE control law

In this section, the proposed servomechanism-based SDRE control law is presented. So far, the disturbances in the control systems have been compensated in feedforward scheme via use HODOs per control channel. However, the suppression of the disturbances in feedback control with so called servomechanism technique has gained attentions among researchers. The principal servomechanism-based SDRE control diagram is depicted in Figure 5.6.

Let's consider the autonomous, infinite-horizon, nonlinear regulator problem for minimizing the performance index in equation (5.27).

Concerning the states x and control u subject to the nonlinear differential constraints

$$\dot{\mathrm{x}} = \mathrm{f}(\mathrm{x}) + \mathrm{B}(\mathrm{x})\mathrm{u} \tag{5.55}$$

where $\mathrm{Q}(\mathrm{x}) \geq 0$ and $\mathrm{R}(\mathrm{x}) > 0$ for all x and $\mathrm{f}(\mathrm{x}) = 0$

The SDRE approach for obtaining a suboptimal, locally asymptotically stabilizing solution to a problem (5.55) is direct parametrisation to bring nonlinear dynamics to the state-dependent coefficients (SDC) form

$$\dot{x} = A(x)x + B(x)u \tag{5.56}$$

where $A(x)x = f(x)$.

In the multi-variable form it is well known that if $f(x)$ is a continuously differentiable function of x, there is an infinite number of ways to factor $f(x)$ into $A(x)x$. To find a valid solution of the SDRE, the pair $\{A(x), B(x)\}$ has to be point-wise stabilizable in the linear sense for all x in the domain of interest.

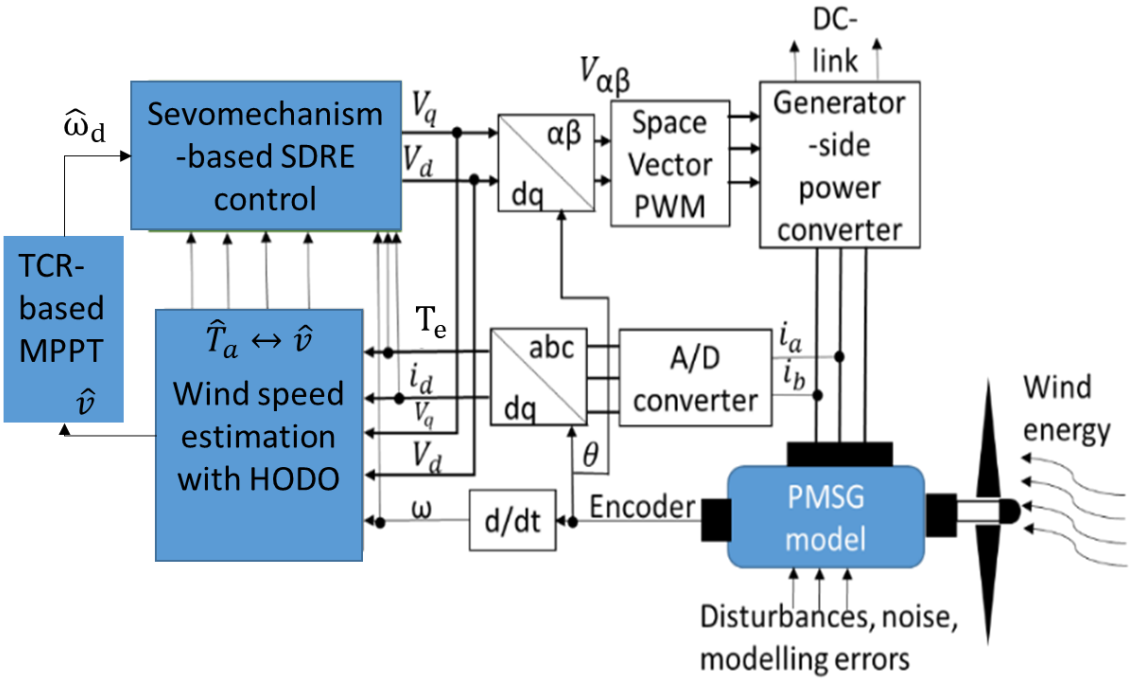

Figure 5.6. The proposed servomechanism-based SDRE control

- Solving state-dependent Riccati equation

$$A^T(x)P(x) + P(x)A(x) - P(x)BR^{-1}(x)B^TP(x) + Q = 0 \tag{5.57}$$

To obtain $P(x) \geq 0$.

- Constructing SDRE-based nonlinear output feedback control law

$$u = -R^{-1}B^TP(x)x \tag{5.58}$$

where states vector of the angular shaft speed error, electromagnetic torque error, and d-axis stator current, $x^T = [\tilde{\omega} \quad \tilde{T}_e \quad i_{ds}]$.

To perform the following command, the SDRE controller can be implemented through the servomechanism technique [9] by augmenting the system with an additional state, integral to angular shaft speed error

$$\dot{\bar{x}} = \bar{A}(\bar{x})\bar{x} + \bar{B}u \tag{5.59}$$

Where augmented state and control matrices will be;

$$\bar{A}(\bar{x}) = \begin{bmatrix} 0 & I \\ A(x) & 0 \end{bmatrix}, \bar{B} = \begin{bmatrix} 0 \\ B \end{bmatrix} \tag{5.60}$$

where augmented states vector become $\bar{x}^T = [\int \tilde{\omega} dt \quad \tilde{\omega} \quad \tilde{T}_e \quad i_{ds}]$ by adding the integral of the angular shaft speed error.

Introducing the error dynamics given by equations in (5.15)

The proposed the control inputs V_q and V_d consists only of feedback terms as compensation terms have been eliminated;

$$V_q = u_{fbq}, \; V_d = u_{fbd} \tag{5.61}$$

where u_{fbq} - q-axis nonlinear output feedback control part; u_{fbd} - d-axis nonlinear output feedback control part, respectively.

Let's recall the three-dimensional error dynamics with formed state-space (5.22) and (5.23) of the PMSG with nonlinear terms [15], [16],[54]

By augmenting the additional state of integral of the angular shaft speed error with the state and control vectors the state-space matrices become as follows;

$$\bar{A}(\bar{x}) = \begin{bmatrix} 0 & 1 & 0 & 0 \\ 0 & -\frac{B_{vf}}{J_{ri}} & -\frac{1}{J_{ri}} & 0 \\ 0 & -\frac{\lambda_m PK}{L} & -\frac{R_s}{L} & -PL\tilde{\omega} \\ 0 & 0 & \frac{PL}{K}\tilde{\omega} & -\frac{R_s}{L} \end{bmatrix}, \bar{B} = \begin{bmatrix} 0 & 0 \\ 0 & 0 \\ \frac{K}{L} & 0 \\ 0 & \frac{1}{L} \end{bmatrix} \tag{5.62}$$

The matrix $\bar{A}(\bar{x})$ in the equation (5.62) can be expressed as follows;

$$\bar{A}(\tilde{x}) = \bar{A}_0 + \Delta\bar{A}(\bar{x}). \tag{5.63}$$

where the state matrix $\tilde{A}(\tilde{x})$ which can be cast as a constant matrix A_0 and coefficients of the state-dependent incremental matrix is the function of $\tilde{\omega}$, $\Delta\bar{A}(\tilde{\omega})$.

$$\bar{A}_0 = \begin{bmatrix} 0 & 1 & 0 & 0 \\ 0 & -\frac{B_{vf}}{J_{ri}} & -\frac{1}{J_{ri}} & 0 \\ 0 & -\frac{\lambda_m PK}{L} & -\frac{R_s}{L} & 0 \\ 0 & 0 & 0 & -\frac{R_s}{L} \end{bmatrix}, \Delta\bar{A}(\bar{x}) = \begin{bmatrix} 0 & 0 & 0 & 0 \\ 0 & 0 & 0 & 0 \\ 0 & 0 & 0 & -\tilde{\omega}PL \\ 0 & 0 & \tilde{\omega}\frac{PL}{K} & 0 \end{bmatrix} \tag{5.64}$$

To have a solution for the SDRE, the point-wise detectability condition should be satisfied. This is accomplished by penalizing $\int \tilde{\omega} dt$, an integral state with the

corresponding non-zero diagonal elements $\bar{Q}(\bar{x})$. Finally, the integral servomechanism-based SDRE nonlinear output feedback control law will be in the form as:

$$u = -K(\bar{x})\bar{x} = -K(\bar{x})\tilde{\omega} = R^{-1}\bar{B}^{T}P(\bar{x})\tilde{\omega}, \quad K: \mathcal{R}^{n} \to \mathcal{R}^{p\times n} \tag{5.65}$$

where $P: \mathcal{R}^{n} \to \mathcal{R}^{n\times n}$ satisfies ARE and for the nonlinear system and $P(\bar{x})$ is a unique symmetric and positive definite solution of the following SDRE control problem:

$$P(\bar{x})A(\tilde{x}) + \bar{A}(\bar{x})^{T}P(\bar{x}) - P(\bar{x})\bar{B}R^{-1}\bar{B}^{T}P(\bar{x}) + Q = 0 \tag{5.66}$$

As a result, the state-dependent optimal gain matrix $\bar{K}$ can also be expressed as the sum of constant and state-dependent matrices:

$$u(t) = -(K_0 + \Delta K(\bar{x}))\tilde{\omega} \tag{5.67}$$

where

$$K_0 = R^{-1}\bar{B}^{T}P_0 \qquad \Delta K(\bar{x}) = R^{-1}\bar{B}^{T}\Delta P(\bar{x}) \tag{5.68}$$

Allowing the nonlinearities in the system, the solution of the SDRE terms can be approximated in the nonlinear output feedback control system design. Its flexibility is defined by finding the state-dependent weighting matrix. The Taylor series expansion can be used to obtain the approximated solution of its nonlinear dynamics.

5.5.2.Solving of servomechanism-based SDRE control by Taylor series expansion

The SDRE control problem can be approximated by Taylor series expansion and solved numerically. However, the numerical solution by applying the Taylor series expansion method can give approximated solution as in the works [5], [13].

$$\Delta\bar{A}(\bar{x}) = \begin{bmatrix} 0 & 0 & 0 & 0 \\ 0 & 0 & 0 & 0 \\ 0 & 0 & 0 & -\tilde{\omega}PL \\ 0 & 0 & \tilde{\omega}\frac{PL}{K} & 0 \end{bmatrix} = \tilde{\omega}\begin{bmatrix} 0 & 0 & 0 & 0 \\ 0 & 0 & 0 & 0 \\ 0 & 0 & 0 & -PL \\ 0 & 0 & \frac{PL}{K} & 0 \end{bmatrix} = \tilde{\omega}\Delta\bar{A}_C \tag{5.69}$$

The equation (5.70) is ARE corresponding to ($\bar{A}_0$, $\bar{B}$) and equations (5.71) and (5.72) are algebraic Lyapunov's equations are formulated. It should be noted that the local solution of the SDRE converges due to $A(\tilde{x})$ is a continuous matrix and B is the constant matrix.

$$P_0\bar{A}_0 + \bar{A}_0^{T}P_0 - P_0\bar{B}R^{-1}\bar{B}^{T}P_0 + Q = 0 \tag{5.70}$$

$$P_1(\bar{A}_0 - \bar{B}R^{-1}\bar{B}^{T}P_0) + (\bar{A}_0^{T} - \bar{B}R^{-1}\bar{B}^{T}P_0)P_1 + P_0\Delta\bar{A}_C + \Delta\bar{A}_C P_0 = 0 \tag{5.71}$$

$$P_1(\bar{A}_0 - \bar{B}R^{-1}\bar{B}^{T}P_0) + (\bar{A}_0^{T} - \bar{B}R^{-1}\bar{B}^{T}P_0)P_n + P_n\Delta\bar{A}_C + \Delta A_C^{T}P_{n-1} - \sum_{k=1}^{n-1} P_k\bar{B}R^{-1}\bar{B}^{T}P_{n-k} = 0 \tag{5.72}$$

Finally, the near-optimal integral servomechanism-based nonlinear output feedback control law is

$$\mathrm{u^N(x) = -(R^{-1}\bar{B}^T\left(\sum_{n=0}^{N}(\tilde{\omega})^n P_n\right)\tilde{x} = -\left(\sum_{n=0}^{N}(\tilde{\omega})^n K_n\right)\tilde{x}},\qquad (5.73)$$

where N is the number of the SDRE terms computed offline, and $\mathrm{P_n}$ are constant matrices, obtained by solving the following ARE (5.70) and ALE (5.71) and (5.72). The detailed algorithm of solving SDRE control problem is given in Figure 5.7.

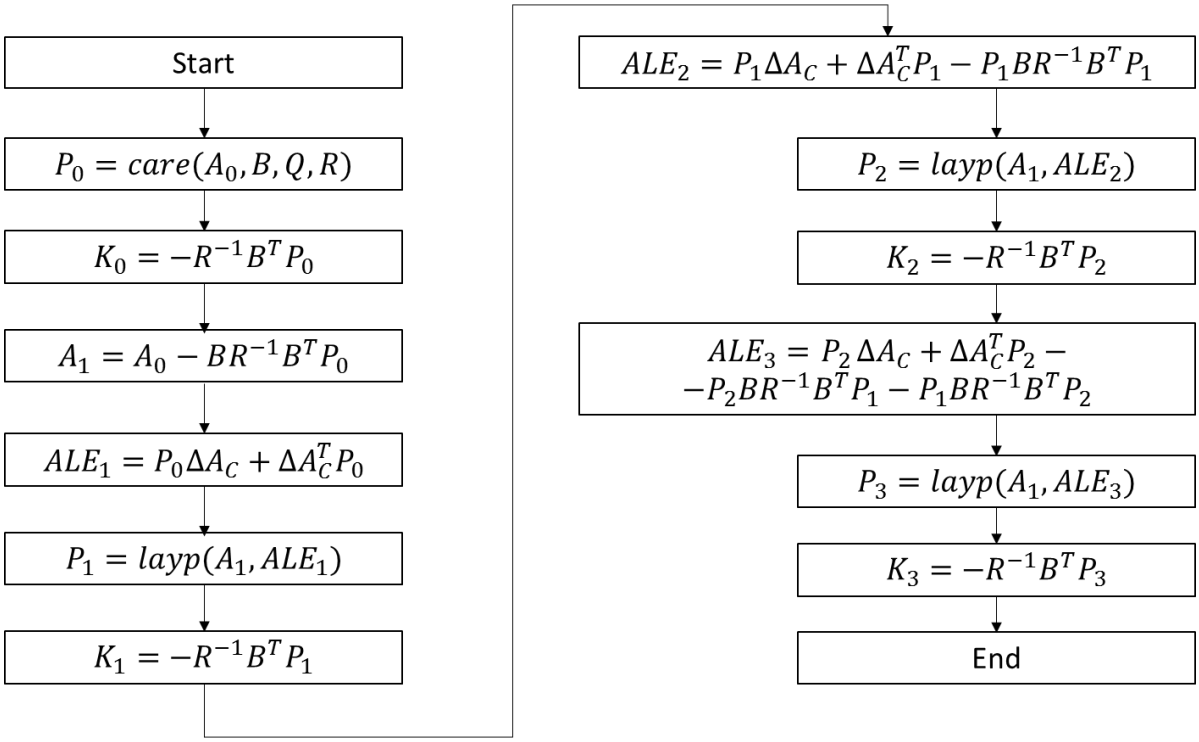

Figure 5.7. Calculation algorithm of SDRE terms with N=3

The solutions of ARE and ALEs can be computed offline using Matlab's functions ***care*** and ***layp.*** In the algorithm, the computing the number of computing SDRE terms is three, N=3.

The performance of the servomechanism-based SDRE control does not have compensation terms nor HODOs for model uncertainty with noise compensation. Similar to the SDRE-based ISMC method, the HODO is used to estimate the wind speed to define the reference for the angular shaft speed in the variable–speed WECS. The performance of the servomechanism-based SDRE control system will be presented and compared with the conventional SDRE method in the corresponding simulation results section.

5.6. Summary of Chapter 5

The DOBC with linear and nonlinear controller are proposed to improve the performances of control systems in the PM synchronous machine applications. Firstly, the switching output feedback control law based SMC is designed for the PMSM system. Secondly, the discrete-time PI-PI control system equipped with a back-calculation anti-windup scheme has been designed for the PMSM speed regulation. The HODO is synthesized with designed feedback controllers to compensate the esternal disturbances, such as load torque, friction, unmodelled dynamics etc. Thirdly, the HODOs-based ISMC is proposed to handle disturbances to extract more power in the WECS whereas SDRE technique is adopted to cope with nonlinear dynamics of the system. Finally, the servomechanism-based SDRE control technique is proposed to reduce the impact of the disturbances in maximizing power extraction of the WECS with only feedback control. In the following sismulation and experimental results chapter, the performances of the presented control systems will be demonstrated and analysed under certain operational conditions.

Chapter 6: Simulations and experimental results of the PMSM speed regulations with DOBC

6.1.Introduction

In this chapter, simulations and experimental results of the proposed control systems for PMSM speed control application will be presented under speed variations, load torque disturbances, and parameter variations scenarios. Firstly, HODO-based SMC with switching output feedback control law performance will be produced and compared with conventional PI –PI control speed tracking performance. Secondly, HODO-based discrete-time PI speed controller's performances are evaluated experimentally under speed variations and load torque disturbances. The mean absolute percentage errors of the angular shaft speed, percentage of overshoot, settling time, maximum estimation error of load torque, percentage of steady-state error are considered as evaluation criteria of the performance.

6.2.Simulation results of switching output feedback control law-based SMC with HODO

To confirm the effectiveness of the proposed switching output feedback control law (SOFCL) based SMC synthesized with HODO. The proposed control system performance is compared with LQR and PI-PI control methods. Let us consider a surface-type PMSM with the nominal parameters given in Table 6.1.

Table 6.1. The PMSM technical parameters

Motor parameters	**Symbol**	**Value**
Rated power	P_n (hp)	1
Rated phase current	I_{rated} (A)	3.94
Rated torque	T_{rated} $(N \cdot m)$	3.9
Permanent magnetic flux coefficient	λ_m (V·s/rad)	7.92×10^{-2}
Winding resistance Ph-Ph	R_s (Ohm)	0.99
Winding inductance Ph-Ph	L (mH)	5.82
Rotor's moment of inertia	J_{ri} (kg·m^2)	12.08×10^{-4}
Number of poles	P	6
Viscous damping coefficient	b (N·m/(rad/s))	3×10^{-4}

The speed reference $251.2\ \mathrm{rad}/s.$ is equivalent to 400 RPM. Then, the coefficients of the system model (3.26) are given as

$$k_1 = 3539.6;\ k_2 = 0.2484;\ k_3 = 4968.8;$$

$$k_4 = 170.1;\ k_5 = 13.6;\ k_6 = 171.82;$$

Choosing tuning gains according to Remark 5.1 and equations (5.7) and (5.8) the gain matrices are chosen as;

$$Q = \begin{bmatrix} 1000000 & 0 & 0 \\ 0 & 1 & 0 \\ 0 & 0 & 1 \end{bmatrix}, R = \begin{bmatrix} 0.5 & 0 \\ 0 & 0.5 \end{bmatrix}$$

By applying ***care*** function in MATLAB with arguments A, B, Q, and R, the solution of the Riccati equation, P –positive-definite solution matrix can be obtained.

A space vector pulse width modulation (SVPWM) technique is used to regulate the phases of currents flowing out of the SPMSM.

HODO gains to estimate load torque disturbance are chosen according to Theorem 4.1, $L_1 = 50, L_2 = 25, \text{and } L_3 = 12.5.$

To demonstrate the superiority of this method, the simulation results are compared against the conventional cascaded PI-PI control and LQR methods.

Case 1: Speed Transient Response with nominal parameters

1) The desired speed (ω_d): $251.2\ \mathrm{rad/s} \rightarrow -251.2\ \mathrm{rad/s} \rightarrow 251.2\ \mathrm{rad/s}.$

2) Nominal motor parameters as in Table 6.1.

3) Constant load torque disturbance $T_L = 1\ \mathrm{N \cdot m}$ is applied

4) No load torque variation.

Case 2: Speed Transient Response with 150% parameter variations

1) The desired speed (ω_d)*:* $251.2\frac{\mathrm{rad}}{\mathrm{s}} \rightarrow -251.2\ \mathrm{rad/s} \rightarrow 251.2\ \mathrm{rad/s}.$

2) 150% motor parameters (R_s, L, J_{ri}) variations i.e., $R_s = 1.485\ \Omega,\ L = 8.73\ \mathrm{mH},$ and $J_{ri} = 18.1 \times 10^{-4}\ \mathrm{kg \cdot m^2}, \lambda_m = 11.87 \times 10^{-2} \mathrm{V \cdot s/rad}$:3)

3) Constant load torque disturbance $T_L = 1.5\ \mathrm{N \cdot m}$ is applied

4) No load torque variation.

Case 3: Load Torque Transient Response with parameter variations.

1) The desired speed is kept at constant $\omega_d = 251.2\ \mathrm{rad/s}.$

2) 150% motor parameters (R_s, L, J_{ri}) variations i.e., $R_s = 1.485\ \Omega, L_s = 8.73\ \mathrm{mH},$ and $J_{ri} = 18.1 \times 10^{-4}\ \mathrm{kg \cdot m^2}, \lambda_m = 11.87 \times 10^{-2} \mathrm{V \cdot s/rad}.$

3) Load torque variation, T_L : $1\ \mathrm{N \cdot m} \rightarrow 2\ \mathrm{N \cdot m} \rightarrow 1\ \mathrm{N \cdot m}.$

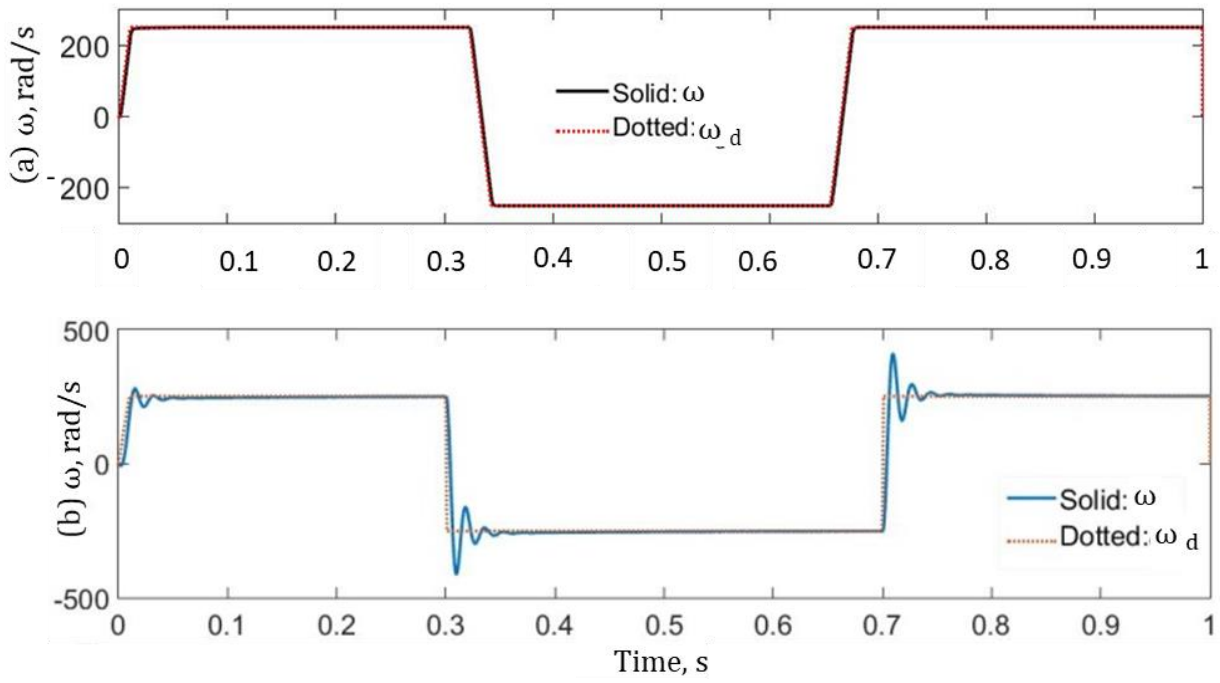

Figure 6.1. The angular shaft speed response under case 1: (a) The proposed SOFCL-based SMC method with HODO; (b) PI-PI method without HODO

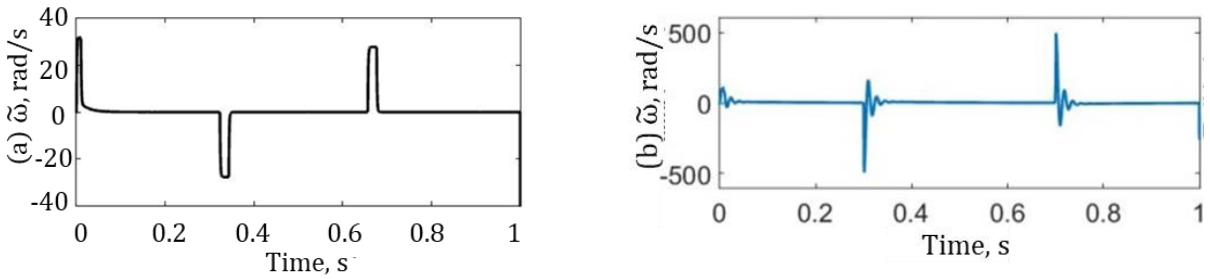

Figure 6.2. The angular shaft speed errors under case 1: (a) The proposed SOFCL-based SMC method with HODO; (b) PI-PI method without HODO

In cases 1 and 2, the speed response of the PMSM model is examined when desired speed (ω_d) varies but load torque (T_L) is constant under nominal parameters and some parameters variations of $R_s, L, J_{ri}, \lambda_m$ respectively. However, in the case 3, the speed response under the load torque disturbances is examined with 150% of $R_s, L, J_{ri}, \lambda_m$ variations. While the HODO observer has been integrated into the speed controller to compensate the load torque disturbance, the SMC is suppress the model uncertainty with the feedback control. The angular shaft speed responses, their errors, direct and quadrature currents, the load torque estimations under the proposed SOFCL-based SMC

with HODO compensation and conventional PI-PI control without HODO in the cases 1, 2, and 3 are shown below.

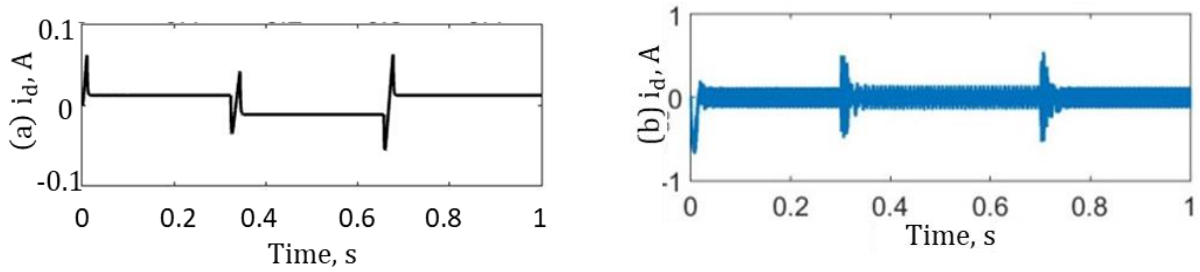

Figure 6.3. The direct current response in the case 1: (a) The proposed SOFCL-based SMC method with HODO; (b) PI-PI method without HODO

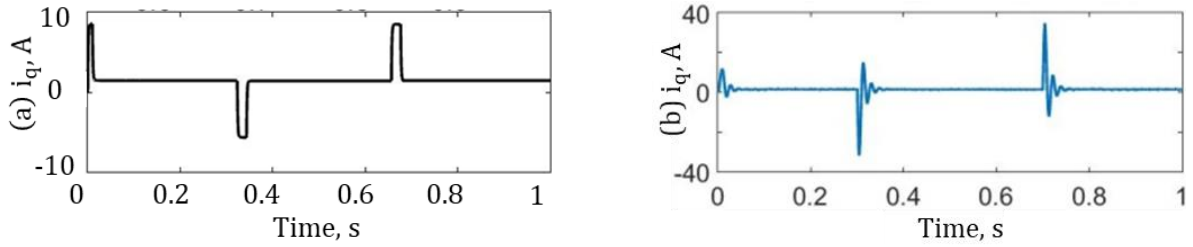

Figure 6.4. The quadrature current response in the case 1: (a) The proposed SOFCL-based SMC method with HODO; (b) PI-PI method without HODO

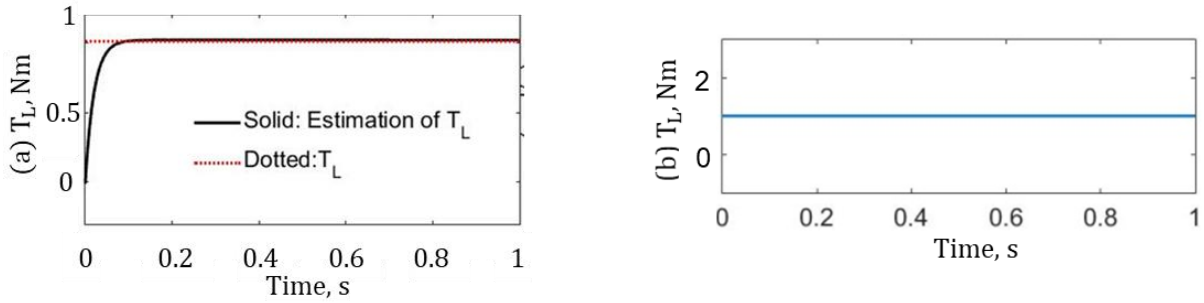

Figure 6.5. The applied load torque and its estimation in the case 1: (a) The proposed SOFCL-based SMC method with HODO; (b) PI-PI method without HODO

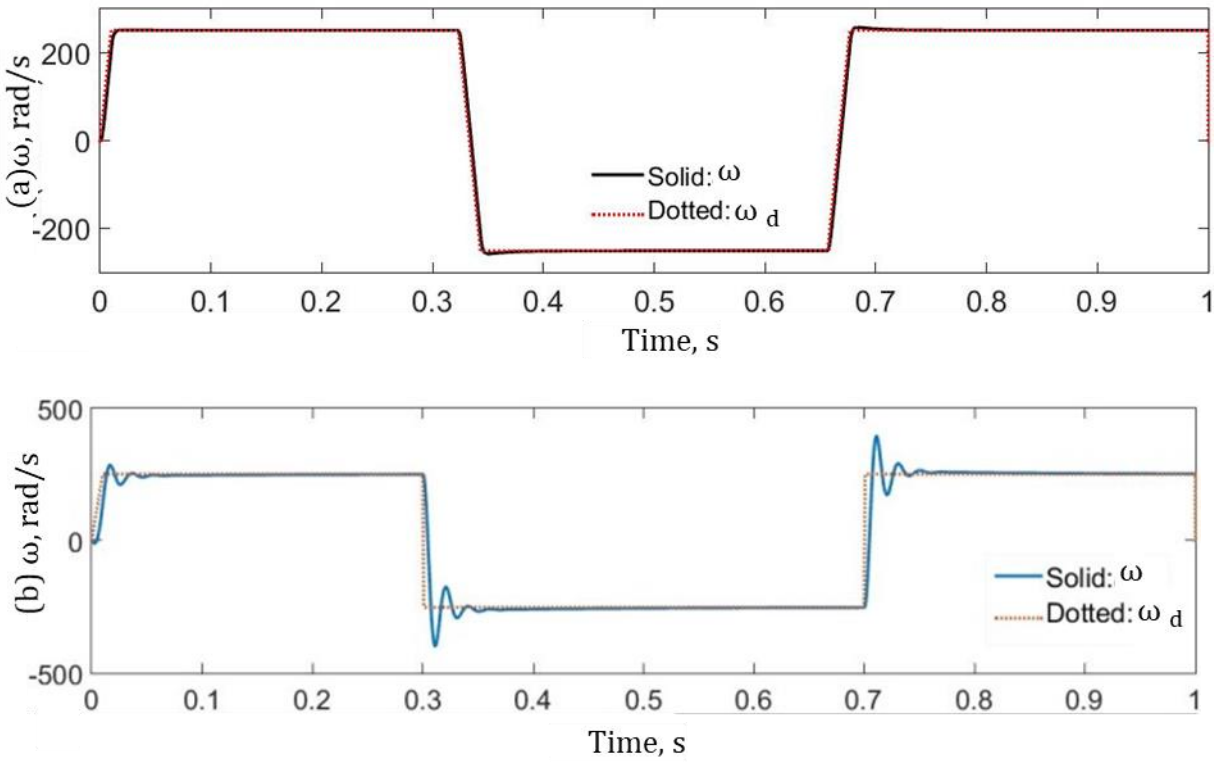

Figure 6.6. The angular shaft speed response in the case 2: (a) The proposed SOFCL-based SMC method with HODO; (b) PI-PI method without HODO

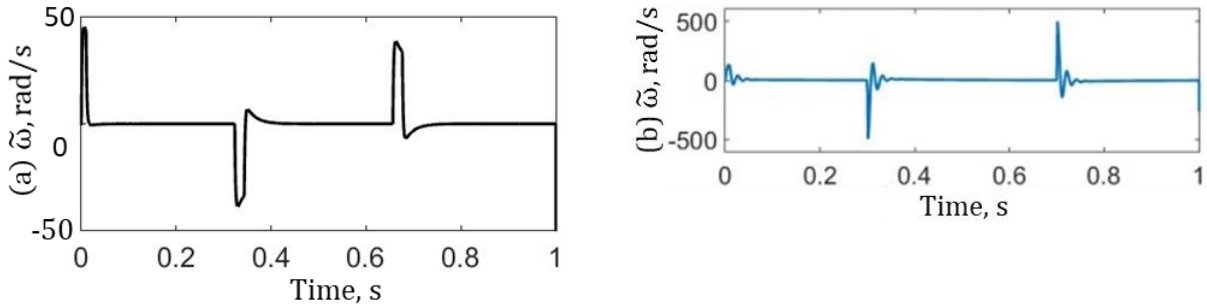

Figure 6.7. The angular shaft speed errors in the case 2: (a) The proposed SOFCL-based SMC method with HODO; (b) PI-PI method without HODO

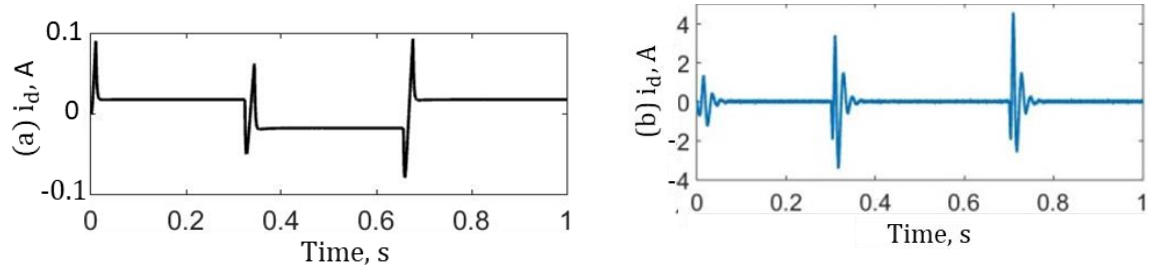

Figure 6.8. The direct current response in the case 2: (a) The proposed SOFCL-based SMC method with HODO; (b) PI-PI method without HODO

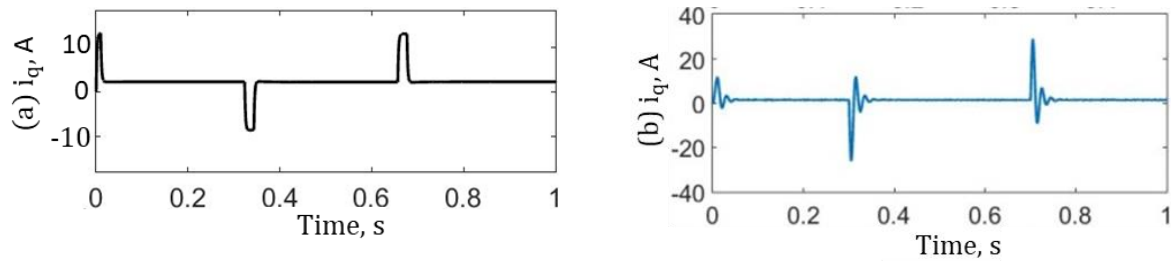

Figure 6.9. The quadrature current response in the case 2: (a) The proposed SOFCL-based SMC method with HODO; (b) PI-PI method without HODO

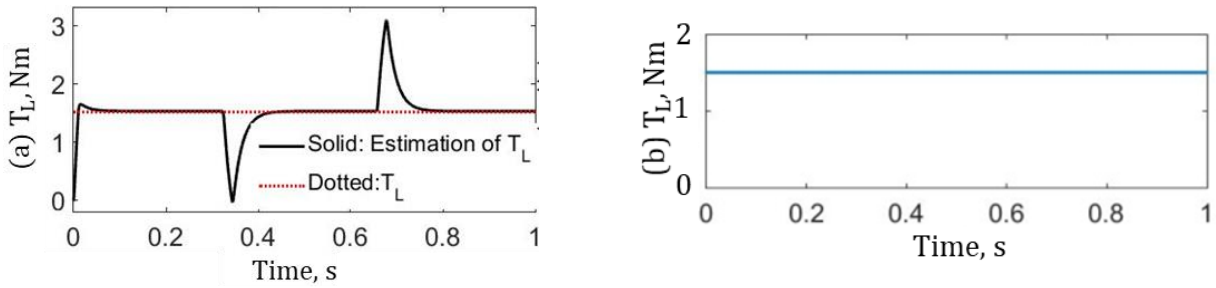

Figure 6.10. The applied load torque and its estimation in the case 2: (a) The proposed SOFCL-based SMC method with HODO; (b) PI-PI method without HODO

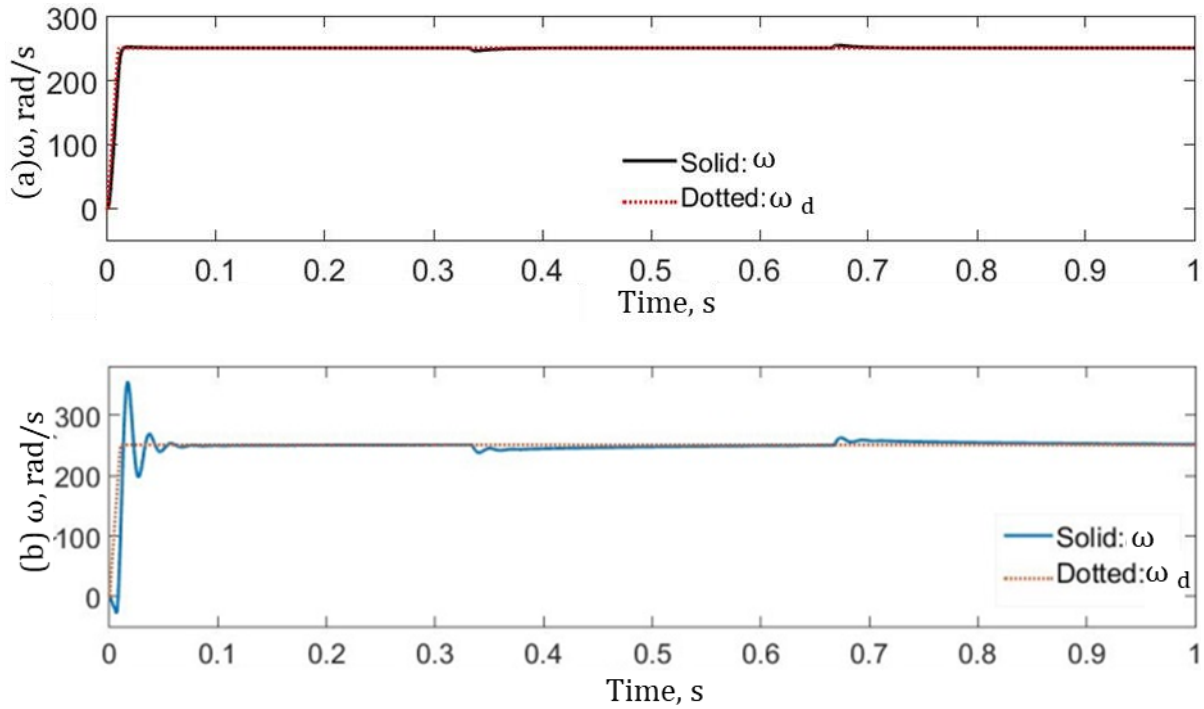

Figure 6.11. The angular shaft speed response in the case 3: (a) The proposed SOFCL-based SMC method with HODO; (b) PI-PI method without HODO

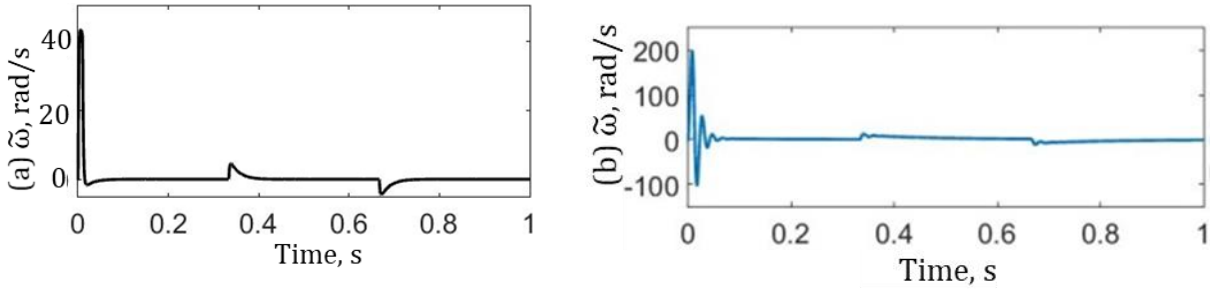

Figure 6.12. The angular shaft speed errors in the case 3: (a) The proposed SOFCL-based SMC method with HODO; (b) PI-PI method without HODO

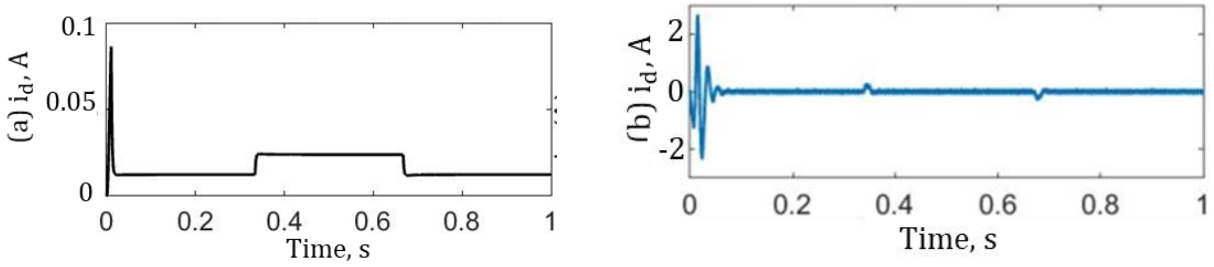

Figure 6.13. The direct current response in the case 3: (a) The proposed SOFCL-based SMC method with HODO; (b) PI-PI method without HODO

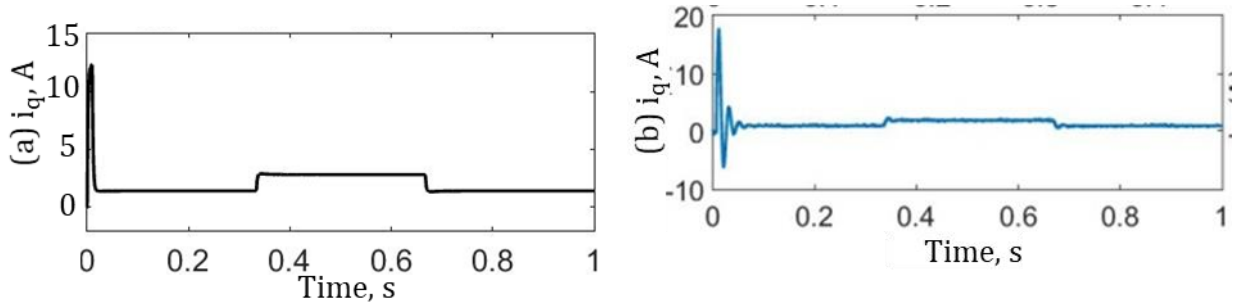

Figure 6.14. The quadrature current response in the case 3: (a) The proposed SOFCL-based SMC method with HODO; (b) PI-PI method without HODO

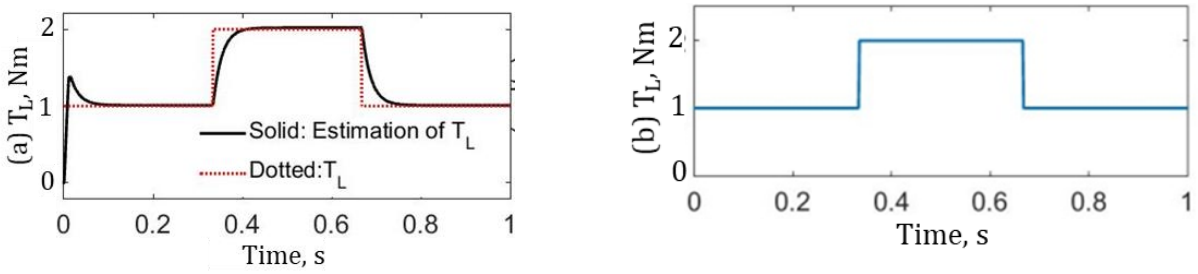

Figure 6.15. The applied load torque and its estimation in the case 3: (a) The proposed SOFCL-based SMC method with HODO; (b) PI-PI method without HODO

The simulation results of the proposed SOFCL-based SMC with HODO has demonstrated its superiority under speed, parameter variations, and load torque disturbance described in the cases 1, 2, and 3. Particularly, the maximum angular shaft speed errors, $\tilde{\omega}$ exist during the transient times reaching to 12.74%, 18.15%, and 17.24 % in case 1 (Figure 6.2, (a)), case 2 (Figure 6.7, (a)), and case 3 (Figure 6.12, (a)) cases, respectively. However, in the conventional PI-PI control method, the maximum angular shaft speed errors are 43.1% (Figure 6.2, (b)), 52.1% (Figure 6.7, (b)), and 79.5% (Figure 6.12, (b)) in three cases respectively, which are larger for 3.38, 2.87, and 4.61 times than in the proposed method.

In terms of overshoot, the PI-PI control method has shown the poor performance, for example it has 11.55% (Figure 6.1, (b)), 13.5% (Figure 6.6, (b)), and 41.4% (Figure 6.11, (b)) in three cases respectively. In the contrast, the proposed SOFCL-based SMC with HODO control system does not have overshoots. The detailed comparative performance of the two methods is summarized in Table 6.2.

The settling times for the proposed control method are 0.01 sec, 0.016 sec, and 0.019 sec in the cases 1, 2 and 3, which are faster in the cases 1 and 2 by 1.4 and 1.17 times than in the conventional PI-PI method. However, the settling time with 0.09 sec does not have a difference in the case 3 in both methods.

In the proposed control, the angular shaft speed steady-state errors are not considerable and almost around zero with nominal parameters. For example, its MAPEs are equal to 0.073% and 0.026% in cases 1 and 3. However, it reaches 0.31% in the case 2 which is still 9.9 times less than in the PI-PI control method.

It should be noted that the load torque observer does not work 100% accurately in all cases due to estimation errors in transient and steady-state periods. In case 1, the average estimated load torque error is 0.066 Nm which is higher for 6.6% from reference (Figure 6.5, (a)). Similarly, the case where some parameter variations are introduced, the estimation of load torque error reaches 1.87% (Figure 6.10, (a)). In addition, it can be seen that the motor speed (ω) is very stable during the transient time when the load torque suddenly changes from 1 to 2 Nm and vice versa (Figure 6.11).

The gains of both PI controllers are determined by the tuning rule, and the bandwidths are designed as $\omega_{\mathrm{speed}} = 2\pi \cdot 16\ \mathrm{rad/s}$ and $\omega_{\mathrm{current}} = 2\pi \cdot 160\ \mathrm{rad/s}$, respectively [5], [99].

Table 6.2. Performance of the proposed SOFCL-based SMC with HODO

Evaluation criteria and cases		**Control schemes**		**Improved by**
		SOFCL+HODO	**(PI) Courtesy of [5]**	
Absolute mean speed error within transient, %	Case 1: with nominal parameters	12.74	43.1	70.44%
	Case 2: with 150% parameter variations	18.15	52.1	65.16%
	Case 3: under load torque disturbance	17.24	79.5	78.31%
Overshoot,%-	Case 1: with nominal parameters	-	11.5	100%
	Case 2: with 150% parameter variations	0.23	13.5	98.3%
	Case 3: 150% parameter variations and load torque disturbance	0.66	41.4	98.4%
Settling time, sec	Case 1: with nominal parameters	0.025	0.07	64.29%
	Case 2: with 150% parameter variations	0.05	0.07	28.57%
	Case 3: 150% parameter variations and load torque disturbance	0.05	0.09	44.44%
Maximum estimation error of load torque within transient, Nm	Case 1: with nominal parameters	0.934	-	n/a
	Case 2: with 150% parameter variations	1.472	-	n/a
	Case 3: 150% parameter variations	0.9	-	n/a

Evaluation criteria and cases		Control schemes		Improved by
		SOFCL+HODO	(PI) Courtesy of [5]	
	and load torque disturbance			
Steady-state error, %	Case 1: with nominal parameters	0.073	2.33	96.87%
	Case 2: with 150% parameter variations	0.31	3.07	89.9%
	Case 3: 150% parameter variations and load torque disturbance	0.026	1.63	98.4%

6.3.Experimental results of HODO-based discrete-time PI-PI control system for PMSM speed regulation

The PMSM drive prototyping kit configuration manufactured by Lucas-Nuelle GmbH is shown in Figure 6.16. It is used to test the proposed HODO-based PI-PI control system with a back-calculation anti-windup scheme. The experimental setup comprises a surface-mounted PMSM (SPMSM) that is coupled with 1024 pulses incremental position encoder and self-cooled asynchronous servo-brake with a resolver operated with a servo-machine test bench acting as a load. The control algorithm is written in MATLAB/Simulink (R2016b) environment then the code generated by Code Composed Studio 5 is sent to the servo-converter for real-time experiment control. Note, after loading the code, no modification of gains is allowed. For a new configuration and modification of gains, the code generation has to be performed again. The switching frequency of the self-commutated converter is set to 8 kHz which allows to reduce the sizes of the semiconductor components and fit to the space requirements. The parameters of the surface-mounted PMSM are listed in Table 6.3.

The performance of the proposed HODO-based discrete-time PI-PI control system are compared with of the PI-PI control system without disturbance observer. Moreover, the performances of HODO and first-order disturbance observer (FODO) based PI-PI control systems with back-calculation anti-windup scheme are also evaluated. Two cases

with speed variations and load torque disturbance have been investigated. The control systems' parameters are given in Table 6.4.

Table 6.3. The PMSM technical parameters

Motor parameters	Symbol	Value
Rated power	P_n (W)	300
Torque constant	K_{tRMS}	0.41
Voltage constant	K_{eRMS}	26.1
Permanent magnetic flux coefficient	λ_m	0.089
Winding resistance	R_s (Ohm)	4.74
Winding inductance	L (mH)	8.6
Rotor's moment of inertia	J (kg·cm^2)	0.33
Number of poles	z_p	8
A static moment of friction	C_f (Nm)	0.014
Hysteresis losses coefficient	C_{hys}	0.08
Viscous damping coefficient	b	0.002
Eddy currents coefficient	c_{ed}	0.0015
Eddy currents damping coefficient	d_{ed}	0.003

Table 6.4. The control system's parameters

Controllers and Observers	Parameters and Gains
Discrete-time PI speed controller gains	$K_p = 0.057$, $T_i = 0.04$
Upper and lower output saturations for speed controller	4, -4
Discrete-time PI current controllers gains	$K_p = 17.1$, $T_i = 0.0018$
Upper and lower output saturations for speed controller	200, -200
$\hat{d}$ observer gains	L_{11}=500, L_{12}=250, L_{13}=100

The discrete-time PI speed controller's upper saturation limit should be set to 4 or more and lower saturation limit should be set to -4 or lower due which give adequate the reference quadrature current to respond to the speed commands. The PI current

controler'supper saturation limit should be set as 200 or less and the lower saturation limit should be set to -200 or higher due to overcurrent issue in power electronics.

Case 1: Speed Transient Response with nominal parameters

1) The desired speed (ω_d): $0\ \text{RPM} \rightarrow 1000\ \text{RPM}$.

2) Constant load torque $T_L = 0.5\ \text{Nm}$.

3) No load torque disturbance.

Case 2: Load Torque Transient Response

1) The desired speed $\omega_d = 1000\ \text{RPM}$.

2) Load torque disturbance $T_L = 0\ \text{Nm} \rightarrow 0.5\ \text{Nm}$.

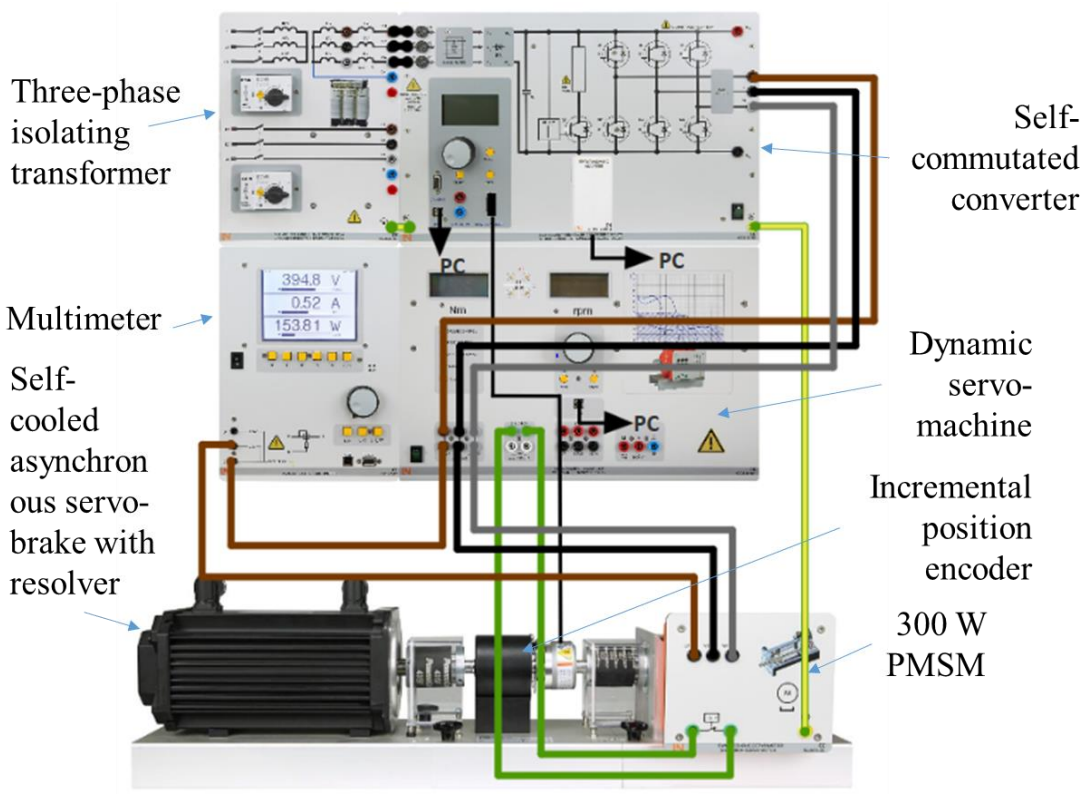

Figure 6.16. DSP-based experimental setup for PMSM control (manufactured by Lucas-Nuelle GmbH)

The smooth trapezoidal-shaped reference speed is used for the PMSM as in [28]. However, the load torque disturbance has been applied step-wise.

The experimental results of the proposed HODO-based discrete-time PI speed controller under two operational cases are given below. Its performance is assessed against the PI speed controller without DO and FODO-based PI speed controller. The reference tracking direct and quadrature currents (i_q, i_d,) are shown in Figures 6.19-

6.20, 6.23-6.24. The mechanical speed of the PMSM (ω) and the estimated total disturbances ($\hat{d}$) are shown and compared with load torque reference values in Figure 6.17-6.18, 6.21-6.22. The detailed evaluation of the performance of the proposed HODO-based discrete time PI speed controller is summarised in Table 6.5.

Table 6.5. Performance of the proposed HODO-based PI speed control with an anti-windup scheme

Evaluation Criteria		**PI with AW**	**FODO-based PI with AW**	**HODO-based PI with AW**	**Improvement, %**
Mean absolute percentage error of the mechanical speed,%	Case 1	6.38	2.961	0.8107	53.59/ 87.29
	Case 2	0.0816	0.02	0.008	75.49/ 90.2
Maximum speed error, RPM	Case 1	-479	-156	-163	67.43/ 65.97
	Case 2	-35	-27	-29	22.86/ 17.14
Settling time, s	Case 1	0.39	0.14	0.14	64.1/ 64.1
	Case 2	0.24	0.11	0.12	54.17/ 50
MAPETDE, %	Case 1	-	3.123	18.422	n/a
	Case 2	-	26.2161	138.0714	n/a
Absolute mean error of i_q, %	Case 1	0.068	0.2285	0.3183	n/a
	Case 2	0.4928	0.2285	0.1956	n/a
Mean value of i_d, mA	Case 1	11.45	-3.55	33.565	n/a
	Case 2	-36.34	-3.55	-36.265	n/a
MTDEE, mNm	Case 1	-	1273	1294	n/a
	Case 2	-	731	828	n/a

Based on the experimental results shown below, the settling time and absolute mean mechanical speed errors of FODO/HODO-based control are improved considerably (settling time under *case 1*: 64.1/64.1%, *case 2*: 54.17/50%; absolute mean mechanical speed error under *case 1*: 53.59/87.29%, *case 2*: 75.49/90.2%). While maximum mechanical speed error under FODO/HODO-based control in *case 1* is decreased by 67.43/65.97%, in *case 2* this criterion is decreased by 22.86/17.14%. The absolute mean of the total disturbance estimations is 3.123/18.422% and 26.2161/138.0714% for *cases 1* and *2*, respectively. The mean absolute percentage error of the total disturbance (MAPETDE) is estimated with respect to the load torque reference, hence the big error occurs. The absolute mean error of the q-axis current is 0.2285/0.3183% and 0.2285/0.1956% for *cases 1* and *2*, respectively. The mean values of the d-axis current are -3.55/-33.565 and -3.55/-36.265 for *cases 1* and *2*, respectively.

The maximum total disturbance estimation error (MTDEE) is 1273/1294 mNm and 731/828 mNm for *cases 1* and *2*, respectively. There is no overshoot in transient time due to the round-shaped reference in both cases.

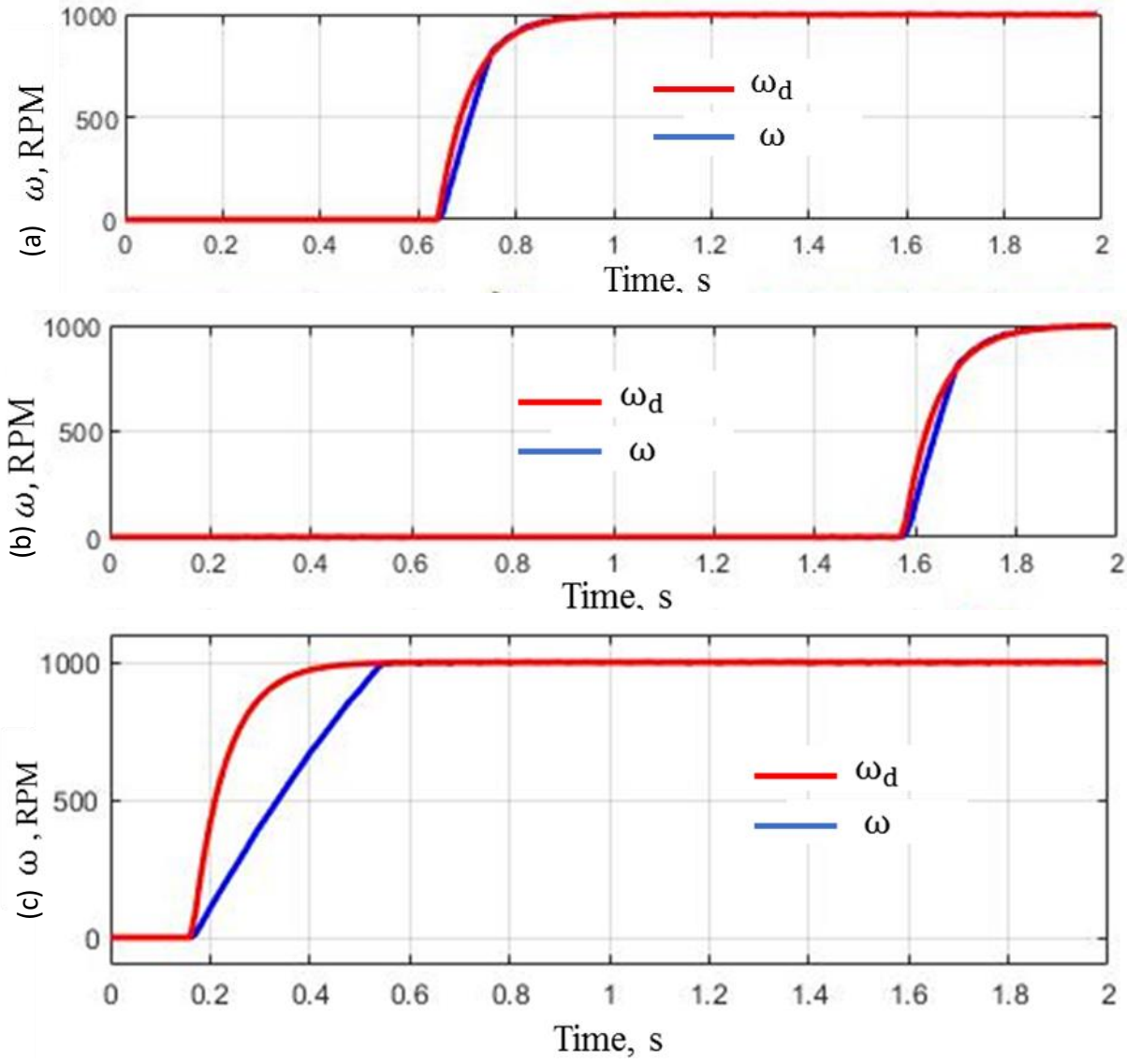

Figure 6.17. The angular shaft speed response in the case 1: (a) the proposed HODO-based discrete-time PI speed controller with the anti-windup scheme; (b) FODO-based discrete-time PI speed controller; (c) discrete-time PI speed controller without DO

The total disturbance has been estimated with FODO and HODO which demonstrate fluctuations around load torque reference, especially during the transient time (Figure 6.18 (a) and 6.18(b). The pulsating torque/current ripples are caused by time-varying flux due to eddy currents in the PMSM system caused by uneven surface of the rotor of the machine. Also, these ripples are reflected in the d-q currents plots.

The speed errors are the most significant during the transient time for both cases of the baseline control system.

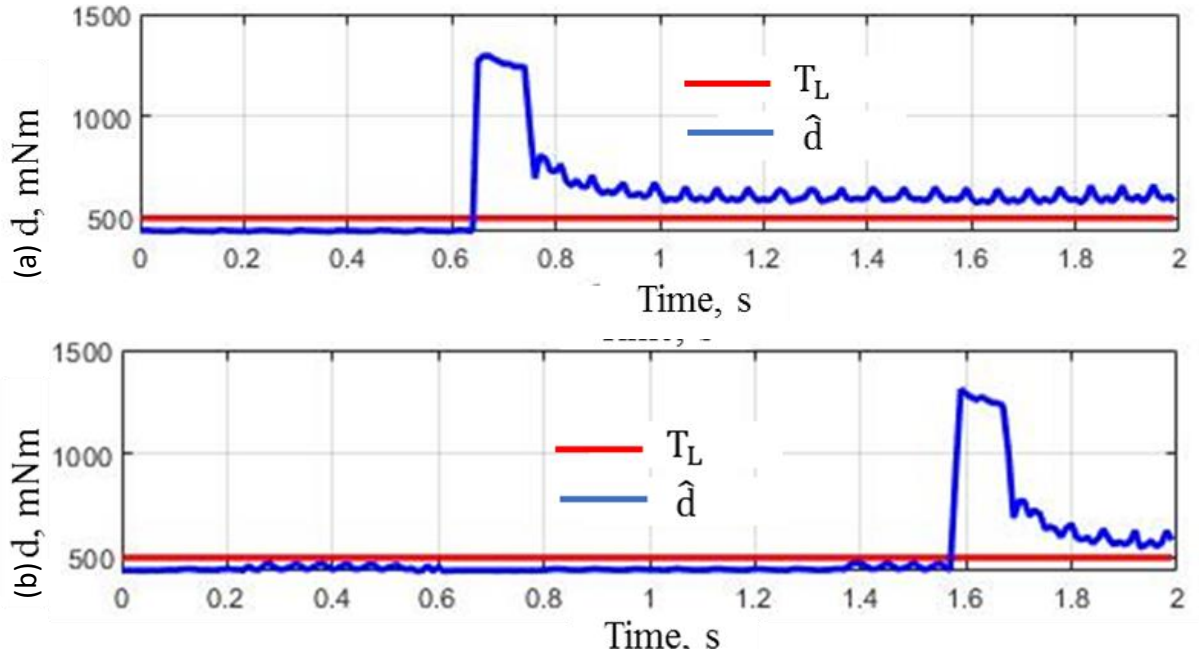

Figure 6.18. The estimated total disturbance including load torque in the case 1: (a) HODO; (b) FODO

Note that the results of estimated total disturbance ($\hat{d}$) and the load torque T_L are shown due to difficulties to measure the total disturbance precisely in the real-time experiment (Figures 6.22(a), 6.22(b)). There are some mismatches between total and load torque disturbances.

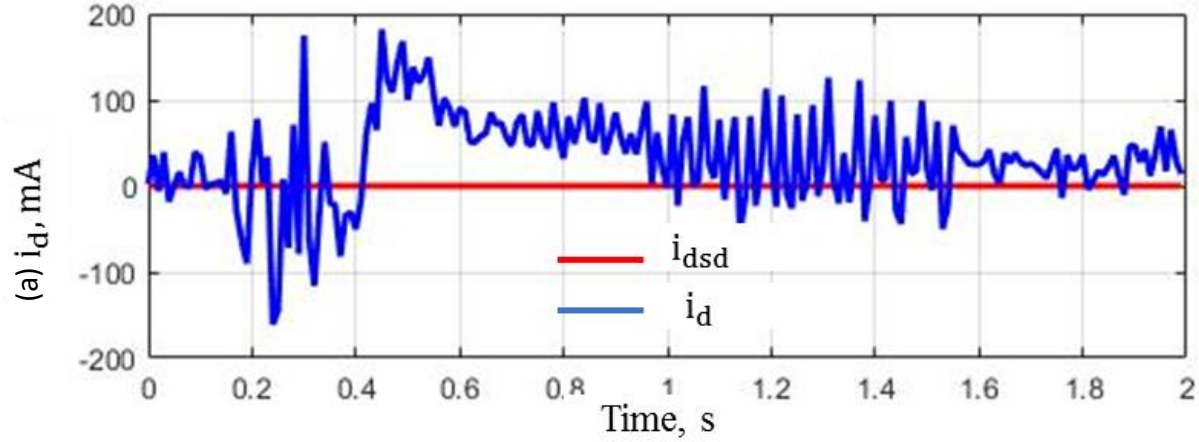

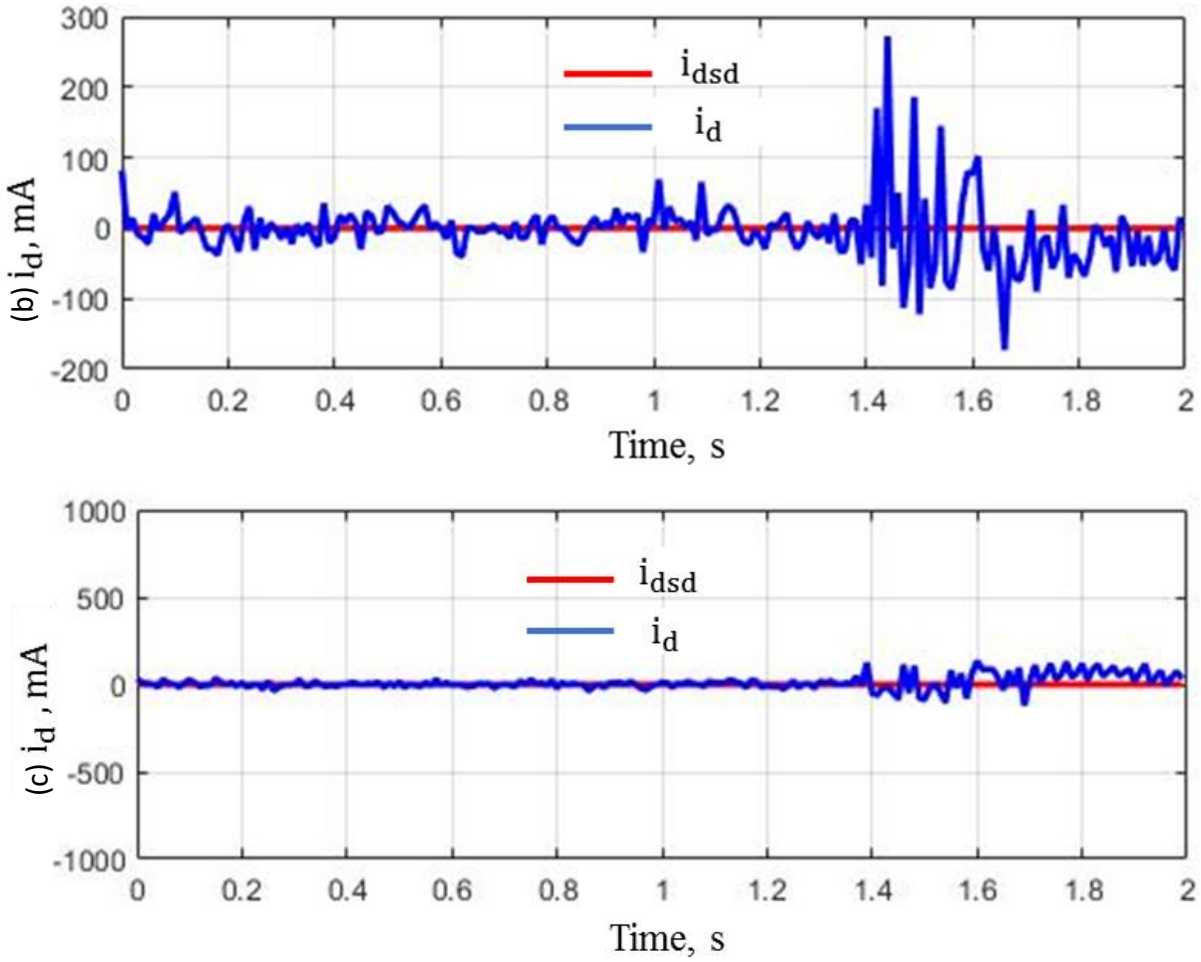

Figure 6.19. The direct current responses in the case 1: (a) the proposed HODO-based discrete-time PI speed controller with the anti-windup scheme; (b) FODO-based discrete-time PI speed controller; (c) discrete-time PI speed controller without DO

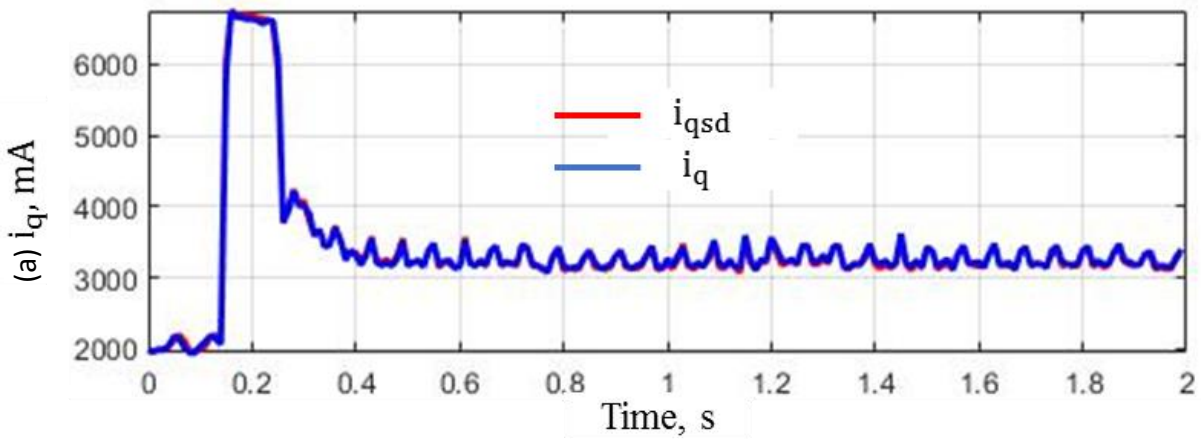

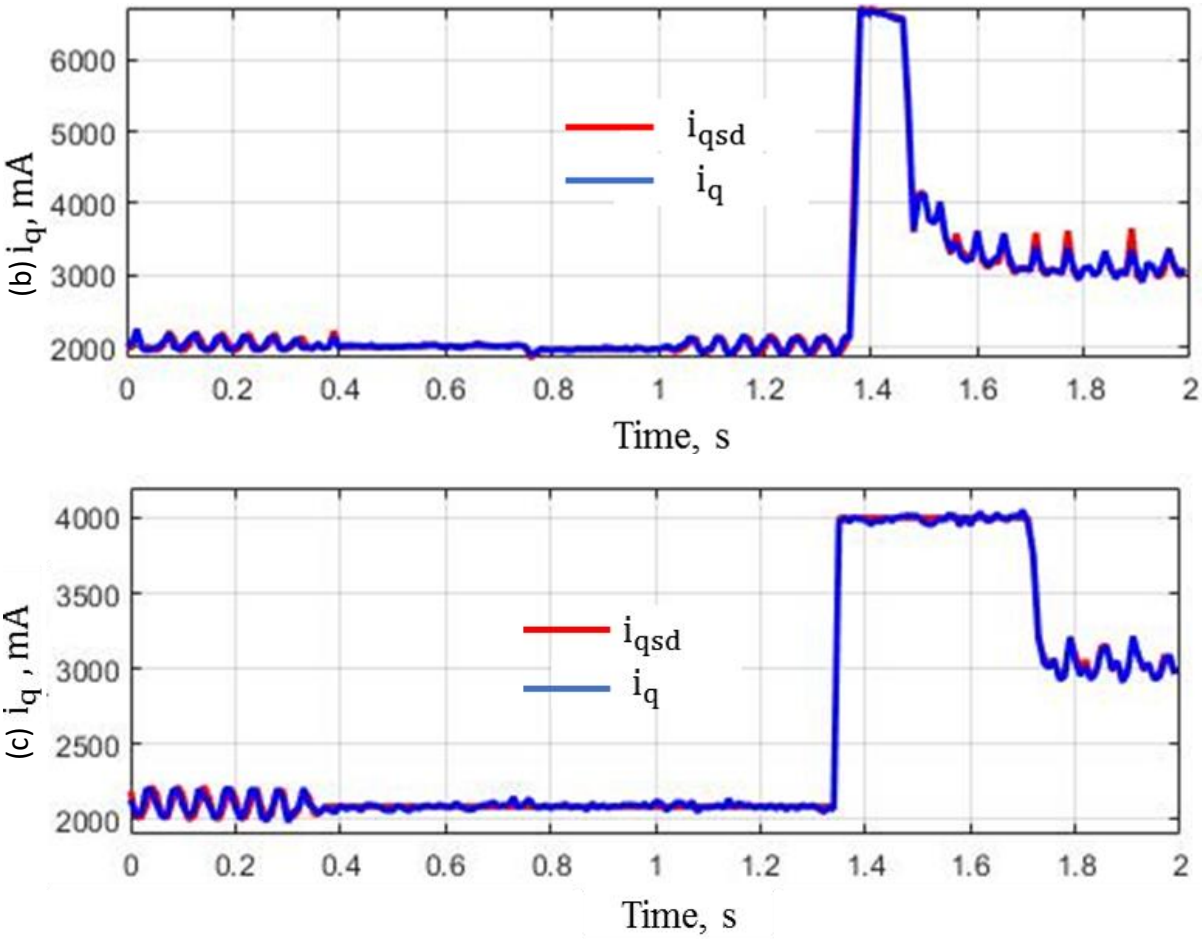

Figure 6.20. The quadrature current responses in the case 1: (a) the proposed HODO-based discrete-time PI speed controller with the anti-windup scheme; (b) FODO-based discrete-time PI speed controller; (c) discrete-time PI speed controller without DO

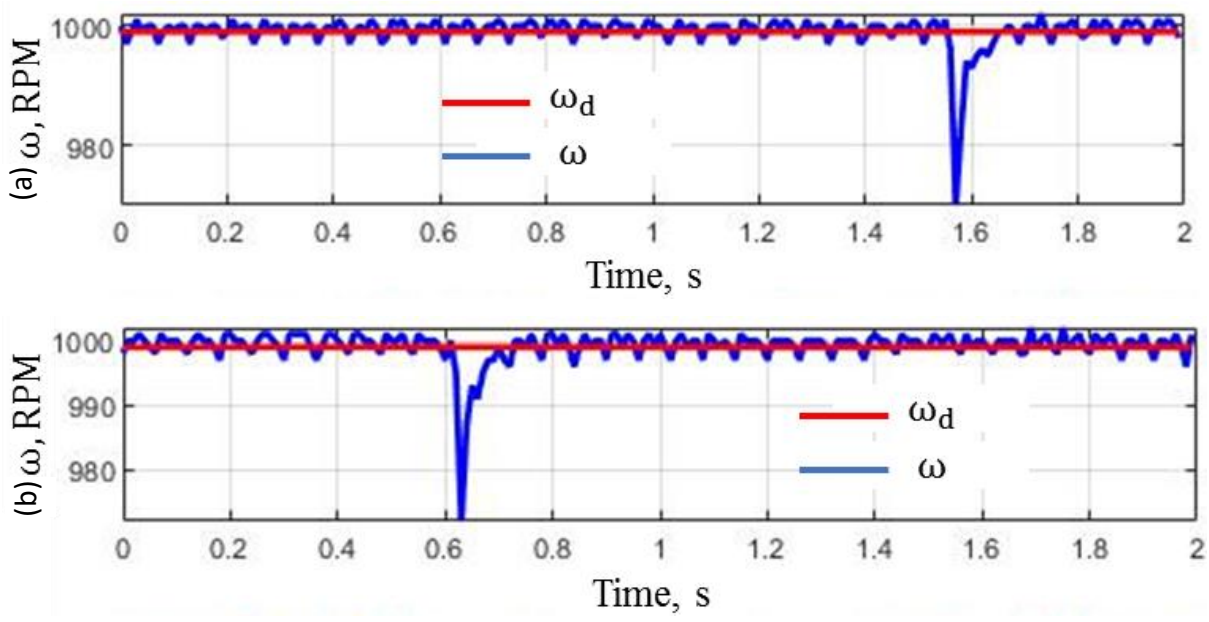

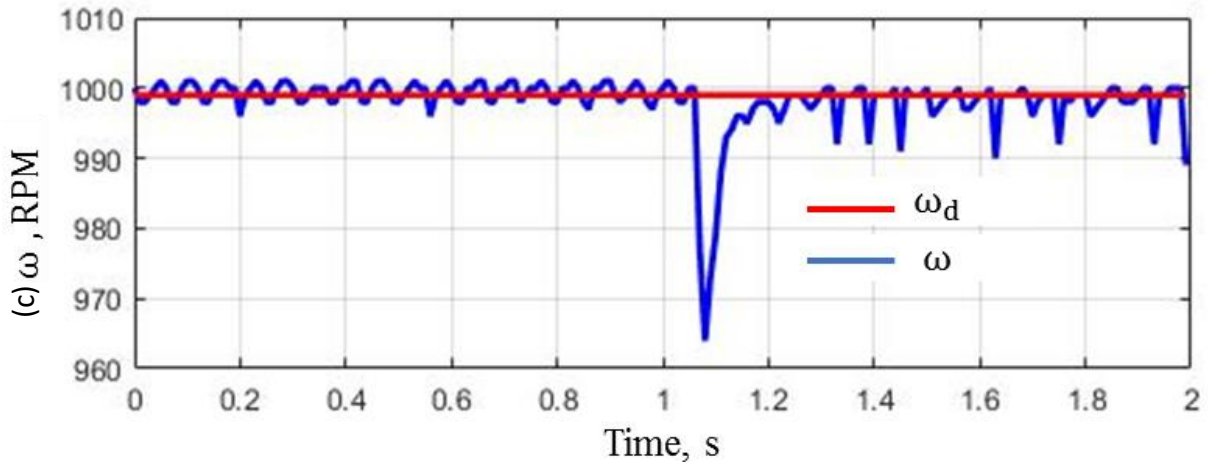

Figure 6.21. The angular shaft speed response in the case 2: (a) the proposed HODO-based discrete-time PI speed controller with the anti-windup scheme; (b) FODO-based discrete-time PI speed controller; (c) discrete-time PI speed controller without DO

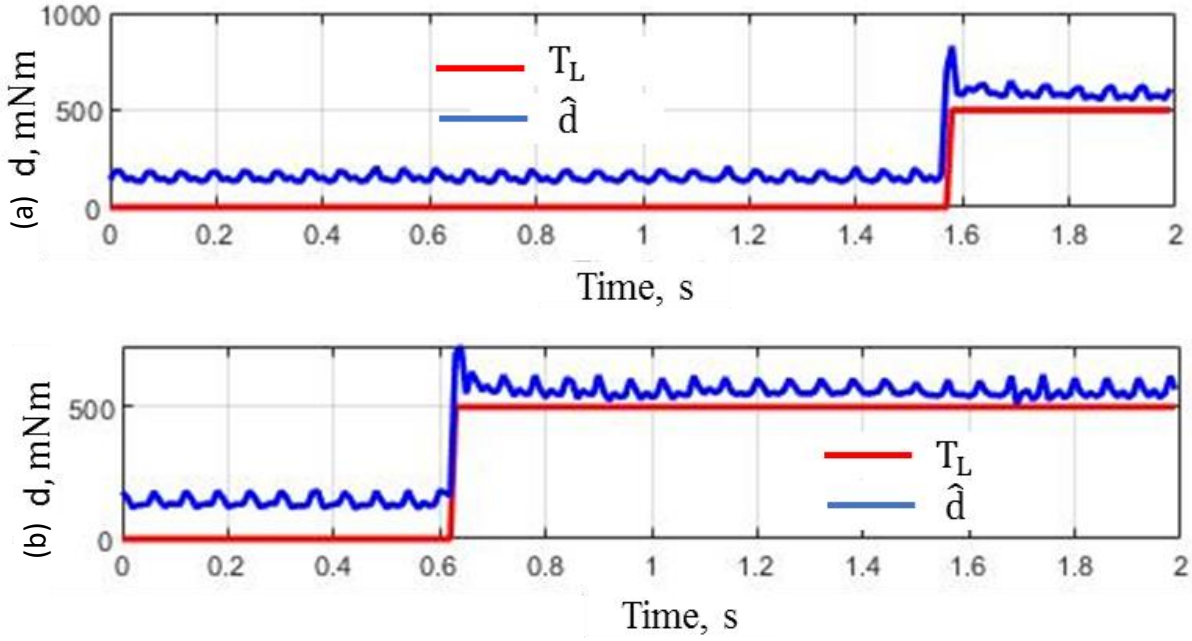

Figure 6.22. The estimated total disturbance including load torque in the case 1: (a) HODO; (b) FODO

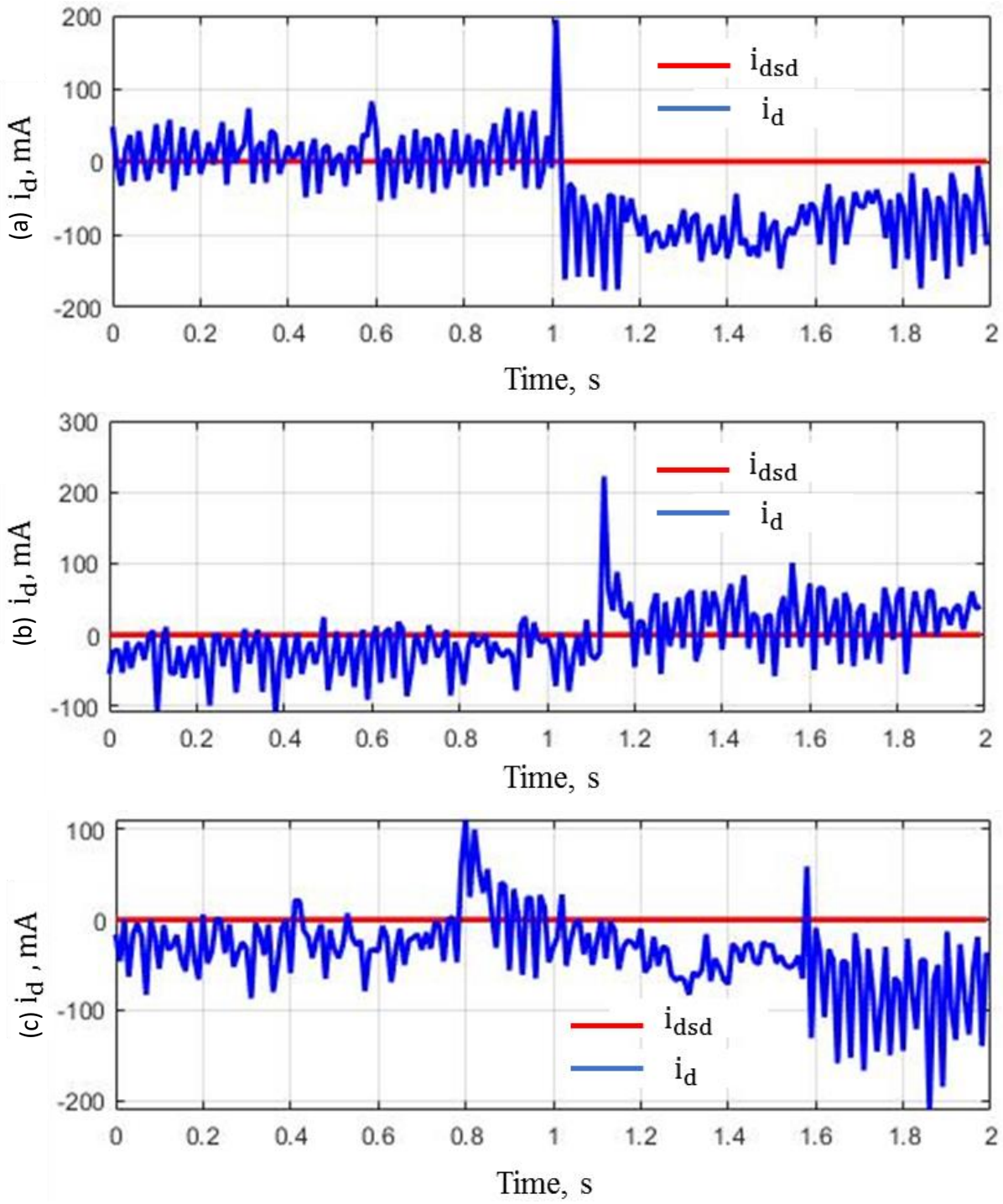

Figure 6.23. The direct current responses in the case 2: (a) the proposed HODO-based discrete-time PI speed controller with the anti-windup scheme; (b) FODO-based discrete-time PI speed controller; (c) discrete-time PI speed controller without DO

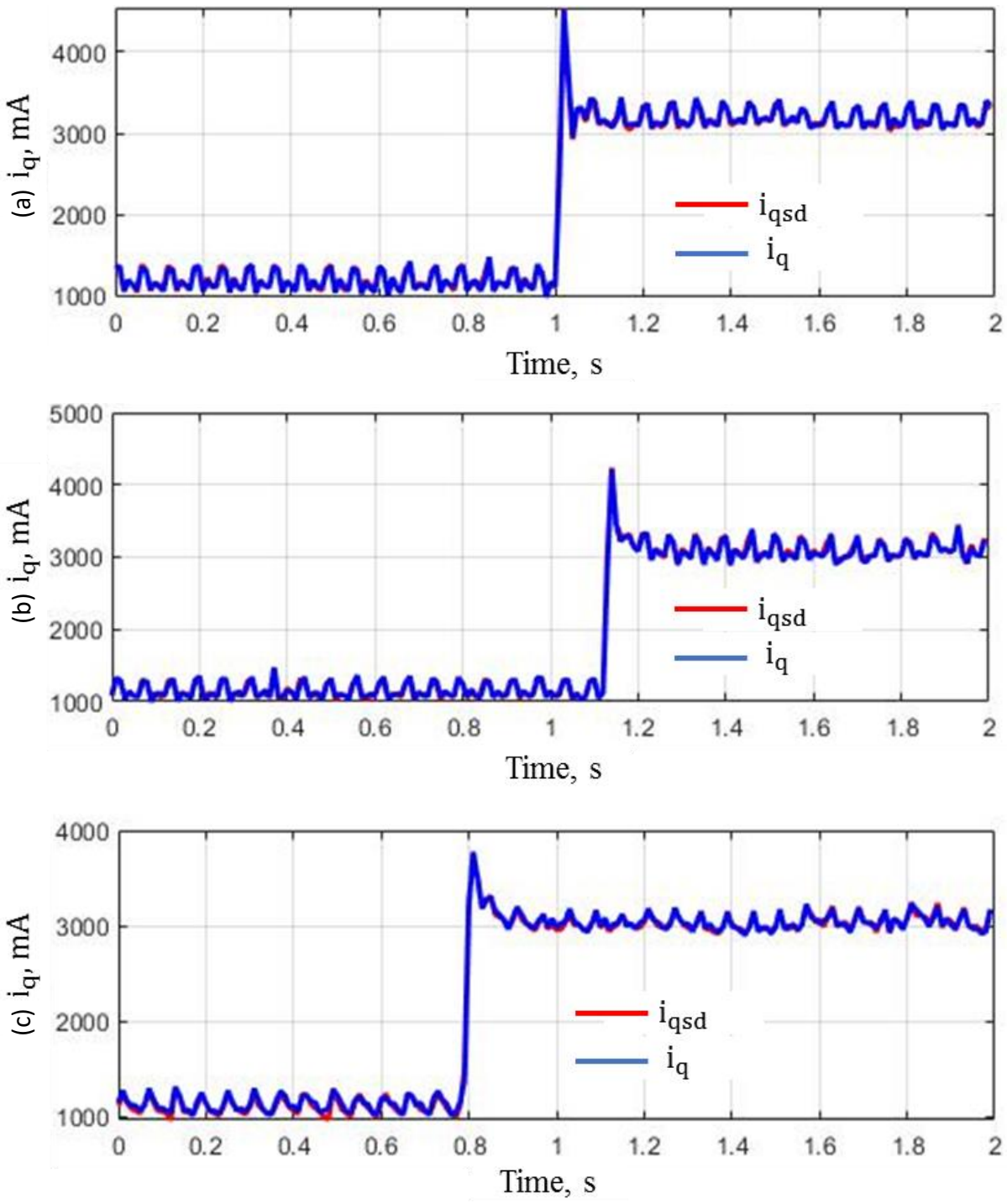

Figure 6.24. The quadrature current responses in the case 2: (a) the proposed HODO-based discrete-time PI speed controller with the anti-windup scheme; (b) FODO-based discrete-time PI speed controller; (c) discrete-time PI speed controller without DO

6.4. Summary of Chapter 6

The HODO-based SMC and PI-PI control systems have been proposed in the PMSM systems' speed regulation. The adopted HODO was used for estimation of load

torque disturbance in the PMSM model. Moreover, the observer was able to estimate the varying nature of the total disturbances including friction, hysteresis, and eddy currents due to the body structure and materials used in building of the PM synchronous machine. The estimated disturbances have been compensated in the speed controllers. The SOFCL-based SMC with HODO has achieved the improvement of the angular shaft tracking transient performance by 70.44% in the nominal case, whereas 65.16%, and 78.31% in parameter variations and load torque disturbance cases respectively. The HODO-based the discrete-time PI speed controller with back-calculation anti-windup scheme has improved the overall performance by 87.29% and 90.2% in speed and load torque variations scenarios respectively. These results demonstrates the effectiveness of integration of disturbance compensation scheme in the speed loop of the control system.

Chapter 7: Simulations results of the HODO-based control systems in WECS application

7.1.Introduction

In this chapter, simulations results of the HODO based proposed control systems to maximize power generation of direct-driven variable-speed WECS are presented under nominal and parameter variations scenarios. Firstly, HODOs-based ISMC with SDRE technique control system's performance are presented and compared with linear feedback-based ISMC, LQR, 1st order SMC under nominal parameters, model uncertainty as well as in presence of vast-varying disturbance, noise, and nonlinear dynamics of PMSG. Secondly, HODO-based SDRE with servomechanism technique control system's performance are presented and compared with conventional SDRE control approach to compensate the model uncertainty with noise in the WECS. The performances are tested in nominal operation and some parameter variations with presence of noise scenarios.

7.2.Simulation results of HODOs-based ISMC with SDRE technique in WECS application

To apply the proposed HODOs-based ISMC with SDRE technique on a machine-side power converter to maximize power extraction from WECS with PMSG, the model of WECS has to be designed in Matlab/Simulink simulation environment. The small power WECS parameters are given in Table 7.1. The control parameters that have been used in simulations are presented in Table 7.2. The wind speed profile is shown in Figure 7.1. The mean value of 12.13 m/sec of wind profile is given according to the study [5]. The power coefficient C_p is analytically estimated and defined as $\lambda_{opt} = 8.09$ and $C_{pmax} = 0.3262$. To consider the performance of the proposed control method under parameter uncertainties, the stator resistance is increased by 20% and inductance is increased by 1% (Table 7.3). To emulate the noise coming from sensors $d_{qn} = 10^5 \sin(t)$ and $d_{dn} = 10^3 \sin(t)$ has been injected into the SPMSM system.

By solving ARE equations (5.33) and Lyapunov equations (5.34) and (5.35) the near-optimal gains matrices are obtained that approximate the solution of the SDRE with N=2, number of terms in Taylor's series

$$K_0 = \begin{bmatrix} -74.8320 & 3.1036 & -0.0000 \\ 0.0000 & -0.0000 & 0.6978 \end{bmatrix}$$

$$K_1 = \begin{bmatrix} 0.0000 & 0.0000 & 0.2603 \\ 0.0020 & 0.0432 & -0.0000 \end{bmatrix}$$

$$K_2 = \begin{bmatrix} -0.0277 & -0.6206 & 0.0000 \\ 0.0000 & 0.0000 & -0.0318 \end{bmatrix}$$

Table 7.1. The WECS with PMSG parameters

Symbol	Quantity	Value	[Unit]
P_{rated}	Rated power	5	kW
R_s	Stator resistance	0.3676	Ω
L	Stator inductance	3.55	mH
λ_m	Magnet flux linkage	0.2867	V·s/rad
J_{ri}	rotor inertia	7.856	kg·m^2
P	Pole pairs	14	-
B_{vf}	Viscous friction coefficient	0.002	kg·m^2/s
R	Rotor radius	1.84	m
ρ	Air density	1.25	kg/m^3

Table 7.2. The control system parameters

Controllers and observers, solver type	Parameters and gains
ISMS: nominal part gains	Q=diag([5000 10 1]), R=diag([1 1])
SDRE terms, N	2
Matlab solver type	care & lyap
ISMC: discontinuous part gains	k=100
Small value for continuous approximation	δ=0.001
T_a observer gains d_q–axis disturbance observer's gains d_d–axis disturbance observer's gains	L_{11}=50, L_{12}=250, L_{13}=500 L_{21}=200, L_{22}=500, L_{23}=1000 L_{31}=200, L_{32}=500, L_{33}=1000

The simulations of HODOs-based ISMC with SDRE technique to control power converter in the WECS show stable results under some parameter variations, and better flexibility in choosing the control parameters.

Table 7.3. The simulation scenarios

Scenario	Parameter variations
1	Nominal parameters in Table 6.5.
2	$\mathrm{R_s} = +20\%, \mathrm{L} = +1\%$

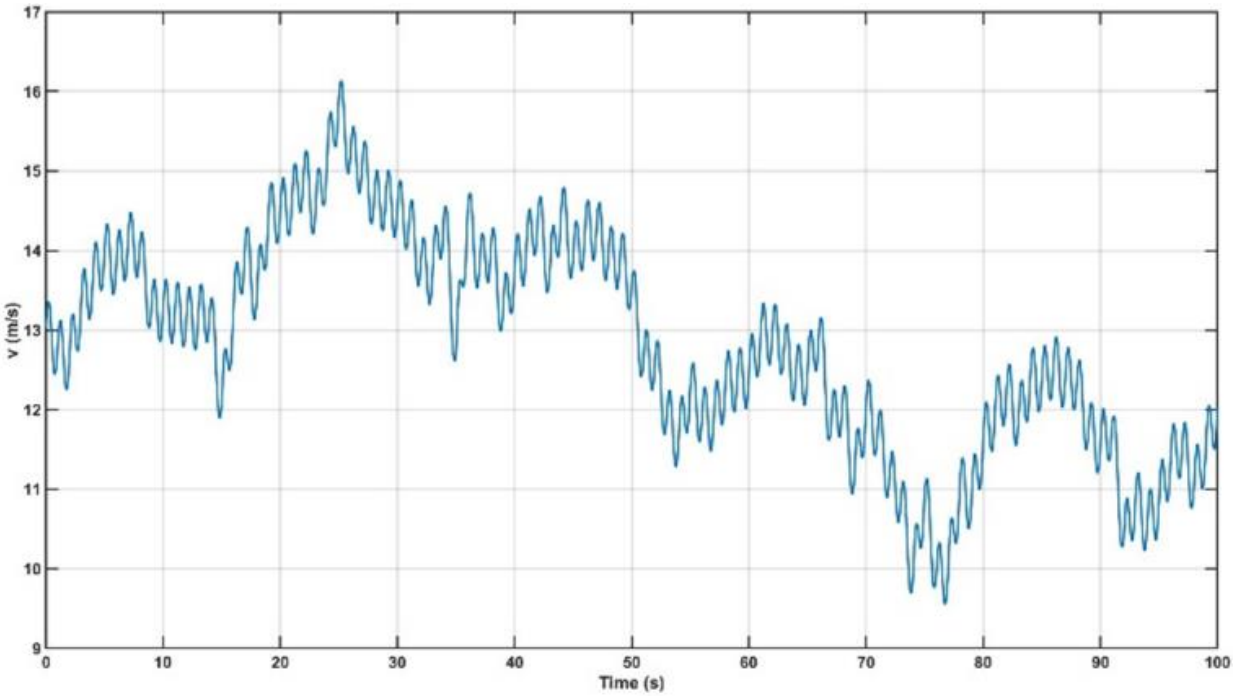

Figure 7.1. Wind speed (v) profile with means values of 12.13 m/sec

The performance of the proposed HODOs-based ISMC with SDRE control system under nominal parameters (scenario 1) with N=1 and N=2 is listed in Table 7.4 and depicted in Figures. 7.2-7.8. The performance has been assessed by the mean absolute percentage error of angular shaft speed, $|\tilde{\omega}|$ and mean absolute percentage error of the electromagnetic torque, $|\tilde{\mathrm{T}}_\mathrm{e}|$.

The proposed HODOs-based ISMC with SDRE technique with N=1 and N=2 have been analysed and compared with other control methods namely, LQR based optimal control method published in [15], linear output feedback-based ISMC method [8], and 1st order SMC method [7]. It should be noted that the ISMC control method with N=0 is the same as the LQR–based ISMC proposed in [8].

The graphs demonstrate the angular shaft speed tracking the variable reference with N=1 (Figure 7.2(a)) and N=2 (Figure 7.2(b)) which is depends on wind speed. The errors between the reference and actual speed where the proposed control system with N=1 and N=2 are demonstrated in Figure 7.3 for scenario 1. Moreover, the actual electromagnetic torque, (T_e) tracking the reference electromagnetic torque (T_{ed}) followed by the electromagnetic torque errors' graphs ($\tilde{T}_e$) are depicted in Figures 7.4 and 7.5 respectively. Finally, direct current, (i_d), q-axis sliding variable (σ_1), and d-axis sliding variable (σ_2) are shown in Figure 7.6, Figure 7.7, and Figure 7.8 for N=1 and N=2 respectively.

The proposed control method with more number of approximating terms has superior performance. As it is difficult to visualize the difference, the proposed control performance has been evaluated by MAPE criteria, where the MAPE of the angular shaft speed is 0.0702% and MAPE of the electromagnetic torque is 1.1709% with N=2. In total, the MAPE of the angular shaft speed with N=2 is reduced for SDRE with N=1 by 0.16%, LQR by 0.25%, SDRE with N=0 by 0.25%, and SMC by 0.22% respectively. Similarly, the MAPE of the electromagnetic torque is decreased for SDRE with N=1 by 2.4%, LQR by 3.76%, SDRE with N=0 by 3.74%, and SMC by 3.66% respectively.

Table 7.4. HODO-based ISMC with SDRE control performance

Parameter error	**Method**	**Scenario 1**	**Scenario 2**
Mean absolute percentage error of the angular shaft speed, $\lvert\tilde{\omega}\rvert$, %	SDRE +ISMC, N=1	0.232	0.2337
	SDRE +ISMC, N=2	0.0702	0.0621
	LQR [15]	0.3207	0.3204
	ISMC [8]	0.319	0.3182
	SMC[7]	0.2918	0.2916
Mean absolute percentage error of the electromagnetic torque,$\lvert\tilde{T}_e\rvert$, %	SDRE +ISMC, N=1	3.5697	3.5933
	SDRE +ISMC, N=2	1.1709	1.0398
	LQR [15]	4.9262	4.9237
	ISMC[8]	4.9054	4.8938
	SMC[7]	4.8345	4.8312

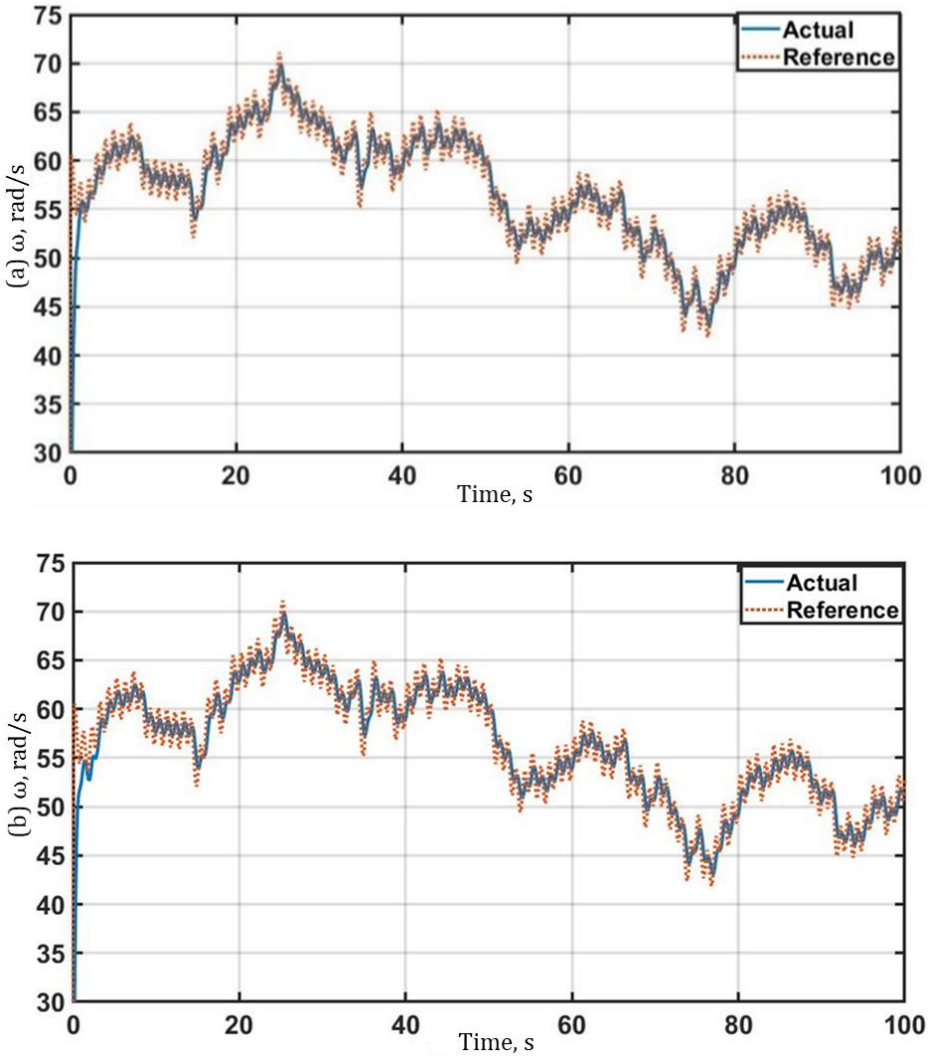

Figure 7.2. The angular shaft speed tracking for Scenario 1: (a) SDRE-based ISMC with HODOs, N=1 (b) SDRE-based ISMC with HODOs, N=2

The proposed method with N=2 has demonstrated robust performance under model uncertainty with noise which is introduced in Scenario 2 (Figures 7.9-7.15). The MAPE of the angular shaft speed composes 0.0621% which is less for 0.17%/0.26%/0.26%/0.23% or 3.76/5.16/512/4.7 times smaller than the proposed control with N=1, LQR, ISMC, SMC based methods, respectively. Similarly, the MAPE of the electromagnetic torque constitutes 1.0398% which is less for 2.55%/3.88%/3.85%/3.79% or 3.46/4.74/4.71/4.65 times smaller than the proposed control with N=1, LQR, ISMC, and SMC methods respectively.

In both scenarios, the sliding variables of the proposed HODO-based ISMC converge to zero (Figures 7.7, 7.8, 7.14, and 7.15). Further increasing the gains of the performance matrix (Q), the gain of discontinuous part and number of terms in the series

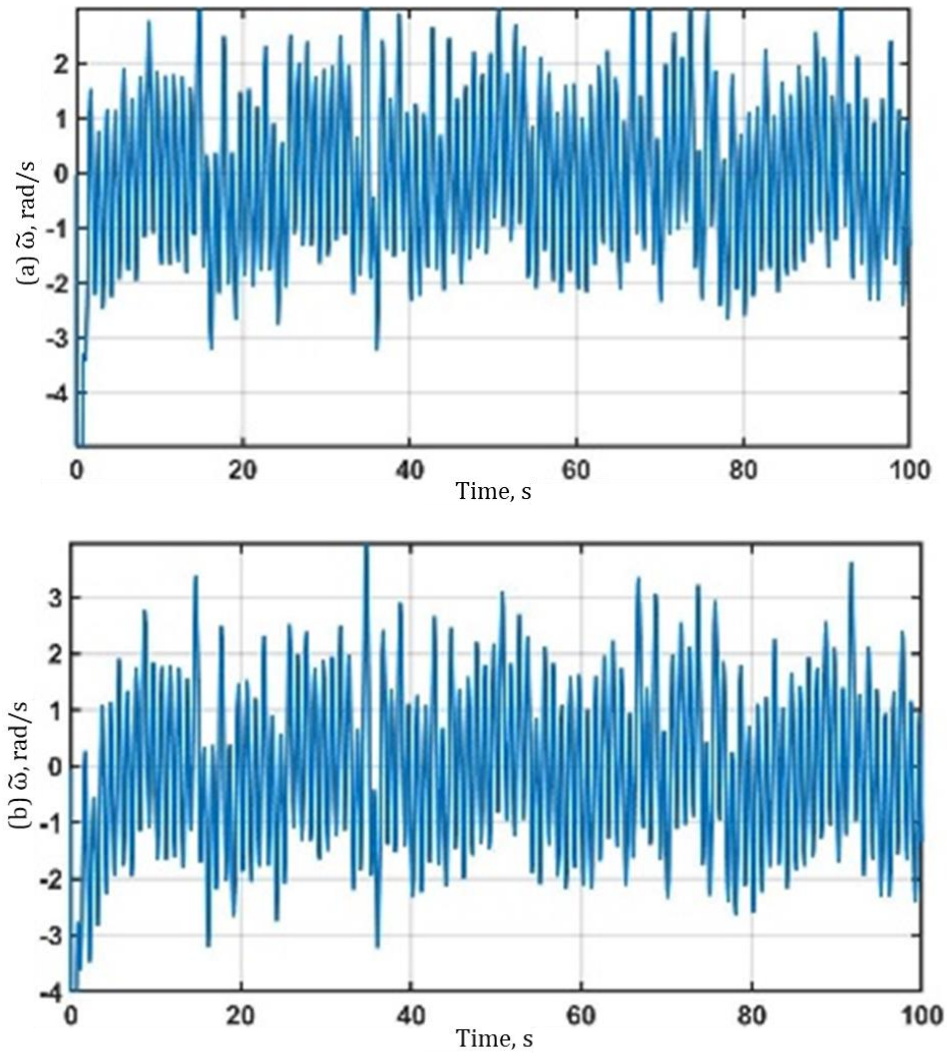

Figure 7.3. The angular shaft speed tracking errors for Scenario 1: (a) SDRE-based ISMC with HODOs, N=1 (b) SDRE-based ISMC with HODOs, N=2

have put more burden on the computational time and jeopardies the stability of the whole system.

In scenario 2, the actual q-axis disturbance (d_q), q-axis disturbance estimation ($\hat{d}_q$), actual d-axis disturbance (d_d), d-axis disturbance estimation ($\hat{d}_d$) have been measured to demonstrate the robustness of the proposed control design under external disturbance, model uncertainty, modelling errors and noise (Figures 6.27 and 6.30).

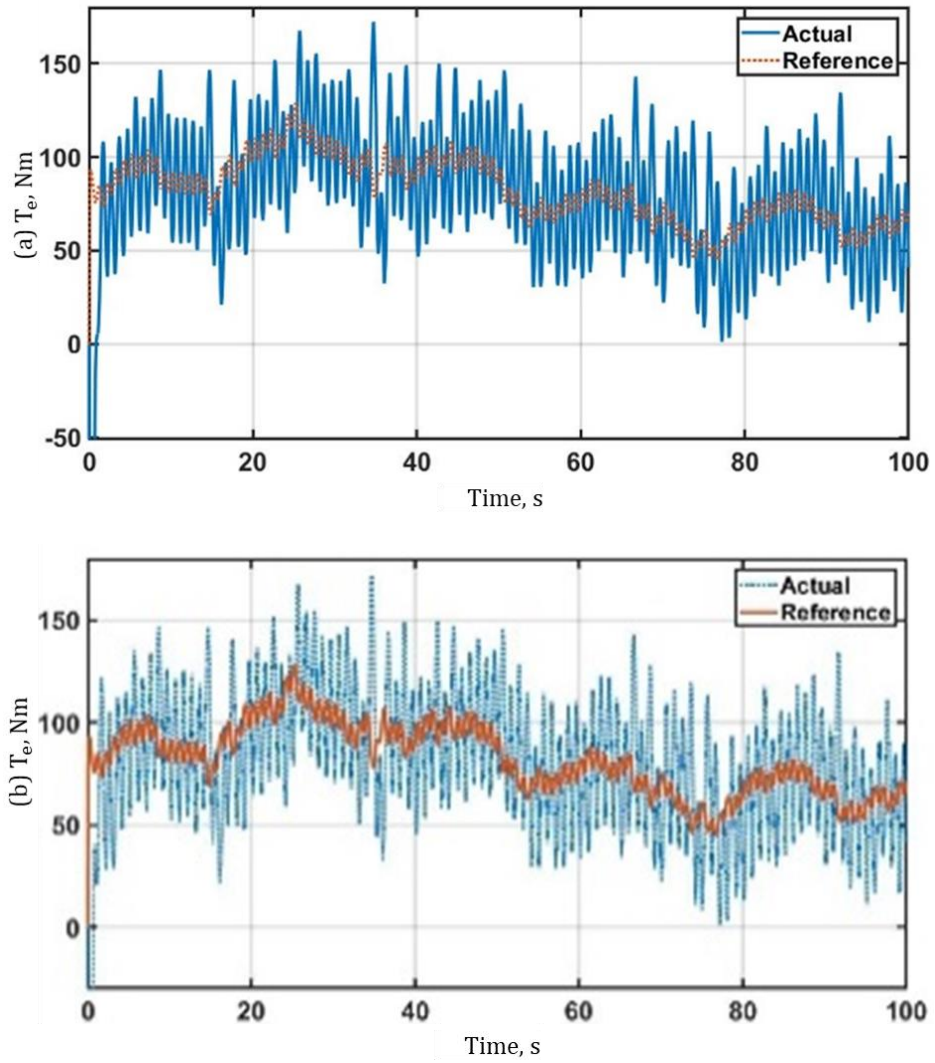

Figure 7.4. The electromagnetic torque tracking for Scenario 1: (a) SDRE-based ISMC with HODOs, N=1 (b) SDRE-based ISMC with HODOs, N=2

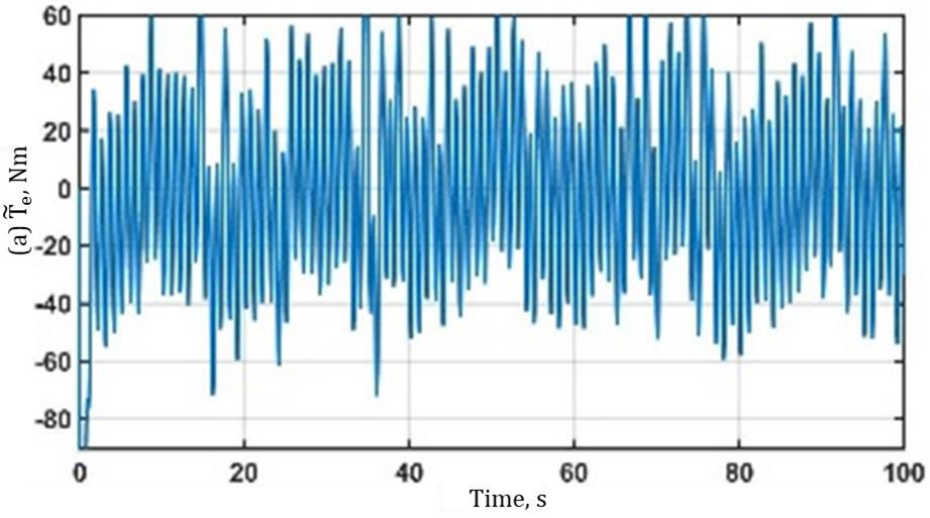

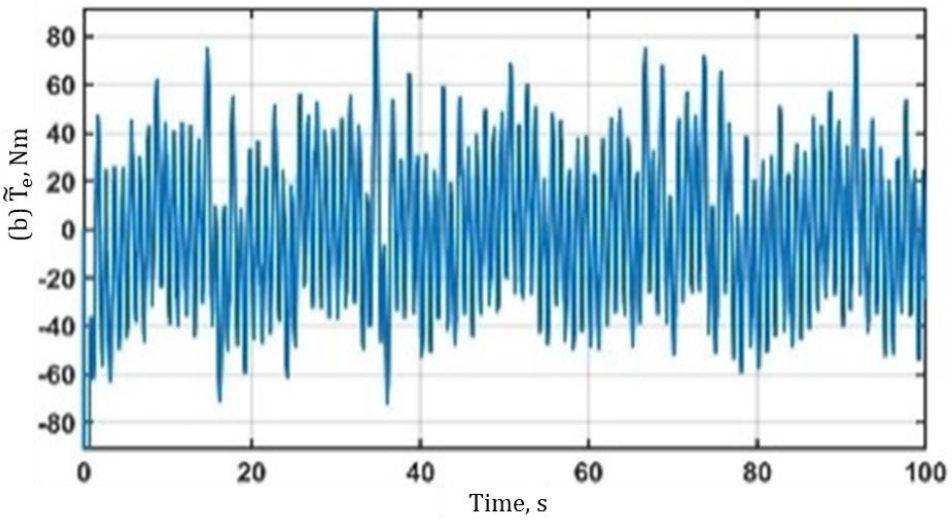

Figure 7.5. The electromagnetic torque tracking errors for Scenario 1: (a) SDRE-based ISMC with HODOs, N=1 (b) SDRE-based ISMC with HODOs, N=2

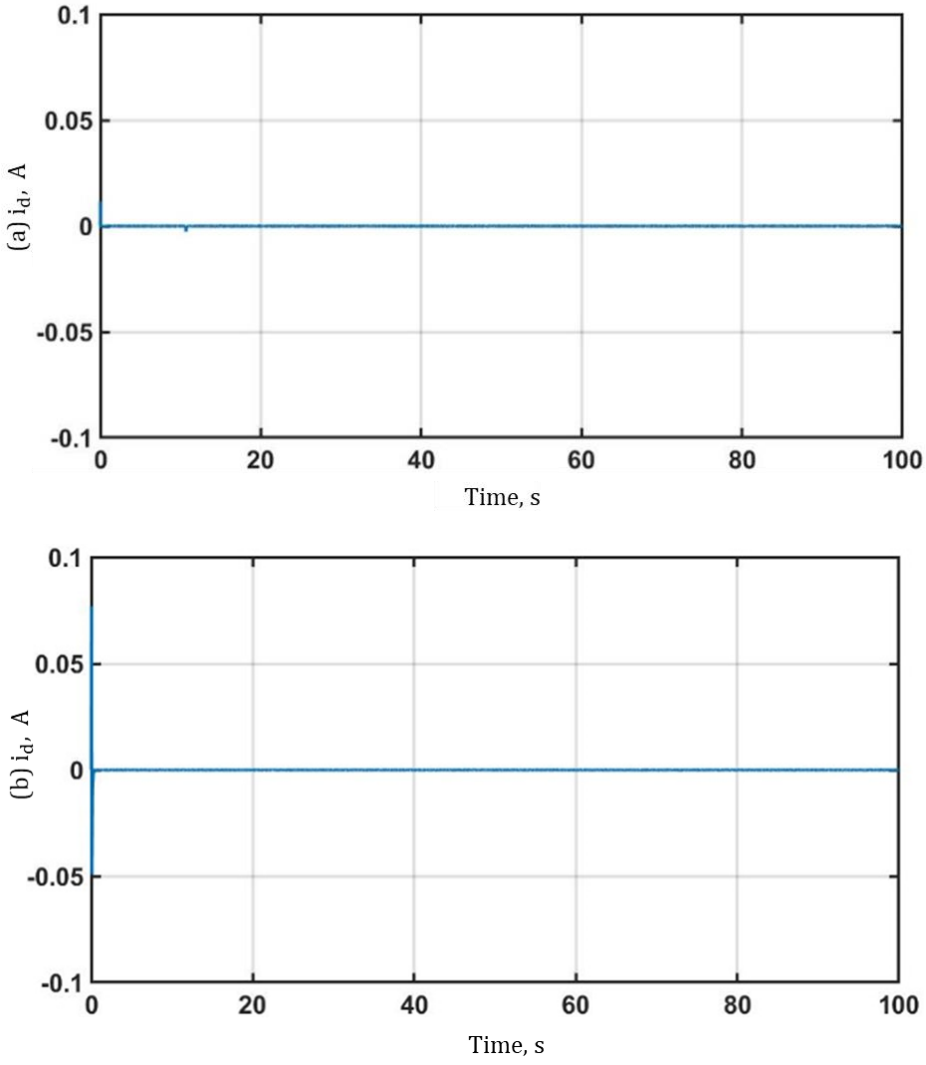

Figure 7.6. The direct current response for Scenario 1: (a) SDRE-based ISMC with HODOs, N=1 (b) SDRE-based ISMC with HODOs, N=2

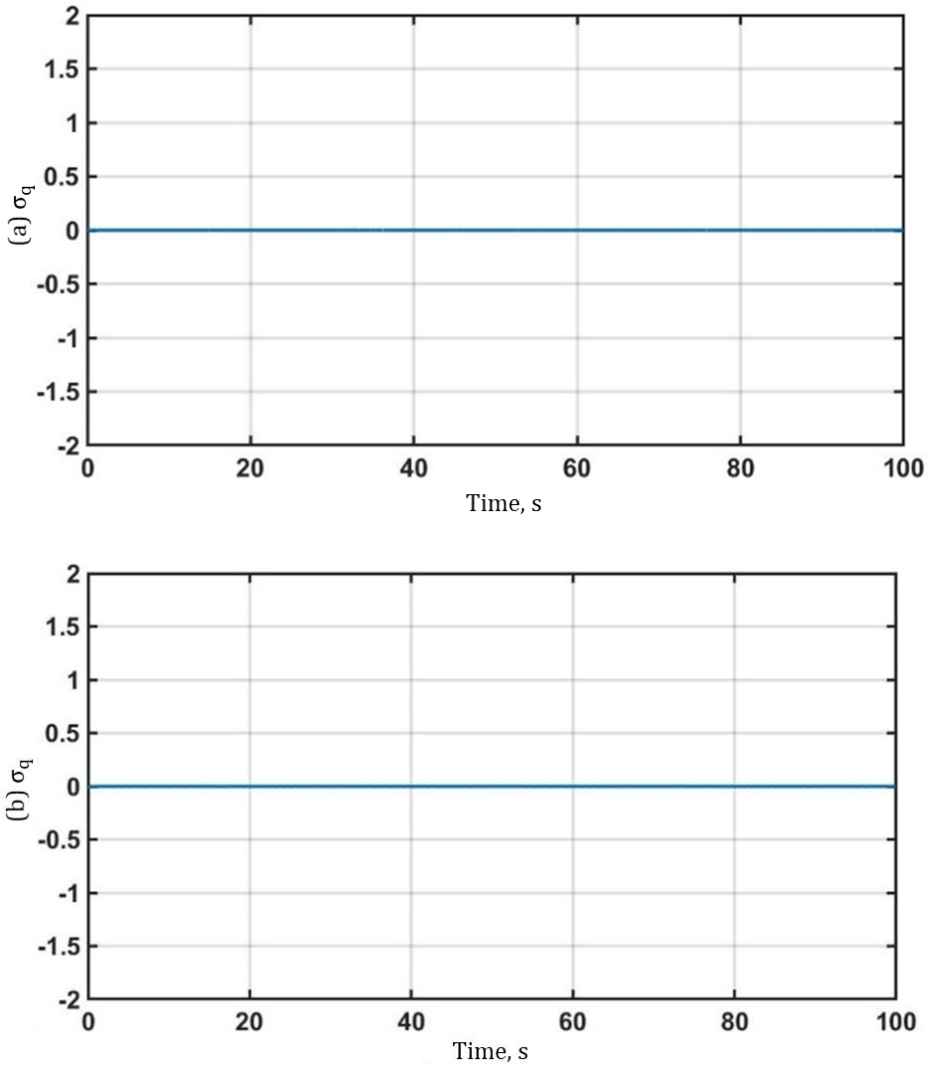

Figure 7.7. The quadrature axes sliding variable response for Scenario 1: (a) SDRE-based ISMC with HODOs, N=1 (b) SDRE-based ISMC with HODOs, N=2

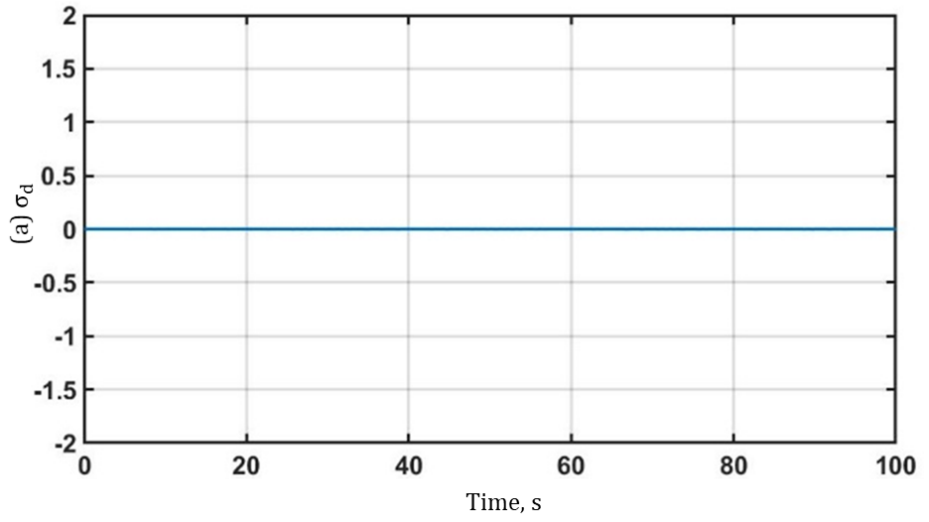

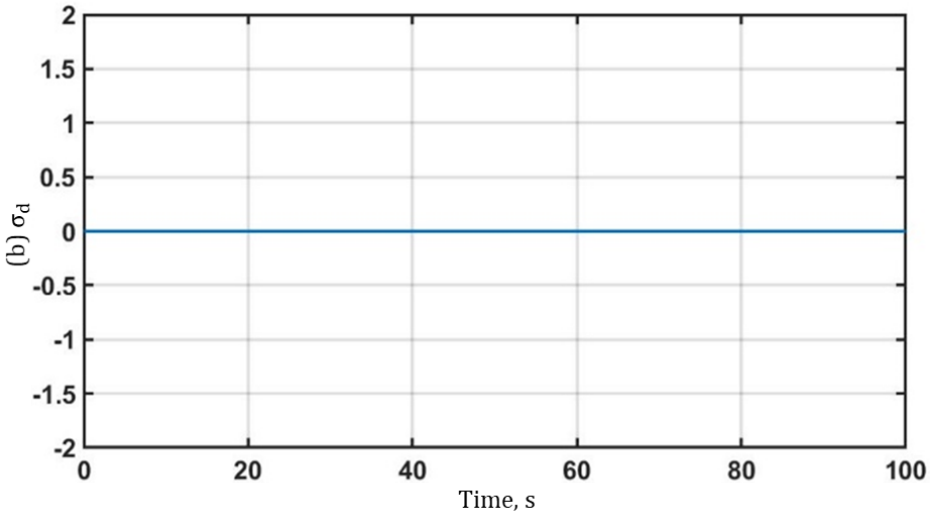

Figure 7.8. The direct axes sliding variable response for Scenario 1: (a) SDRE-based ISMC with HODOs, N=1 (b) SDRE-based ISMC with HODOs, N=2

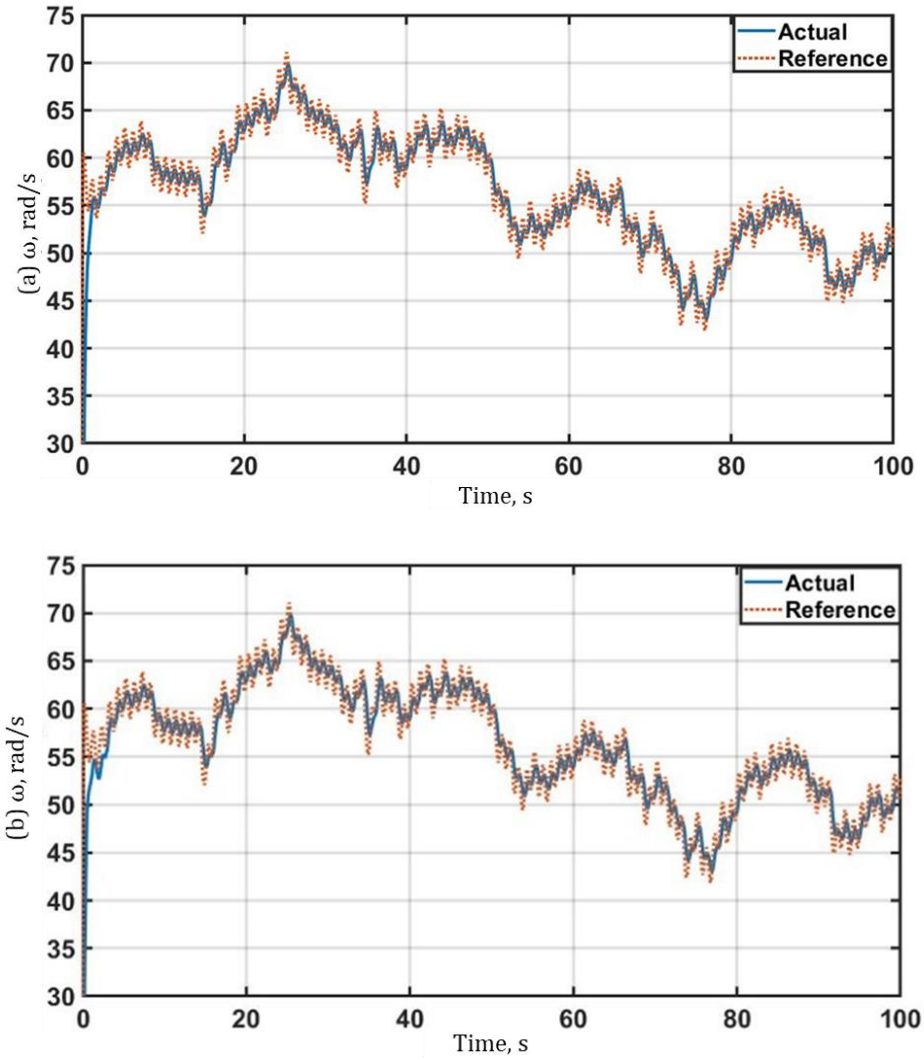

Figure 7.9. The angular shaft speed tracking for Scenario 2: (a) SDRE-based ISMC with HODOs, N=1 (b) SDRE-based ISMC with HODOs, N=2

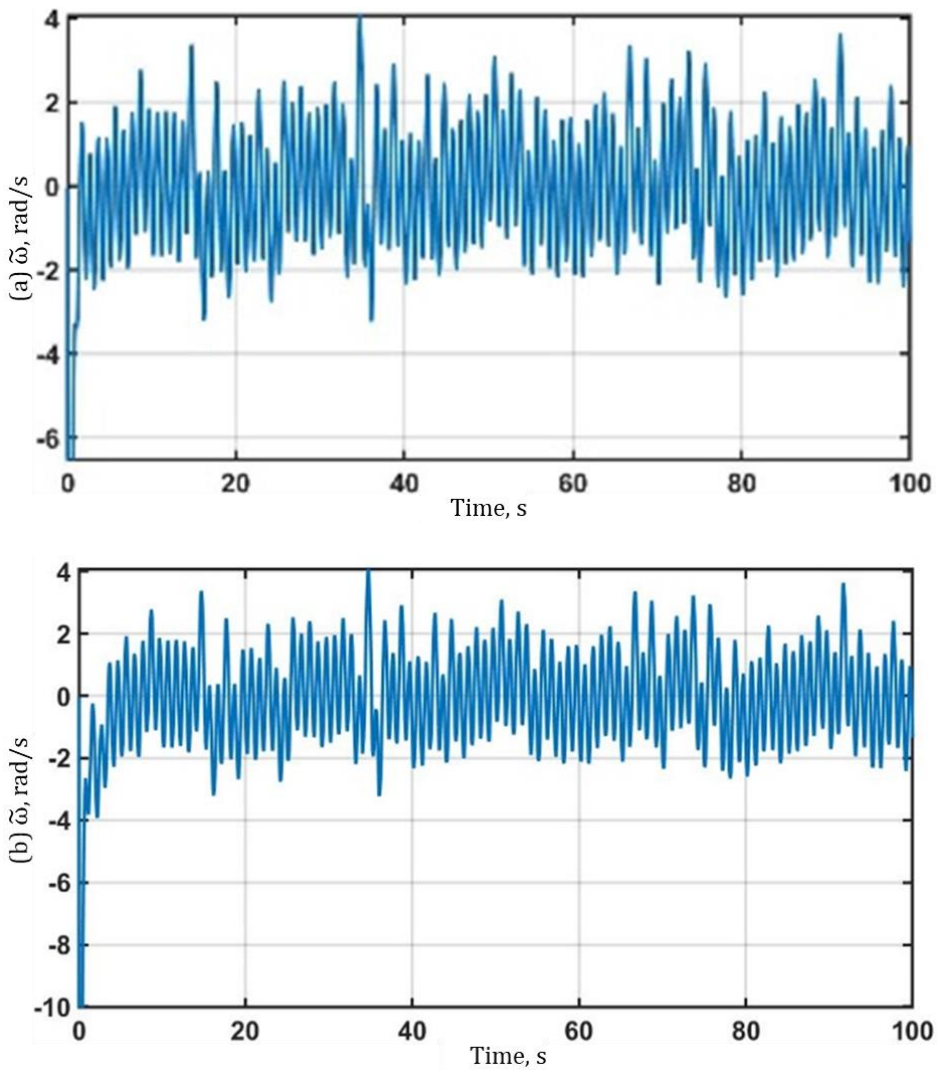

Figure 7.10. The angular shaft speed tracking errors for Scenario 2: (a) SDRE-based ISMC with HODOs, N=1 (b) SDRE-based ISMC with HODOs, N=2

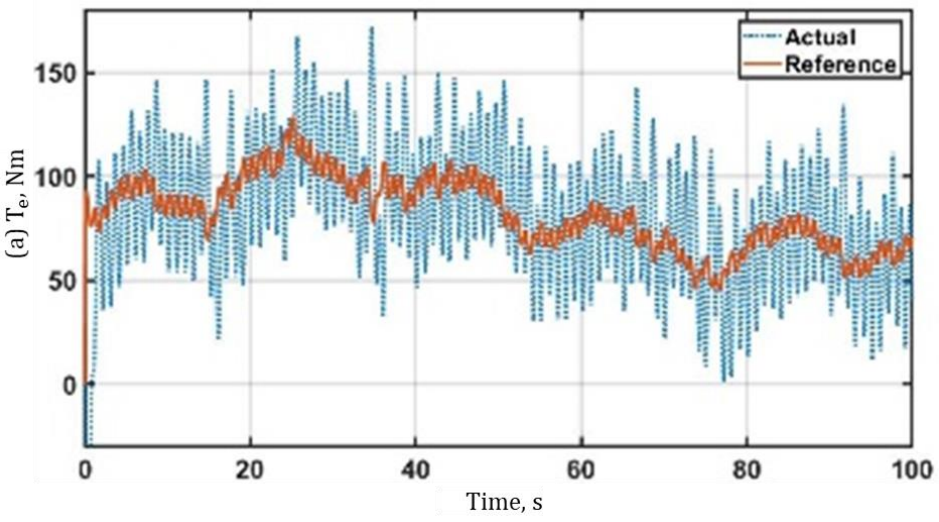

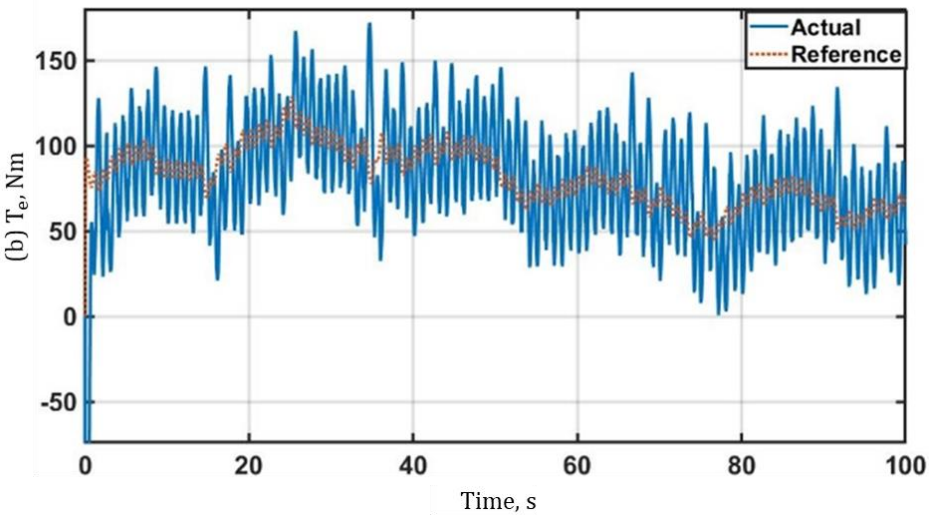

Figure 7.11. The electromagnetic torque tracking for Scenario 2: (a) SDRE-based ISMC with HODOs, N=1 (b) SDRE-based ISMC with HODOs, N=2

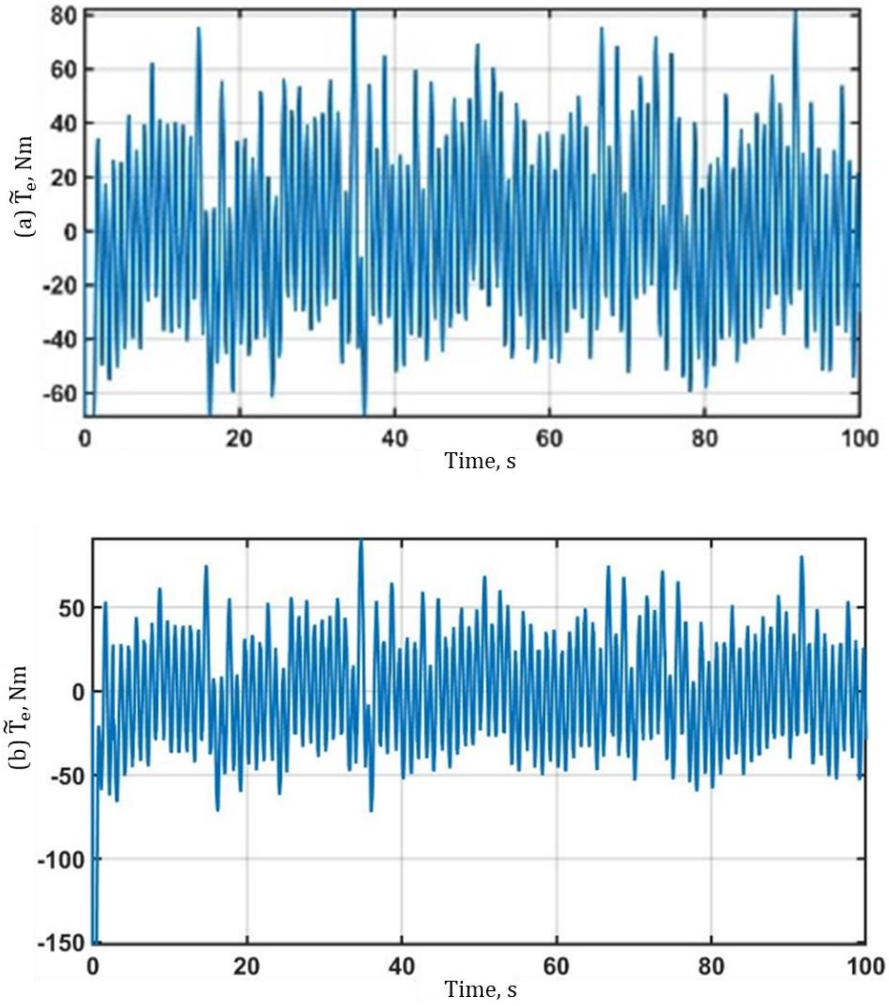

Figure 7.12. The electromagnetic torque tracking errors for Scenario 2: (a) SDRE-based ISMC with HODOs, N=1 (b) SDRE-based ISMC with HODOs, N=2

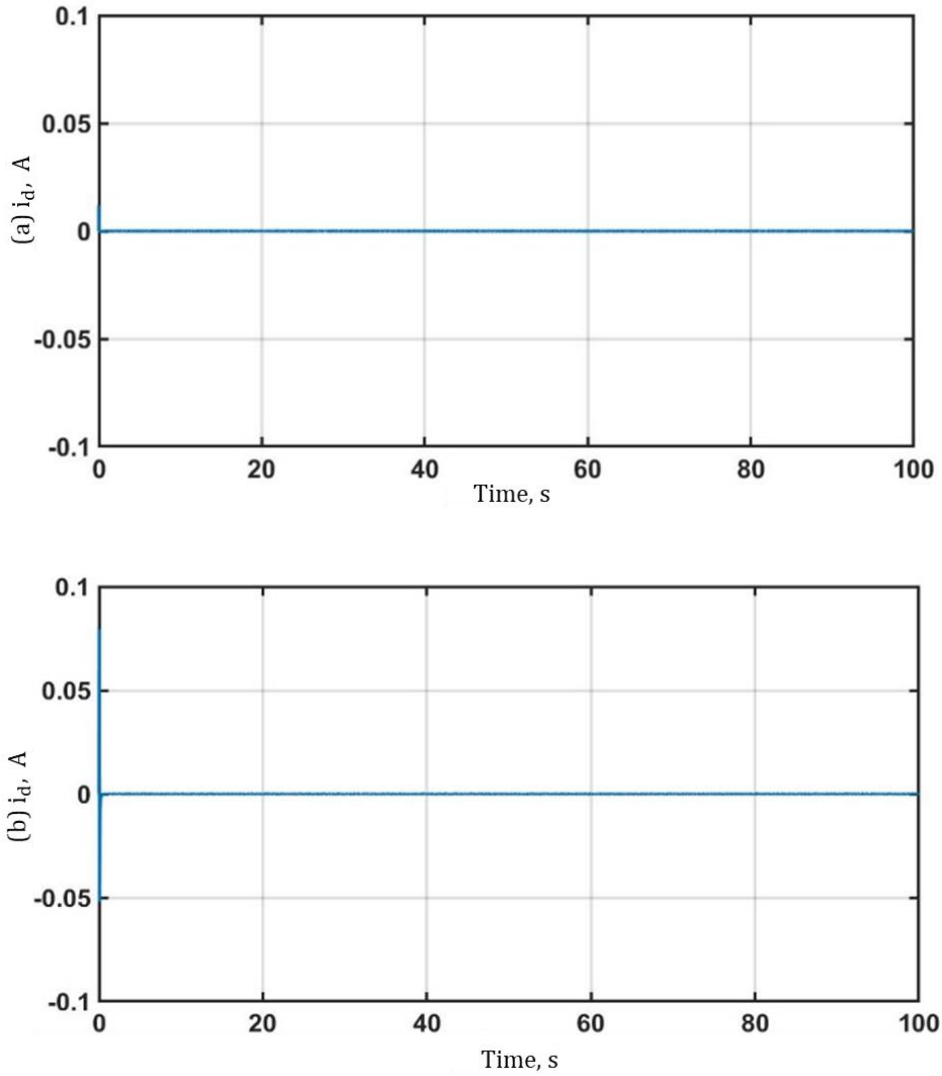

Figure 7.13. The direct current response for Scenario 2: (a) SDRE-based ISMC with HODOs, N=1 (b) SDRE-based ISMC with HODOs, N=2

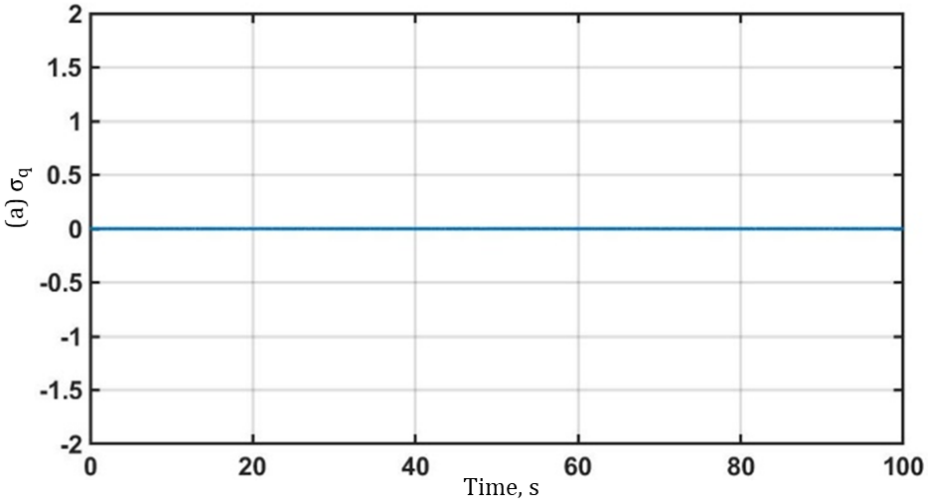

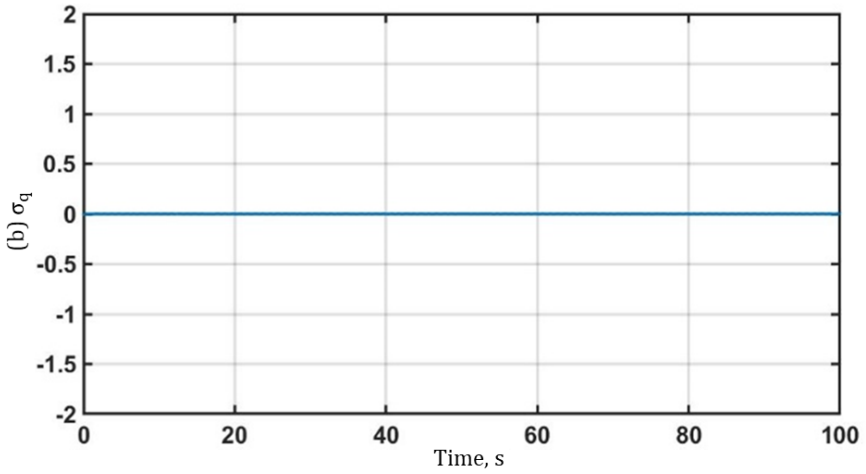

Figure 7.14. The quadrature axes sliding variable response for Scenario 2: (a) SDRE-based ISMC with HODOs, N=1 (b) SDRE-based ISMC with HODOs, N=2

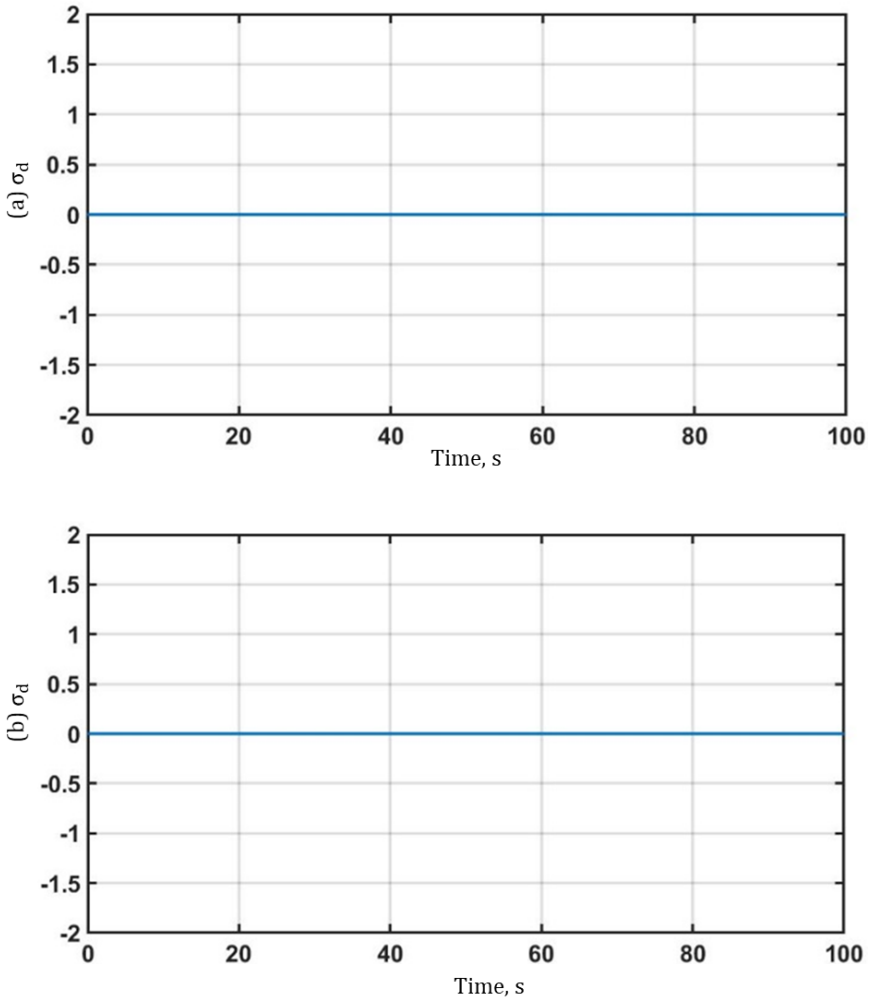

Figure 7.15. The direct axes sliding variable response for Scenario 2: (a) SDRE-based ISMC with HODOs, N=1 (b) SDRE-based ISMC with HODOs, N=2

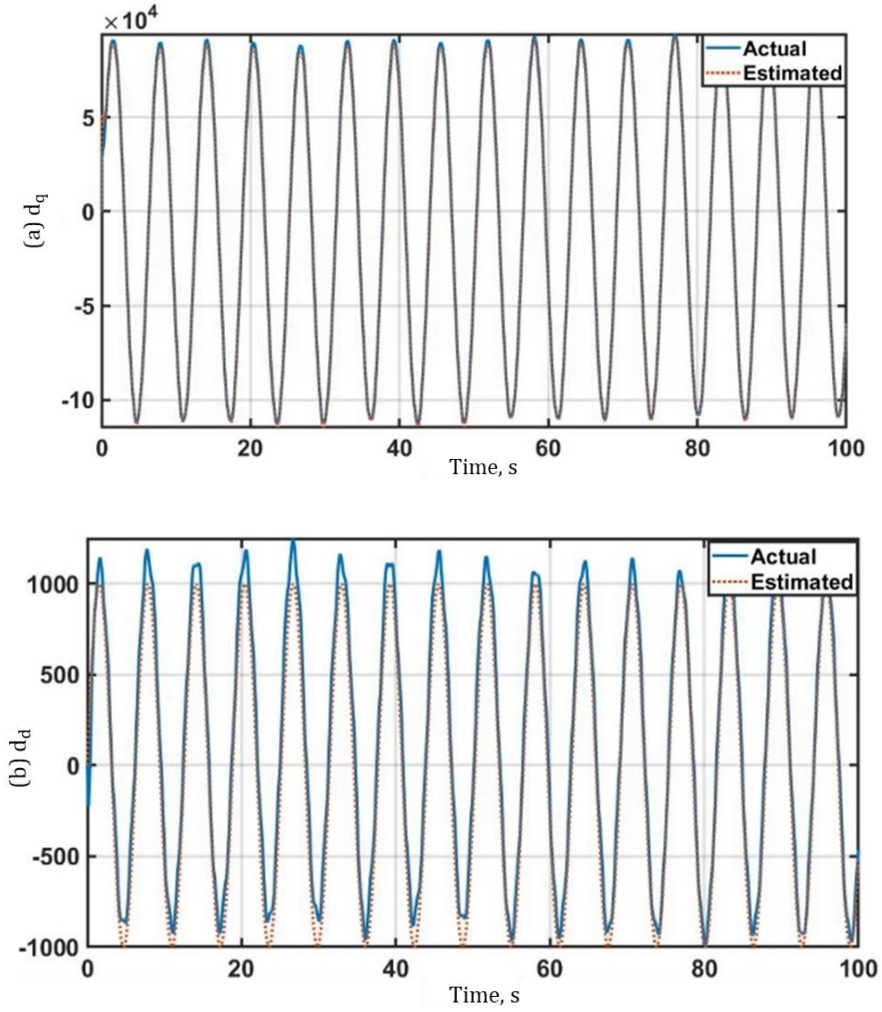

Figure 7.16. The model uncertainty with noise in the system for Scenario 2, N=1: (a) the quadrature axes disturbance estimated by HODO; (b) the direct axes disturbance estimated by HODO

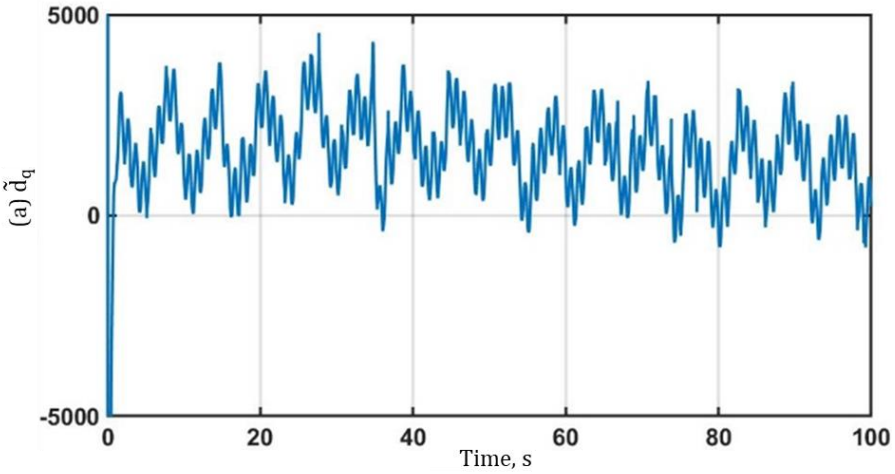

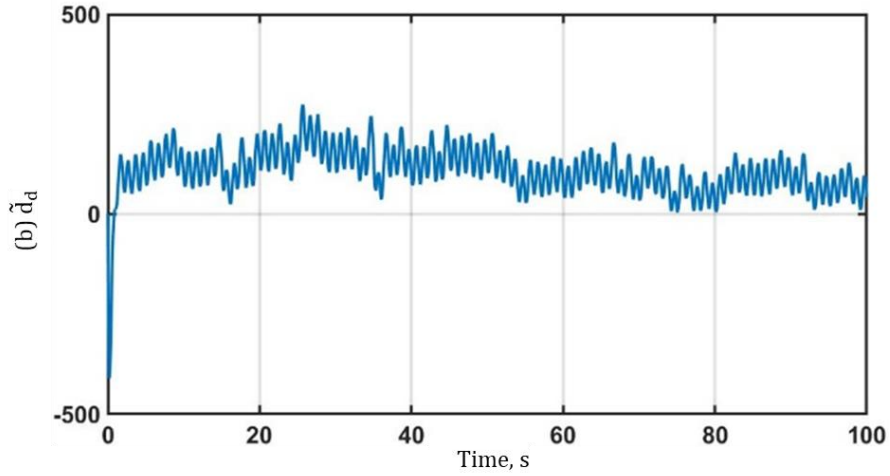

Figure 7.17. The model uncertainty with noise estimations errors in the system for Scenario 2, N=1: (a) the quadrature axes disturbance estimation errors; (b) the direct axes disturbance estimation errors

The model uncertainty caused by some parameter variations with noise are estimated by HODOs ($\hat{d}_q$ and $\hat{d}_d$) for both control channels (Figures 7.16 and 7.18). The estimated disturbances are compensated in feedforward terms of the proposed control system.

7.3. Simulation results of servomechanism-based SDRE control for WECS application

To apply the proposed SDRE control with servomechanism, the Matlab/Simulink simulation model of WECS with PMSG has been formulated. The 5 kW power PMSG-based WECS parameters are given above (Table 7.1). The control settings are given in Table 7.5. The power coefficient C_p is predefined graphically as $\lambda_{opt} = 11$ and $C_{max}^{p} = 0.411$ (Figure 3.7). The wind speed (v) profile with a mean value of 12.13 m/sec is shown in Figure 6.20. To test the performance of the proposed control under various sources of disturbances caused by external factors, incorrect setting of the model parameters in the control system [69] or the impact of increased ambient temperature around PMSG [100], the control parameters have been set (Table 6.9). In scenario 2, the variations of the electrical parameters have been changed that the stator resistance, R_s is extended by 20% and stator inductance L is added 1% from nominal parameters as in [9] (Table

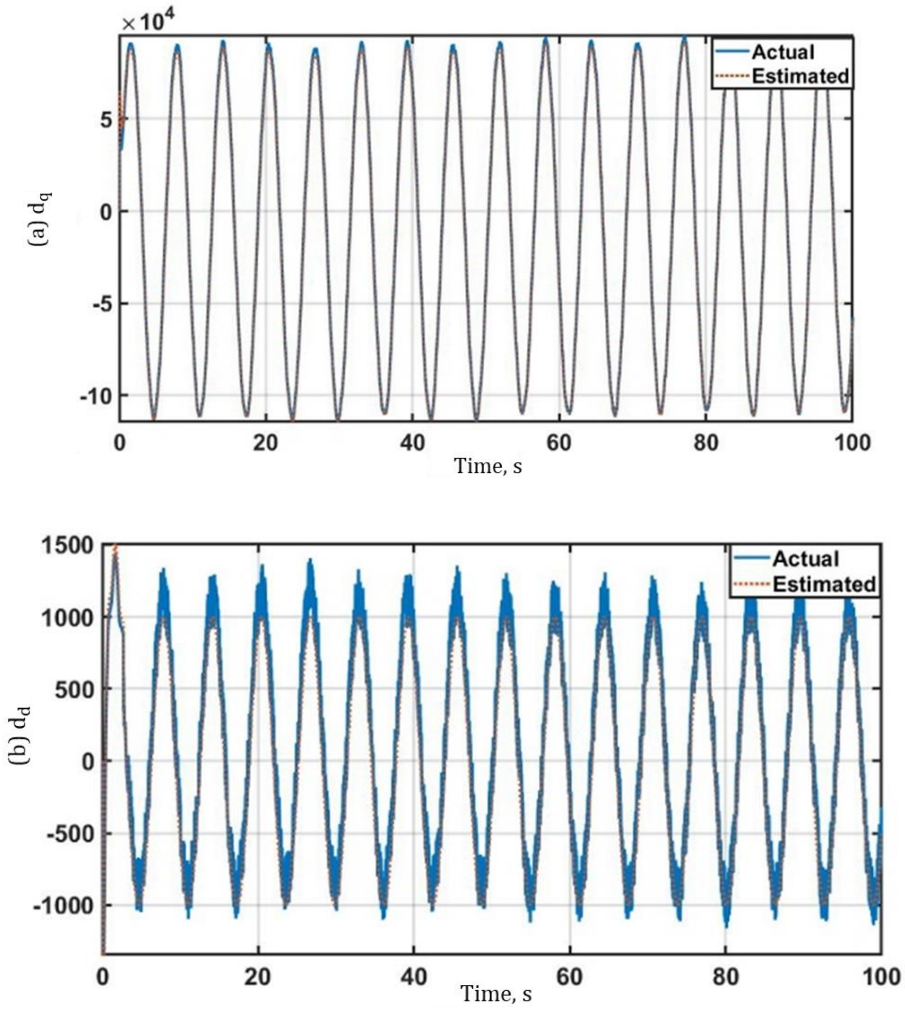

Figure 7.18. The model uncertainty with noise in the system for Scenario 2, N=2: (a) the quadrature axes disturbance estimated by HODO; (b) the direct axes disturbance estimated by HODO

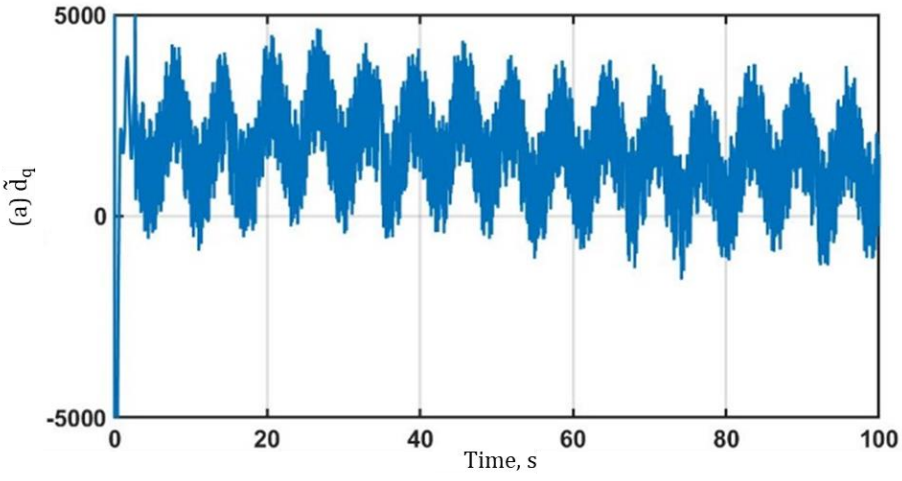

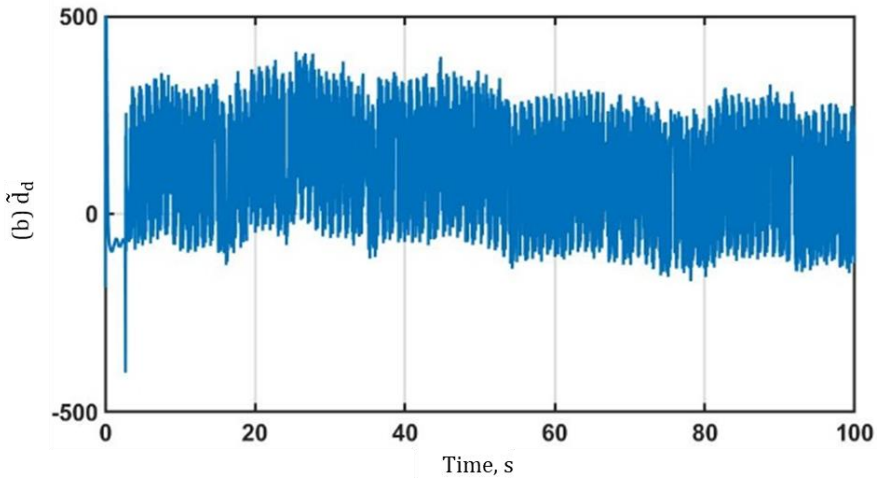

Figure 7.19. The model uncertainty with noise estimations errors in the system for Scenario 2, N=2: (a) the quadrature axes disturbance estimation errors; (b) the direct axes disturbance estimation errors

6.7). Also, to evaluate the proposed HODO-based SDRE control with servomechanism under noise $d_{qn} = 10^5 \sin(t)$ and $d_{dn} = 10^3 \sin(t)$ has been injected into the WECS.

Table 7.5. The servomechanism-based SDRE control system parameters

Controllers and Observers, solver type	**Parameters and Gains**
SDRE tuning gains	Q=diag([1 10000 1000 1]), R=diag([0.0005 0.0005])
SDRE terms, N	3
Observers for compensations of parameters uncertainties, modelling errors and noise	No
Matlab solvers' commands	***care & lyap***
HODO's observer gains for estimation of aerodynamic torque, T_a	L_{11}=50, L_{12}=250, L_{13}=500

By solving ARE equations (5.70) and Lyapunov equations (5.71) and (5.72) with N = 1, 2, 3 number of terms of Taylor's series, the near-optimal gains matrices can be obtained.

The simulations of the proposed near-optimal control with servomechanism demonstrate the improvements in tracking the angular shaft speed in the WECS than with conventional SDRE control using HODOs compensation techniques even under some parameters variations, external disturbance and noise [9], [16], [17]. The performance of the absolute angular shaft speed error under the proposed HODO-based near-optimal control with servomechanism is presented in Table 7.6.

It has been estimated that the MAPEs of the angular shaft speed tracking of the proposed control are improved under scenarios 1 and 2: with N=0 by 69.51% and 69.06%; with N=1 by 69.15% in both cases; with N=2 by 78.58% and 77.99%; with N=3 by 80.67% and 80.05% respectively. The angular shaft speed tracking errors $\tilde{\omega}$ of the servomechanism-based SDRE control with N=0,1,2,3 as well as the conventional SDRE control with N=2 are shown in Figures 7.25 and 7.29 for both scenarios.

Table 7.6. The performance of the proposed SDRE control with servomechanism for the WECS application

Assessment criteria and cases		**Scenario 1**	**Scenario 2**	**Improved by, %**
MAPE of angular shaft speed tracking, $\lvert\tilde{\omega}\rvert$	Conventional SDRE N=2 [9]	2.1957	2.2171	n/a
	LQR-based Integral SMC [8]	2.2361	2.2361	-1.84/-0.85
	Proposed SDRE with N=0 [8]	0.6694	0.6859	69.51/ 69.06
	Proposed SDRE with N=1	0.6681	0.684	69.15/ 69.15
	Proposed SDRE with N=2	0.4704	0.4879	78.58/ 77.99
	Proposed SDRE with N=3	0.4245	0.4423	80.67/80.05

Continued Table 7.6.

Assessment criteria and cases		**Scenario 1**	**Scenario 2**	**Improved by, %**
MAPE of electromagnetic torque, $\lvert\widetilde{T}_e\rvert$	Conventional SDRE N=2 [9]	4.8227	4.8246	n/a
	LQR-based Integral SMC [8]	4.8227	4.8227	-/0.04
	Proposed SDRE with N=0 [8]	4.8672	4.8678	-0.896/ -0.895
	Proposed SDRE with N=1	4.8644	4.8636	-0.837/-0.808
	Proposed SDRE with N=2	4.8576	4.8633	-0.697/-0.802
	Proposed SDRE with N=3	4.8797	4.8877	-1.155/-1.308
MAE of direct current, $\lvert i_d\rvert$, A	Conventional SDRE N=2 [9]	0.0084	0.000483	n/a
	LQR-based Integral SMC [8]	0.000476	0.000475	0.007924/0.000006
	Proposed SDRE with N=0 [8]	0.8481	0.7277	0.8397/0.727217
	Proposed SDRE with N=1	0.8843	0.764	0.8759/0.760517
	Proposed SDRE with N=2	0.8856	0.765	0.8772/0.764517
	Proposed SDRE with N=3	0.6145	-0.7415	0.6061/-0.741983
MAPE of aerodynamic torque estimation, $\lvert\widetilde{T}_a\rvert$	For all cases is unchanged	0.0738	0.0703	N/a

It should be noted that the LQR-based linear output feedback controller [15], [16], and ISMC with linear feedback of the nominal part [8], [9] produce the acceptable results

in nominal scenario. However, their performance is sensitive to the model uncertainty with noise, and nonlinear dynamics of the system. The MAPEs of electromagnetic torque of the proposed control are increased under scenario 1 and 2: with N=0 by 0.896% and 0.895%; with N=1 by 0.837% and 0.808%; with N=2 by 0.697% and 0.802%; with N=3 by 1.155% and 1.308% respectively. The comparisons of the transient response of electromagnetic torque tracking reference under proposed and conventional SDRE controls are shown in Figures 7.26 and 7.30. Also, the MAE of the direct current is increased under proposed control with N=0 by 0.8397A and 0.727217A; with N=1 by 0.8759A and 0.760517A; with N=2 by 0.8772A and 0.764517A; with N=3 by 0.6061A and 0.741983A for scenario 1 and 2 respectively. The comparisons of the transient response of direct current converging to zero under proposed and conventional SDRE controls are shown in Figures 7.27 and 7.31.

In scenario 2, the parameters variations of R_s and L due to changing ambient temperature as well as noise are caused. The PMSG's model uncertainty (d_q, and d_d) with noise injected into the WECS for assessing the robustness of the proposed control system are shown in Figure 7.32 (a) and (b).

It should be noted, that the proposed servomechanism-based SDRE nonlinear output feedback controller does not use disturbance observers' compensation techniques. According to the optimal control practices, further tuning gain matrices Q and R towards increasing require more control efforts to improve the tracking performance. Also, increasing the number of the approximating terms of SDRE solution (N) makes the simulation of the model complex even with available high-performance computers.

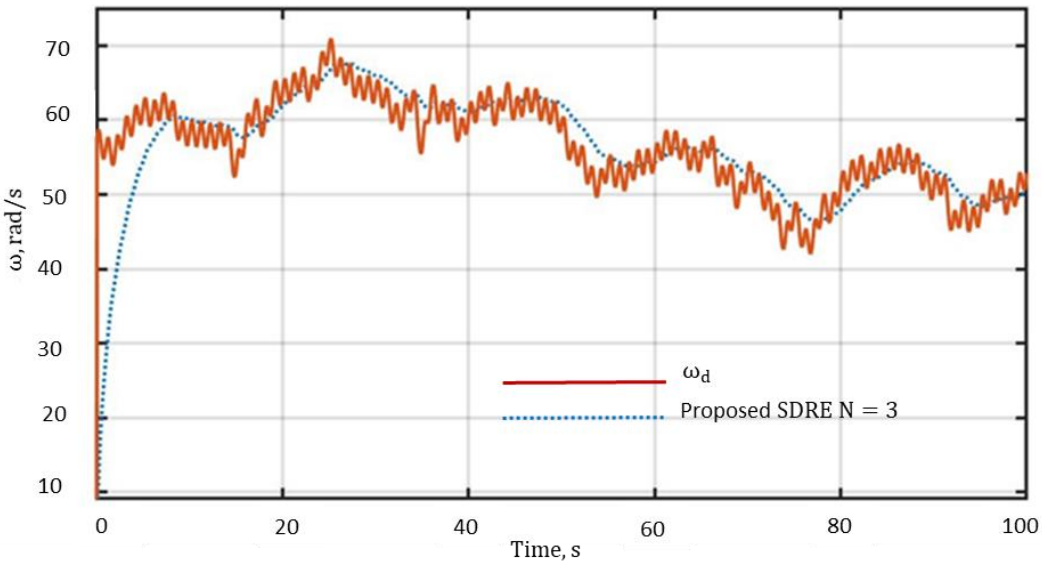

Figure 7.20. The angular shaft speed tracking under the proposed servomechanism-based SDRE control for Scenario 1, N=3

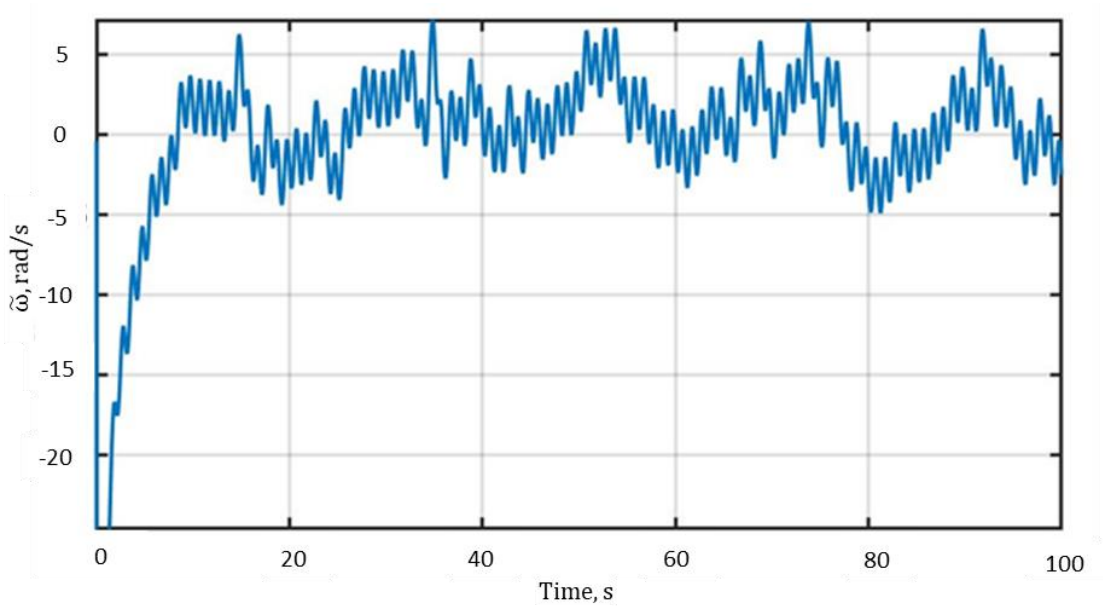

Figure 7.21. The angular shaft speed tracking errors under the proposed servomechanism-based SDRE control for Scenario 1, N=3

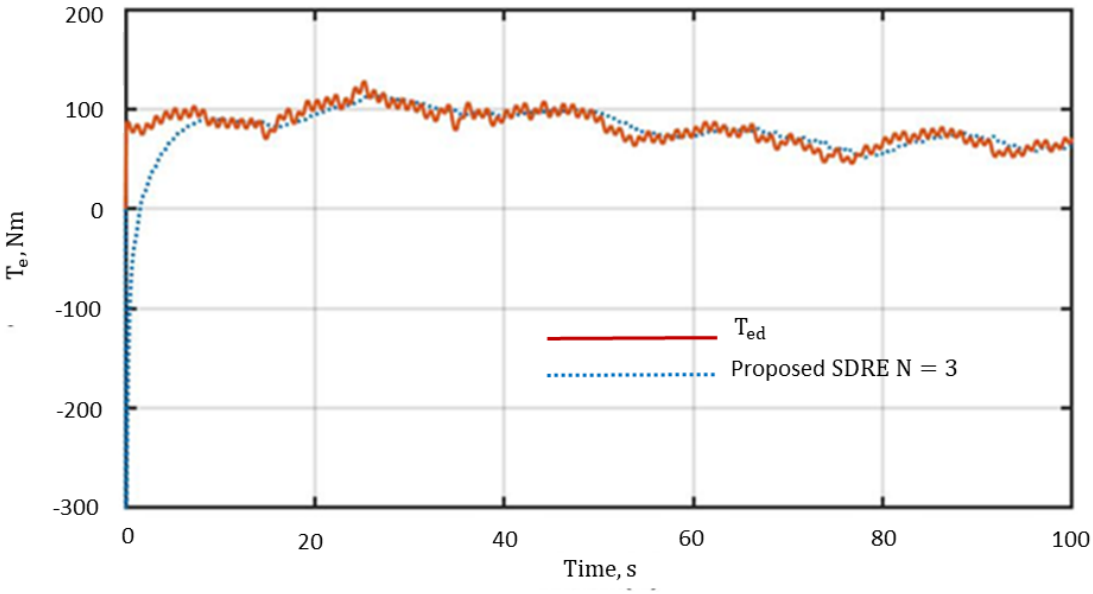

Figure 7.22. The electromagnetic torque tracking under the proposed servomechanism-based SDRE control for Scenario 1, N=3

While the MAPE criterion is suitable to evaluate the controller's performance between the defined nominal parameters and maximum possible model uncertainty cases (scenarios 1 and 2), the root means square error (RMSE) criterion is suitable for evaluation of controllers' statistics with Gaussian distribution [101]. This criterion can demonstrate the performance of the proposed control scheme with randomly distributed parameters in case of the model uncertainty of the controlled system. The RMSE of angular shaft speed for the proposed method with various numbers of Taylor series approximated terms have been

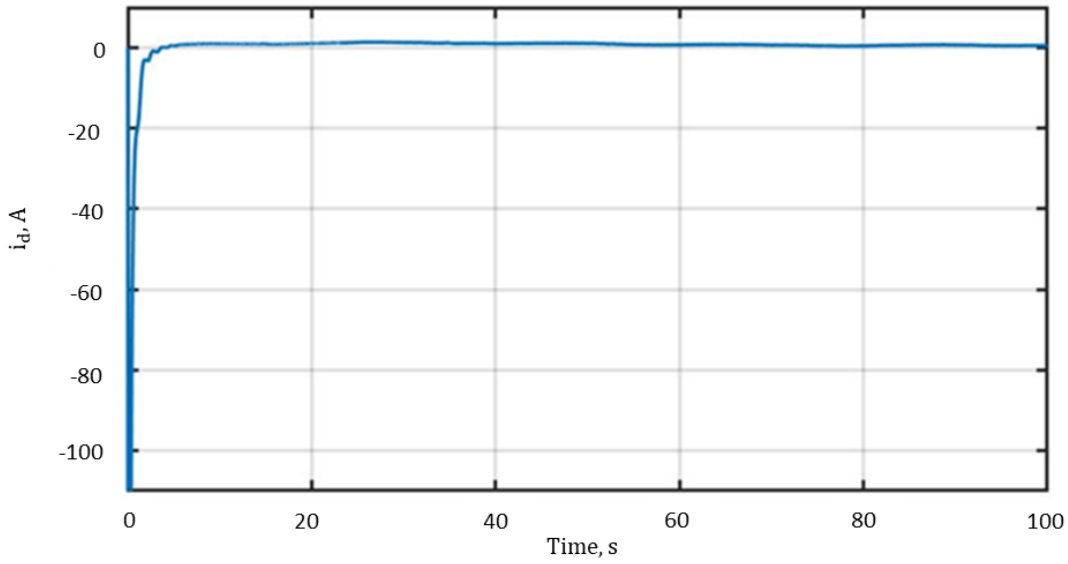

Figure 7.23. The direct current response under the proposed servomechanism-based SDRE control for Scenario 1, N=3

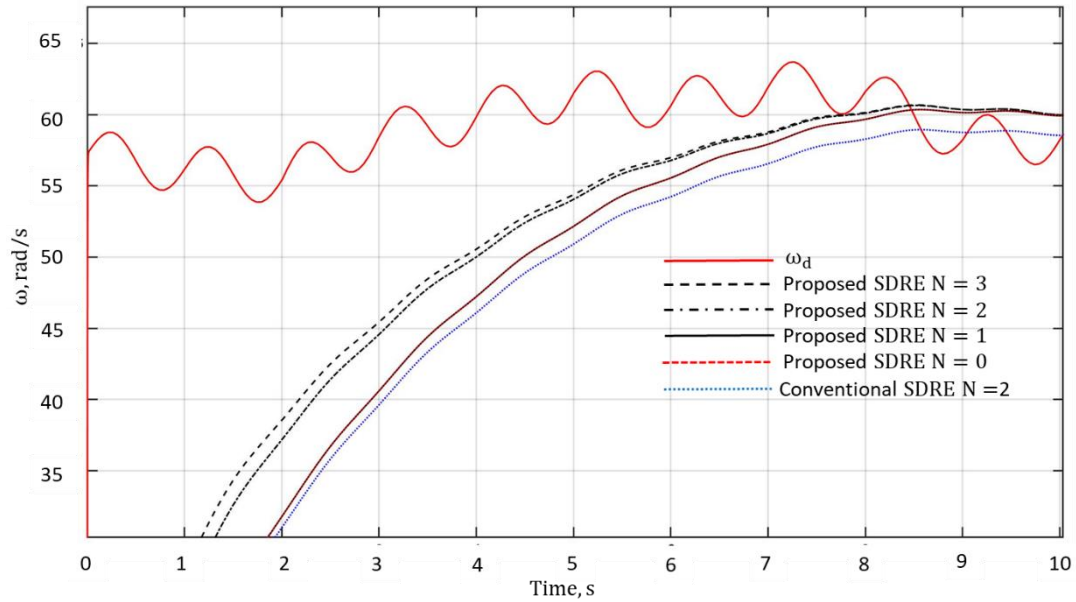

Figure 7.24. The comparison of the angular shaft speed transient responses under the proposed servomechanism-based SDRE control and conventional SDRE with HODOs compensation for Scenario 1

evaluated against conventional HODOs-based SDRE control. The proposed HODO-based near-optimal control with servomechanism with N=0, 1, 2, and 3, the RMSE of $\tilde{\omega}$ are 4.1166, 3.936, 2.26 and 2.0575 respectively (Table 7.7).

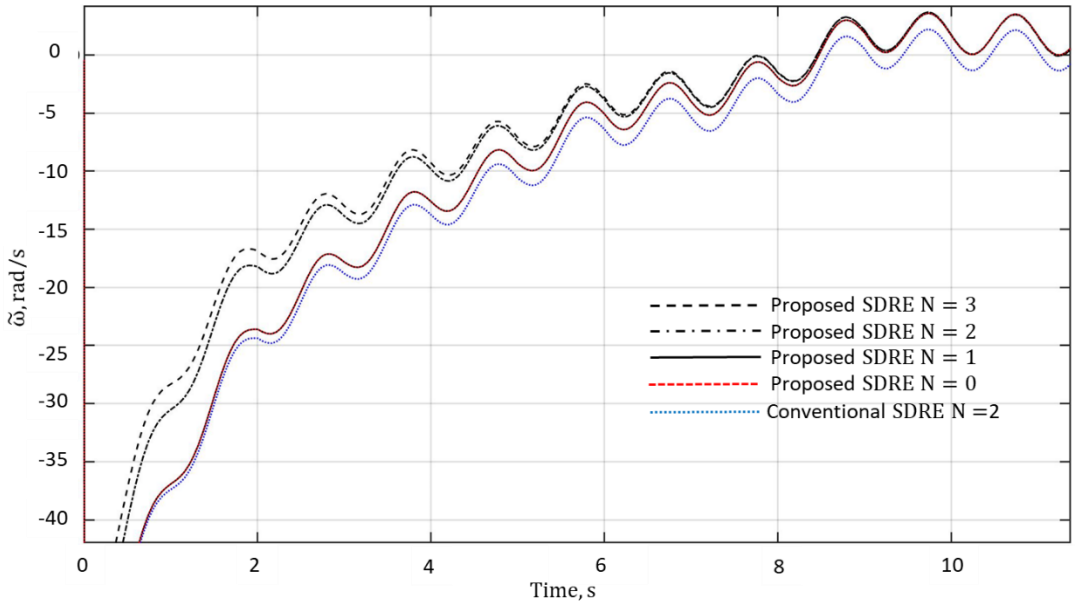

Figure 7.25. The comparison of the angular shaft speed errors under the proposed servomechanism-based SDRE control and conventional SDRE with HODOs compensation for Scenario 1

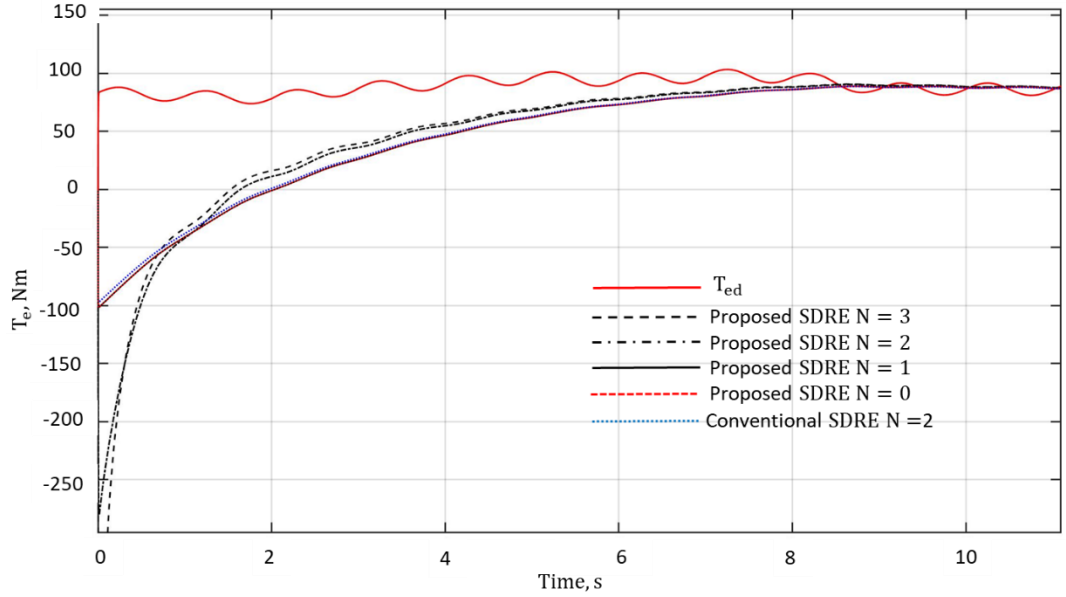

Figure 7.26. The comparison of the electromagnetic torque transient responses under the proposed servomechanism-based SDRE control and conventional SDRE with HODOs compensation for Scenario 1

Although the performances of the proposed control system with N=0, 1, 2, and 3 Taylor's series approximating terms can demonstrate a significant insight into the proposed control, its performance with randomly ranged system parameters is not provided. To facilitate the additional evaluation of the proposed control method are given as in[102], the

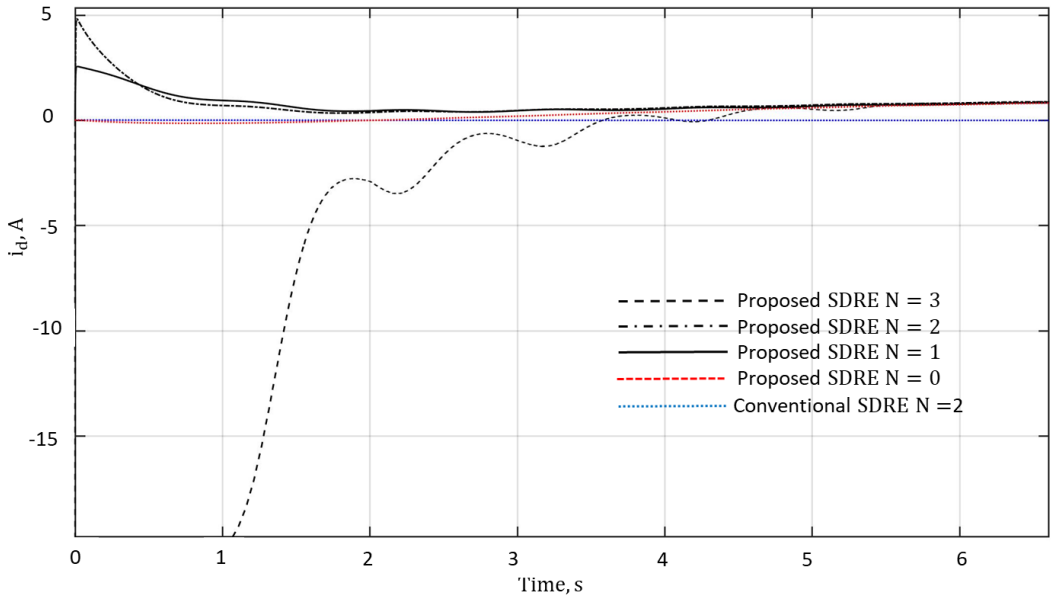

Figure 7.27. The comparison of the direct current transient responses under the proposed servomechanism-based SDRE control and conventional SDRE with HODOs compensation for Scenario 1

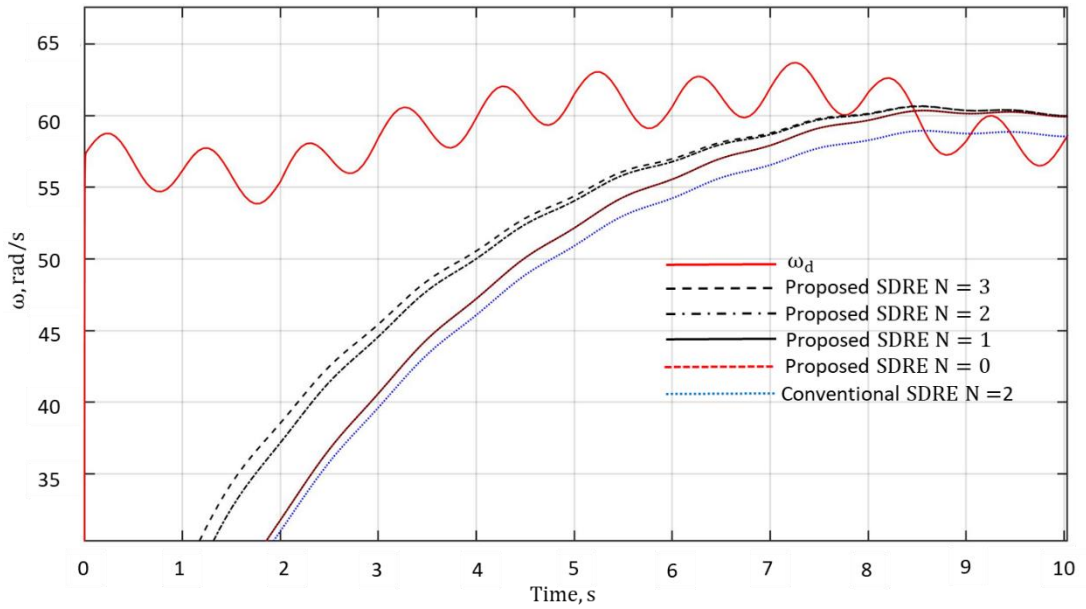

Figure 7.28. The comparison of the angular shaft speed transient responses under the proposed servomechanism-based SDRE control and conventional SDRE with HODOs compensation for Scenario 2

20 simulations with the identical wind profile, as well as tuning gain matrices have been run for all considered controllers. The random variations of the parameters between the

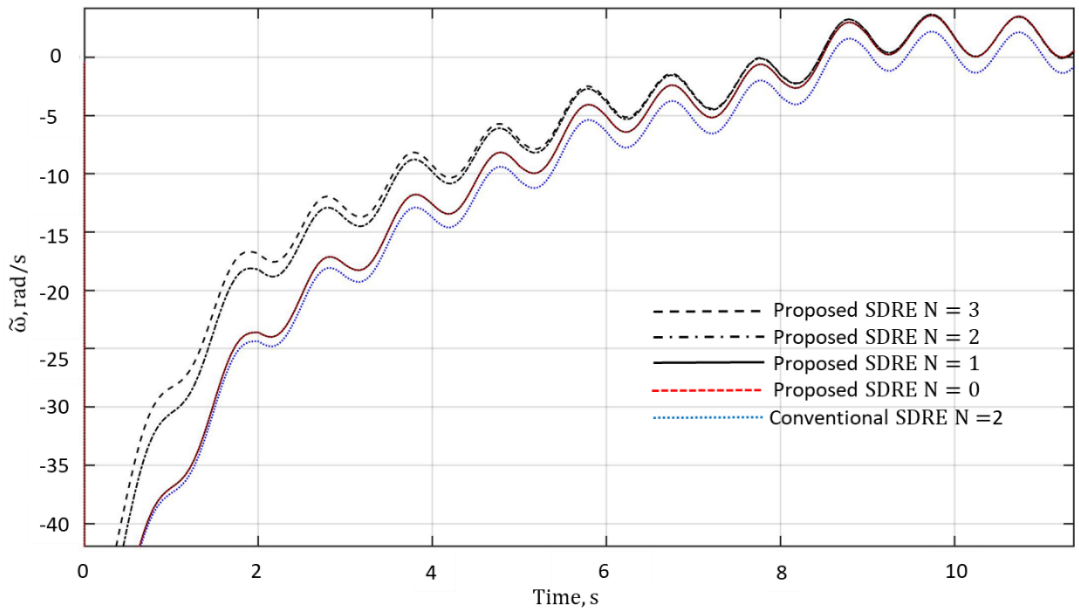

Figure 7.29. The comparison of the angular shaft speed errors under the proposed servomechanism-based SDRE control and conventional SDRE with HODOs compensation for Scenario 2

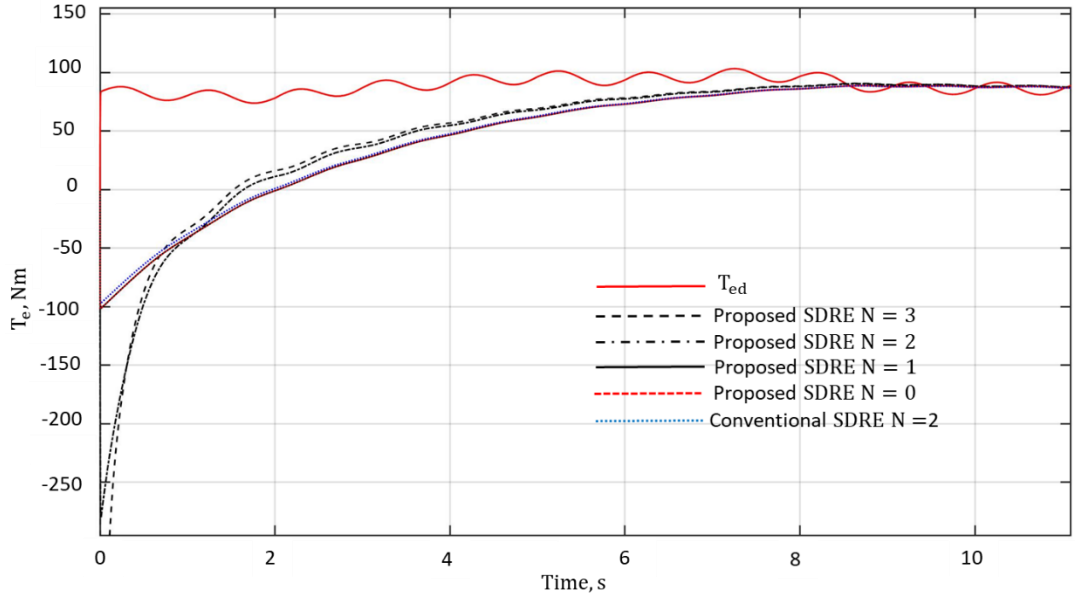

Figure 7.30. The comparison of the electromagnetic torque transient responses under the proposed servomechanism-based SDRE control and conventional SDRE with HODOs compensation for Scenario 2

nominal value and the maximum allowed values are ranged from their nominal values, R_s within 100% - 120%, and L 100% - 101% respectively.

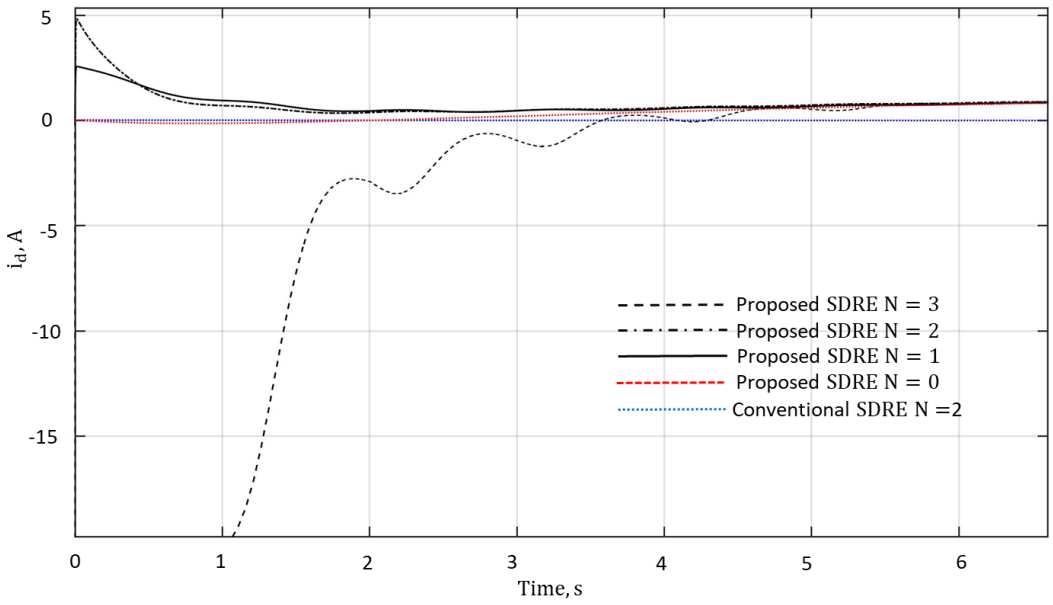

Figure 7.31. The comparison of the direct current transient responses under the proposed servomechanism-based SDRE control and conventional SDRE with HODOs compensation for Scenario 2

Table 7.7. The RMSE of the state variables of the proposed control system with one random selection of parameters (L, R_s) in the defined ranges

State variable	**Proposed SDRE with N=0 [8]**	**Proposed SDRE with N=1 [8]**	**Proposed SDRE with N=2 [8]**	**Proposed SDRE with N=3 [8]**	**Conventional SDRE N=2 [9]**	**LQR-based Integral SMC [8]**
$\tilde{\omega}$	4.1166	3.9360	2.26	2.0575	6.8634	3.9633
$\tilde{T}_e$	41.9585	40.1454	5.5659×10^3	5.6797×10^3	21.7313	39.7244
i_d	0.9203	1.3486	59.1551	2.6122×10^3	247.9766	4.7822×10^{-4}

Then, the parameter variations were randomly assigned within a defined range using a uniform probability distribution. The means of RMSEs of the state variables of the proposed control, and the conventional controls are shown in Table 7.8. The results mainly demonstrate the reduction of the mean RMSEs of the angular shaft speed errors in the proposed control while the number of the approximated Taylor's terms is increased. In addition, the proposed control demonstrates the ability to suppress the model uncertainty

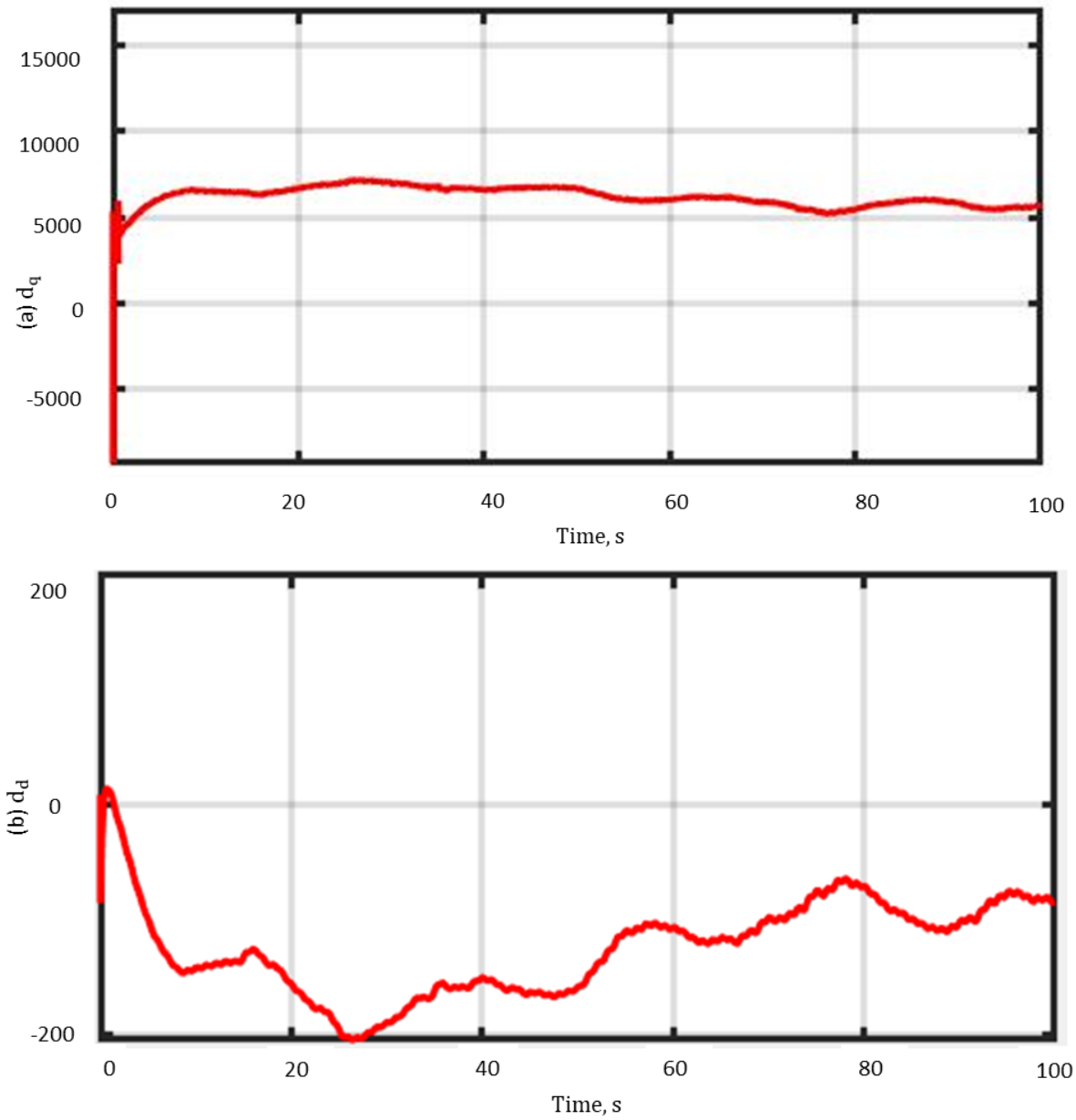

Figure 7.32. The model uncertainty and noise in the WECS injected in Scenario 2: (a) The quadrature axis disturbance quantity b) The direct axis disturbance quantity

with servomechanism based nonlinear feedback control without the use of the compensating scheme.

7.4.Summary of Chapter 7

In this chapter, the simulation results of the proposed SDRE-based ISMC and servomechanism-based SDRE control systems to improve the angular shaft speed

tracking performance in direct-driven variable-speed WECS. The reduction of the tracking errors enable to maximize the power extraction whereas the assumptions that fixing pitch angle and regulation of DC-link voltage are in place.

Table 7.8. The mean of RMSE of the proposed control system for 20 simulations with randomly selected parameters (L, R_s) in the defined ranges

State variable	**Proposed SDRE with N=0 [8]**	**Proposed SDRE with N=1 [8]**	**Proposed SDRE with N=2 [8]**	**Proposed SDRE with N=3 [8]**	**Conventional SDRE N=2 [9]**	**LQR-based Integral SMC [8]**
$\tilde{\omega}$	4.0897	3.8562	2.035	2.0303	6.7851	3.87089
$\tilde{T}_e$	40.458	39.9847	5.5163×10^3	5.6054×10^3	20.2305	39.0210
i_d	0.9145	1.2657	58.0245	2.5301×10^3	245.4103	4.6981×10^{-4}

Firstly, the nominal performance of the proposed SDRE-based ISMC has been presented and evaluated under reduction of the MAPE of angular shaft speed whereas the MAPE of electromagnetic torque and the ME of direct current also are shown. The number of approximating terms of SDRE control has been equal to two where N=0 is identical to the ISMC with linear feedback scheme.

The proposed SDRE-based ISMC with HODOs (N=2) has demonstrated the improvement of MAPE of angular shaft speed by 0.25%/0.25%/0.22% than in LQR, conventional ISMC, and SMC methods respectively. Then, the proposed SDRE-based ISMC with HODOs (N=2) has been tested under parameter variations with noise (scenario 2) where the angular shaft speed tracking has shown the superiority by 0.26%/0.26%/0.23% over LQR, conventional ISMC, and SMC methods respectively. Similarly, the proposed servomechanism-based SDRE control (N=3) has been evaluated under nominal scenario and impact of model uncertainty. The MAPEs of angular shaft speed have been reduced by 80.67% and 80.05% over conventional SDRE control with compensation scheme with HODOs. Furthermore, the proposed control systems' performances have been evaluated under RMSE criterion when the parameters varied with Gaussian distributions. This evaluations has shown that the performance is robust to various source of the disturbances.

Chapter 8: Conclusions and further research

7.1.Conclusions

This chapter will make concluding remarks by summarising of the main contributions associated with the proposed control systems in improvement their performances under influence of the disturbances. Also, it will review the limitations of the proposed control methods and provide the opportunity for further research.

This study aimed to design the control systems which are insensitive to various sources of disturbances in the PM electric machine applications such as servo motor speed control and WECS with PMSG. The simulation and experimental results show that their nominal tracking performances are improved but also in the presence of model uncertainty with noise and external disturbances. Furthermore, the model-based proposed control systems demonstrate to account for the nonlinearities in the systems with SDRE control method.

The key findings of the study have been presented in the 2019 International Conference on System Science and Engineering (ICSSE), 10th International Conference on Smart Grid (icSmartGrid), and published in the pier-reviewed journal such as IEEE Access and Optimal Control Applications and Methods.

The first proposed SOFCL-based SMC has been equipped with HODO to compensate load torque disturbance in the speed controller of the PMSM servo-system. The second proposed discrete-time PI-PI cascade system has been synthesized with HODO for total disturbance compensation in PI speed controller with back-calculation-based anti-windup scheme of the PMSM system. The third proposed SDRE-based ISMC controller has been integrated with HODOs for estimation wind speed and model uncertainty in the WECS. The SDRE control is used to account for nonlinearities whereas DOs estimate the aerodynamic torque which defines reference for the angular shaft in the variable-speed WECS, and the uncertainties associated with parameter variations with noise in the system. Finally, the proposed SDRE control has been developed with servomechanism. While this approach uses HODO for the aerodynamic torque estimation, the HODOs for estimations of the model uncertainty has been eliminated.

There are number of the studies paying attentions to developing the control systems with disturbance rejecting capabilities. However, these studies are too complicated and lacking the detailed explanations to follow the exact implementation algorithms. Moreover, some of them is less suitable for high performance applications due to its requirement for central processing unit (CPU).

While the proposed control systems could improve the tracking performances under presence of various sources of disturbance via DOBC approach, the output regulation method enable to suppress them in the feedback scheme only. Since the servo PMSM and variable speed WECS with PMSG systems are highly nonlinear systems and with effects of various sources of disturbances such as load torque, noise, parameters uncertainties, and modelling errors to facilitate their high performance and stability, the proposed control systems acquire characteristics such as robustness, sensorless, actively rejecting disturbances, and fault-tolerant to facilitate precise tracking of prescribed commands. These characteristics to improve precision of the angular shaft speed regulation in the servo PMSM and maximize power extraction in the WECS application.

The study has some limitations such as in the model based control requires the precise value of the parameters of the machine. Although the electric machine's manufacturer provide the parameters, the parameters changes over long period of exploitation. In addition, the optimal controllers' parameters should be tuned regularly due to realistic operational condition. The WECS application utilises the assumptions that the pitch angle is fixed and DC-link voltage well-regulated for assessing only the performance of control systems of generator-side power converter. Finally, the WECS experimental validation has not been implemented due to project budget and time frame limitations.

8.2.Further research

The research study has proposed DO-based linear and nonlinear feedback controls to facilitate nominal performances in servo PMSM and WECS applications under various source of disturbances. The sensitivity of the proposed SDRE-based ISMC further tuning gain matrices Q and R with increasing number of approximating terms of the near-optimal solution require more detailed attention. Moreover, the closed-loop stability analysis of the HODO-based nonlinear control system require the investigation. However, these aspects of study have not been considered because they are outside of scope of the aim of study.

References list

[1] P. Pillay and R. Krishnan, “Modeling, simulation, and analysis of permanent-magnet motor drives. I. The permanent-magnet synchronous motor drive,” *IEEE Trans. Ind. Appl.*, vol. 25, no. 2, pp. 265–273, 1989, doi: 10.1109/28.25541.

[2] S. Li, J. Yang, W.-H. Chen, and C. Xisong, *Disturbance observer-based control: methods and applications*. Boca Raton-London-New York: CRC Press, 2014.

[3] H. Abu-Rub, A. Iqbal, and J. Guzinski, *High Performance Control of AC Drives with MATLAB/Simulink Models*. John Wiley and Sons, 2012. doi: 10.1002/9781119969242.

[4] X. X. Yin, Y. G. Lin, W. Li, H. W. Liu, and Y. J. Gu, “Fuzzy-Logic Sliding-Mode Control Strategy for Extracting Maximum Wind Power,” *IEEE Trans. Energy Convers.*, vol. 30, no. 4, pp. 1267–1278, 2015, doi: 10.1109/TEC.2015.2422211.

[5] T. D. Do, H. H. Choi, and J.-W. Jung, “SDRE-Based Near Optimal Control System Design for PM Synchronous Motor,” *IEEE Trans. Ind. Electron.*, vol. 59, no. 11, pp. 4063–4074, 2012, doi: 10.1109/TIE.2011.2174540.

[6] L. Qinghua, “Analysis, Design and Cotrol of Permanent Magnet Synchronous Motors for Wide-Speed Operation,” 2005. [Online]. Available: https://scholarbank.nus.edu.sg/handle/10635/15011

[7] B. Sarsembayev, T. Kalganova, Y. Zhetpissov, A. Kaibaldiyev, and T. D. Do, “Sliding mode control with High-order Disturbance Observer Design for Disturbance Estimation in SPMSM,” in *2019 International Conference on System Science and Engineering (ICSSE)*, 2019, pp. 542–547. doi: 10.1109/ICSSE.2019.8823109.

[8] K. Suleimenov, B. Sarsembayev, and T. Do, “Disturbance observer-based integral sliding mode control for wind energy conversion systems,” *Wind Energy*, vol. 23, no. 4, pp. 1026–1047, 2020, doi: 10.1002/we.2471.

[9] B. Sarsembayev, K. Suleimenov, B. Mirzagalikova, and T. D. Do, “SDRE-based Integral Sliding Mode Control for Wind Energy Conversion Systems,” *IEEE Access*, vol. 8, pp. 51100–51113, 2020, doi: 10.1109/access.2020.2980239.

[10] Sarsembayev, B, Zholtayev, D, Do, TD. Maximum power tracking of variable-speed wind energy conversion systems based on a near-optimal servomechanism control system. Optim Control Appl Meth. 2022; 43(3): 904– 924. doi:10.1002/oca.2863

[11] B. Sarsembayev, K. Suleimenov, and T. D. Do, “High Order Disturbance Observer Based PI-PI Control System with Tracking Anti-Windup Technique for Improvement of Transient Performance of PMSM,” *IEEE Access*, vol. 9, pp. 66323–66334, 2021, doi: 10.1109/ACCESS.2021.3074661.

[12] J. W. Jung, V. Q. Leu, T. D. Do, E. K. Kim, and H. H. Choi, “Adaptive PID speed control design for permanent magnet synchronous motor drives,” *IEEE Trans. Power Electron.*,

vol. 30, no. 2, pp. 900–908, 2015, doi: 10.1109/TPEL.2014.2311462.

[13] T. D. Do, S. Kwak, and H. H. Choi, “Suboptimal Control Scheme Design for Interior Permanent-Magnet Synchronous Motors: An SDRE-Based Approach,” *IEEE Trans. Power Electron.*, vol. 29, no. 6, pp. 3020–3031, 2014, doi: 10.1109/TPEL.2013.2272582.

[14] J. Yang, W. Chen, S. Member, S. Li, and S. Member, “Disturbance / Uncertainty Estimation and Attenuation Techniques in PMSM Drives — A Survey,” *IEEE Trans. Ind. Electron.*, vol. 64, no. 4, pp. 3273–3285, 2017.

[15] A. V. Le and T. D. Do, “High-order observers-based LQ control scheme for wind speed and uncertainties estimation in WECSs,” *Optim. Control Appl. Methods*, vol. 39, no. 5, pp. 1818–1832, 2018, doi: 10.1002/oca.2444.

[16] V. P. Vu and T. D. Do, “A novel nonlinear observer-based LQ control system design for wind energy conversion systems with single measurement,” *Wind Energy*, vol. 22, no. 8, pp. 1134–1147, 2019, doi: 10.1002/we.2345.

[17] V. P. Vu and T. D. Do, “Observer-Based LQR for Wind Energy Conversion Systems with Single Measurement,” in *Proceedings GTSD -IEEE*, 2018, pp. 77–81. doi: 10.1109/GTSD.2018.8595673.

[18] H. H. Choi, E. K. Kim, D. Y. Yu, J. W. Jung, and T. H. Kim, “Precise PI speed control of permanent magnet synchronous motor with a simple learning feedforward compensation,” *Electr. Eng.*, vol. 99, no. 1, pp. 133–139, 2017, doi: 10.1007/s00202-016-0407-0.

[19] T. D. Do, Y. N. Do, and P. D. Dai, “A robust suboptimal control system design of chaotic PMSMs,” *Electr. Eng.*, vol. 100, no. 3, pp. 1455–1466, 2018, doi: 10.1007/s00202-017-0603-6.

[20] J. Chen, W. Yao, Y. Ren, R. Wang, L. Zhang, and L. Jiang, “Nonlinear adaptive speed control of a permanent magnet synchronous motor: A perturbation estimation approach,” *Control Eng. Pract.*, vol. 85, pp. 163–175, 2019, doi: https://doi.org/10.1016/j.conengprac.2019.01.019.

[21] A. Hezzi, M. N. Abdelkrim, and S. B. Elghali, “Sensorless Backstepping Drive for a Five-Phase PMSM based on Unknown Input Observer,” in *2020 20th International Conference on Sciences and Techniques of Automatic Control and Computer Engineering (STA)*, 2020, pp. 125–130. doi: 10.1109/STA50679.2020.9329327.

[22] G. Huang, J. Li, E. F. Fukushima, C. Zhang, J. He, and K. Zhao, “An improved equivalent-input-disturbance approach for PMSM drive with demagnetization fault,” *ISA Trans.*, vol. 105, pp. 120–128, 2020, doi: https://doi.org/10.1016/j.isatra.2020.06.010.

[23] K. Zhao et al., "Demagnetization-Fault Reconstruction and Tolerant-Control for PMSM Using Improved SMO-Based Equivalent-Input-Disturbance Approach," in IEEE/ASME Transactions on Mechatronics, vol. 27, no. 2, pp. 701-712, April 2022, doi: 10.1109/TMECH.2021.3069787.

[24] L. Xiaoquan, L. Heyun, and H. Junlin, “Load disturbance observer-based control method for sensorless PMSM drive,” *IET Electr. Power Appl.*, vol. 10, no. 8, pp. 735–743, Sep. 2016, doi: 10.1049/iet-epa.2015.0550.

[25] A. Kaibaldiyev, Y. Zhetpissov, B. Sarsembayev, and T. Do, “Combined H- ∞ and Integral Sliding Mode Controllers for Robust Speed Control of Permanent Magnet Synchronous Motor with Load Torque Observer,” in *2019 International Conference on System Science and Engineering (ICSSE)*, 2019, pp. 554–559. doi: 10.1109/ICSSE.2019.8823533.

[26] Y. Jiang, W. Xu, and C. Mu, “Robust Sliding Mode Speed Control with Adaptive Torque Observer for High Performance PMSM,” in *IEEE Vehicle Power and Propulsion Conference (VPPC)*, Oct. 2016, pp. 1–6. doi: 10.1109/VPPC.2016.7791770.

[27] L. Qu, W. Qiao and L. Qu, "An Extended-State-Observer-Based Sliding-Mode Speed Control for Permanent-Magnet Synchronous Motors," in IEEE Journal of Emerging and Selected Topics in Power Electronics, vol. 9, no. 2, pp. 1605-1613, April 2021, doi: 10.1109/JESTPE.2020.2990442.

[28] Y. Wang, H. T. Yu, N. J. Feng, and Y. C. Wang, “Non-cascade backstepping sliding mode control with three-order extended state observer for PMSM drive,” *IET Power Electron.*, vol. 13, no. 2, pp. 307–316, Feb. 2020, doi: https://doi.org/10.1049/iet-pel.2019.0819.

[29] D. Ke, F. Wang, L. He, and Z. Li, “Predictive Current Control for PMSM Systems Using Extended Sliding Mode Observer With Hurwitz-Based Power Reaching Law,” *IEEE Trans. Power Electron.*, vol. 36, no. 6, pp. 7223–7232, 2021, doi: 10.1109/TPEL.2020.3043489.

[30] E. Sariyildiz, R. Oboe, and K. Ohnishi, “Disturbance Observer-Based Robust Control and Its Applications: 35th Anniversary Overview,” *IEEE Trans. Ind. Electron.*, vol. 67, no. 3, pp. 2042–2053, 2020, doi: 10.1109/TIE.2019.2903752.

[31] J. Baran and A. Jąderko, “An MPPT Control of a PMSG-Based WECS with Disturbance Compensation and Wind Speed Estimation,” Energies, vol. 13, no. 23, p. 6344, Dec. 2020, doi: 10.3390/en13236344.

[32] T. D. Do, “Optimal control design for chaos suppression of PM synchronous motors,” *Proc. 2016 2nd Int. Conf. Control Sci. Syst. Eng. ICCSSE 2016*, pp. 88–92, 2016, doi: 10.1109/CCSSE.2016.7784359.

[33] T. D. Do, H. H. Choi, and J.-W. Jung, “Nonlinear Optimal DTC Design and Stability Analysis for Interior Permanent Magnet Synchronous Motor Drives,” *IEEE/ASME Trans. Mechatronics*, vol. 20, no. 6, pp. 2716–2725, 2015, doi: 10.1109/TMECH.2015.2426725.

[34] L. J. Cheng and M. C. Tsai, “Enhanced Model Predictive Direct Torque Control Applied to IPM Motor with Online Parameter Adaptation,” *IEEE Access*, vol. 9, pp. 42185–42199, 2020, doi: 10.1109/ACCESS.2020.2977057.

[35] L. Sun, X. Zhang, L. Sun, and K. Zhao, “Nonlinear speed control for PMSM system using sliding-mode control and disturbance compensation techniques,” *IEEE Trans. Power*

Electron., vol. 28, no. 3, pp. 1358–1365, 2013, doi: 10.1109/TPEL.2012.2206610.

[36] R. Errouissi, A. Al-Durra, and S. M. Muyeen, “Experimental Validation of a Novel PI Speed Controller for AC Motor Drives with Improved Transient Performances,” *IEEE Trans. Control Syst. Technol.*, vol. 26, no. 4, pp. 1414–1421, 2018, doi: 10.1109/TCST.2017.2707404.

[37] R. E. Precup, R. C. David, E. M. Petriu, M. B. Radac, and S. Preitl, “Adaptive GSA-based optimal tuning of PI controlled servo systems with reduced process parametric sensitivity, robust stability and controller robustness,” *IEEE Trans. Cybern.*, vol. 44, no. 11, pp. 2168–2267, 2014, doi: 10.1109/TCYB.2014.2307257.

[38] J. Espina, A. Arias, J. Balcells, and C. Ortega, “Speed Anti-Windup PI strategies review for Field Oriented Control of Permanent Magnet Synchronous Machines,” in *2009 Compatibility and Power Electronics*, 2009, pp. 279–285. doi: 10.1109/CPE.2009.5156047.

[39] K. J. Astrom and T. Hagglung, *Advanced PID Control*. NC, USA: ISA, 2006.

[40] Y. Zhetpissov, A. Kaibaldiyev, and T. D. Do, “PI anti-windup speed control of Permanent Magnet Synchronous Motor based on feedforward compensation,” in *2018 ELEKTRO*, 2018, pp. 1–8. doi: 10.1109/ELEKTRO.2018.8398275.

[41] V. Kumar, P. Gaur, and A. P. Mittal, “ANN based self tuned PID like adaptive controller design for high performance PMSM position control,” *Expert Syst. Appl.*, vol. 41, no. 17, pp. 7995–8002, 2014, doi: 10.1016/j.eswa.2014.06.040.

[42] Y. Shtessel, C. Edwards, L. Fridman, and A. Levant, *Sliding mode control and observation*. New York Heidelberg Dordrecht London: Springer, 2014. doi: 10.1007/978-0-8176-4893-0.

[43] T. D. Do, H. H. Choi, and J.-W. Jung, “θ-D Approximation Technique for Nonlinear Optimal Speed Control Design of Surface-Mounted PMSM Drives,” *IEEE/ASME Trans. Mechatronics*, vol. 20, no. 4, pp. 1822–1831, 2015, doi: 10.1109/TMECH.2014.2356138.

[44] K. D. Young, V. I. Utkin, and Ü. Özgüner, “A control engineer’s guide to sliding mode control,” *IEEE Trans. Control Syst. Technol.*, vol. 7, no. 3, pp. 328–342, 1999, doi: 10.1109/87.761053.

[45] X. Wu, H. Wang, X. Yuan, S. Huang, and D. Luo, “Design and implementation of recursive model predictive control for permanent magnet synchronous motor drives,” *Math. Probl. Eng.*, vol. 2015, pp. 1–10, 2015, doi: 10.1155/2015/431734.

[46] Z. Ma, S. Saeidi, and R. Kennel, “FPGA implementation of model predictive control with constant switching frequency for PMSM drives,” *IEEE Trans. Ind. Informatics*, vol. 10, no. 4, pp. 2055–2063, 2014, doi: 10.1109/TII.2014.2344432.

[47] J. Bae, J. Hwang, J. Park, and D. Kwag, “Modeling and experiments on eddy current damping caused by a permanent magnet in a conductive tube †,” *J. Mech. Sci. Technol.*,

vol. 23, pp. 3024–3035, 2009, doi: 10.1007/s12206-009-0819-0.

[48] H. A. Sodano and J. Bae, “Eddy Current Damping in Structures,” *Shock Vib. Dig.*, vol. 36, no. 6, pp. 469–478, 2004, doi: 10.1177/0583102404048517.

[49] Abdullah, J.-H. Ahn, and H.-Y. Kim, “Effect of Electromagnetic Damping on System Performance of Voice-Coil Actuator Applied to Balancing-Type Scale,” Actuators, vol. 9, no. 1, p. 8, Feb. 2020, doi: 10.3390/act9010008.

[50] G. Luo, R. Zhang, Z. Chen, W. Tu, S. Zhang, and R. Kennel, “A Novel Nonlinear Modeling Method for Permanent-Magnet Synchronous Motors,” *IEEE Trans. Ind. Electron.*, vol. 63, no. 10, pp. 6490–6498, 2016, doi: 10.1109/TIE.2016.2578839.

[51] K. S. Kim, K. H. Rew, and S. Kim, “Disturbance observer for estimating higher order disturbances in time series expansion,” *IEEE Trans. Automat. Contr.*, 2010, doi: 10.1109/TAC.2010.2049522.

[52] B. Nurtay, B. Duisenbay, and T. D. Do, “Direct-torque control system design using maximum torque per ampere method for interior permanent magnet synchronous motors,” in *12th International Conference ELEKTRO 2018, 2018 ELEKTRO Conference Proceedings*, 2018, pp. 1–6. doi: 10.1109/ELEKTRO.2018.8398286.

[53] A. A. Hassan, A. M. Kassem, and A. M. Kassem, “Modeling, Simulation and Performance Improvements of a PMSM Based on Functional Model Predictive Control,” *Arab J Sci Eng*, vol. 38, pp. 3071–3079, 2013, doi: 10.1007/s13369-012-0460-6.

[54] K. Suleimenov, M. H. Ali, and T. D. Do, “Integral Sliding Mode Controller Design for Permanent Magnet Synchronous Machines,” in *Proceeding ICSSE-IEEE*, 2019, pp. 548–553.

[55] G. Feng, C. Lai, and N. C. Kar, “A Closed-Loop Fuzzy-Logic-Based Current Controller for PMSM Torque Ripple Minimization Using the Magnitude of Speed Harmonic as the Feedback Control Signal,” *IEEE Trans. Ind. Electron.*, vol. 64, no. 4, pp. 2642–2653, 2017, doi: 10.1109/TIE.2016.2631524.

[56] G. Oussama and A. Douik, “Comparison between PI and fuzzy controllers in speed control of PMSM,” in *2017 International Conference on Green Energy Conversion Systems (GECS)*, Mar. 2017, pp. 1–7. doi: 10.1109/GECS.2017.8066123.

[57] H. Huang *et al.*, “Fuzzy sliding mode control of servo control system based on variable speeding approach rate,” *Soft Comput.*, vol. 23, no. 24, pp. 13477–13487, 2019, doi: 10.1007/s00500-019-03886-8.

[58] F. A. Bouaziz, Y. Bouteraa, and N. Derbel, “Control energy comparison bweeetn 1st and 2nd order sliding mode approach with application to a SCARA robot,” *13th Int. Multi-Conference Syst. Signals Devices, SSD 2016*, pp. 757–761, 2016, doi: 10.1109/SSD.2016.7473679.

[59] H. C. Liaw and B. Shirinzadeh, “Sliding-mode enhanced adaptive motion tracking control

of piezoelectric actuation systems for micro/nano manipulation," *IEEE Trans. Control Syst. Technol.*, vol. 16, no. 4, pp. 1103–1108, doi: 10.1109/ICARCV.2008.4795674.

[60] M. N. Audin and R. Goban, "Second-order sliding mode control design and experimental application to a servo motor," in *International Conference on Mechanical, System and Control Engineering*, 2017, pp. 141–144. doi: 10.1373/clinchem.2016.270876.

[61] F. M. Zaihidee, S. Mekhilef, and M. Mubin, "Robust Speed Control of PMSM Using Sliding Mode Control (SMC)A Review," *ENERGIES*, vol. 12, no. 1669, pp. 1–27, May 2019, doi: 10.3390/en12091669.

[62] S. H. Zak and S. Hui, "On Variable Structure Output Feedback Controllers for Uncertain Dynamic Systems," *IEEE Trans. Autom. Control*, vol. 38, no. 10, pp. 1509–1512, 1993.

[63] S. K. Bag, S. K. Spurgeon, and C. Edwards, "Output feedback sliding mode design for linear uncertain systems," *IEE Proc. - Control Theory Appl.*, vol. 144, no. 3, pp. 209–216, 1997, doi: 10.1049/ip-cta:19971122.

[64] A. Mehta and B. Bandyopadhyay, "Preliminaries of Sliding Mode Control," in *Frequency-Shaped and Observer-Based Discrete-time Sliding Mode Control*, vol. 2, Springer, 2015, pp. 9–25. doi: 10.1007/978-81-322-2238-5.

[65] Fridman, L., Levant, A. (1996). Higher order sliding modes as a natural phenomenon in control theory. In: Garofalo, F., Glielmo, L. (eds) Robust Control via Variable Structure and Lyapunov Techniques. Lecture Notes in Control and Information Sciences, vol 217. Springer, Berlin, Heidelberg. https://doi.org/10.1007/BFb0027563

[66] H. U. Suleiman, M. B. Mu'azu, T. A. Zarma, A. T. Salawudeen, S. Thomas, and A. A. Galadima, "Methods of Chattering Reduction in Sliding Mode Control: A Case Study of Ball and Plate System," in *2018 IEEE 7th International Conference on Adaptive Science & Technology (ICAST)*, 2018, pp. 1–8. doi: 10.1109/ICASTECH.2018.8506783.

[67] B. (Bin) Wu, Y. Lang, N. Zargari, and S. Kouro, *Power conversion and control of wind energy systems*. Wiley, 2011.

[68] C. H. Lin, "Novel modified Elman neural network control for PMSG system based on wind turbine emulator," *Math. Probl. Eng.*, pp. 1–15, 2013, doi: 10.1155/2013/753756.

[69] R. Errouissi, A. Al-Durra, and M. Debouza, "A novel design of PI current controller for PMSG-based wind turbine considering transient performance specifications and control saturation," *IEEE Trans. Ind. Electron.*, vol. 65, no. 11, pp. 8624–8634, 2018, doi: 10.1109/TIE.2018.2814007.

[70] T. D. Do and H. T. Nguyen, "A Generalized Observer for Estimating Fast-Varying Disturbances," *IEEE Access*, vol. 6, pp. 28054–28063, 2018, doi: 10.1109/ACCESS.2018.2833430.

[71] A. Merabet, K. T. Ahmed, H. Ibrahim, and R. Beguenane, "Implementation of Sliding Mode Control System for Generator and Grid Sides Control of Wind Energy Conversion System,"

IEEE Trans. Sustain. Energy, vol. 7, no. 3, pp. 1327–1335, 2016, doi: 10.1109/TSTE.2016.2537646.

[72] Y. Wang, W. Zhou, J. Luo, H. Yan, H. Pu and Y. Peng, "Reliable Intelligent Path Following Control for a Robotic Airship Against Sensor Faults," in IEEE/ASME Transactions on Mechatronics, vol. 24, no. 6, pp. 2572-2582, Dec. 2019, doi: 10.1109/TMECH.2019.2929224.

[73] R. Errouissi and A. Al-Durra, "A Novel PI-Type Sliding Surface for PMSG-Based Wind Turbine With Improved Transient Performance," *IEEE Trans. Energy Convers.*, vol. 33, no. 2, pp. 834–844, 2018, doi: 10.1109/TEC.2017.2776752.

[74] H. H. H. Mousa, A.-R. Youssef, and E. E. M. Mohamed, "Optimal power extraction control schemes for five-phase PMSG based wind generation systems," *Eng. Sci. Technol. an Int. J.*, no. 23, pp. 144-155, 2020, doi: 10.1016/j.jestch.2019.04.004.

[75] A. Shafiei, B. M. Dehkordi, A. Kiyoumarsi, and S. Farhangi, "A control approach for a small-scale PMSG-Based WECS in the whole wind speed range," *IEEE Trans. Power Electron.*, vol. 32, no. 12, pp. 9117–9130, 2017, doi: 10.1109/TPEL.2017.2655940.

[76] Z. Ma, Z. Yan, M. L. Shaltout, and D. Chen, "Optimal Real-Time Control of Wind Turbine During Partial Load Operation," *IEEE Trans. Control Syst. Technol.*, vol. 23, no. 6, pp. 2216–2226, 2015, doi: 10.1109/TCST.2015.2410735.

[77] I. Jlassi, S. K. El Khil, and N. M. Bellaaj, "Power switch and current sensor fault-tolerant control of PMSG drives for wind turbine systems," *Proc. - SDEMPED 2015 IEEE 10th Int. Symp. Diagnostics Electr. Mach. Power Electron. Drives*, pp. 401–407, 2015, doi: 10.1109/DEMPED.2015.7303721.

[78] Z. Zhang, Z. Li, M. P. Kazmierkowski, J. Rodriguez, and R. Kennel, "Robust Predictive Control of Three-Level NPC Back-to-Back Power Converter PMSG Wind Turbine Systems with Revised Predictions," *IEEE Trans. Power Electron.*, vol. 33, no. 11, pp. 9588–9598, 2018, doi: 10.1109/TPEL.2018.2796093.

[79] T. D. Do, "Disturbance Observer-Based Fuzzy SMC of WECSs Without Wind Speed Measurement," *IEEE Access*, vol. 5, pp. 147–155, 2017, doi: 10.1109/ACCESS.2016.2633271.

[80] H. Jafarnejadsani and J. Pieper, "Gain-scheduled λ1-optimal control of variable-speed-variable-pitch wind turbines," *IEEE Trans. Control Syst. Technol.*, vol. 23, no. 1, pp. 372–379, 2015, doi: 10.1109/TCST.2014.2320675.

[81] V. I. Utkin, "Sliding Mode Control Design Principles and Applications to Electric Drives," *IEEE Trans. Ind. Electron.*, vol. 40, no. 1, pp. 23–36, 1993, doi: 10.1109/41.184818.

[82] C. A. Evangelista, A. Pisano, P. Puleston, and E. Usai, "Receding Horizon Adaptive Second-Order Sliding Mode Control for Doubly-Fed Induction Generator Based Wind Turbine," *IEEE Trans. Control Syst. Technol.*, vol. 25, no. 1, pp. 73–84, 2017, doi:

10.1109/TCST.2016.2540539.

[83] Y. Wang, Y. Xia, H. Li, and P. Zhou, “A new integral sliding mode design method for nonlinear stochastic systems,” *Automatica*, vol. 90, pp. 304–309, 2018, doi: 10.1016/j.automatica.2017.11.029.

[84] S. Kim and S. Kwon, “Nonlinear optimal control design for underactuated two-wheeled inverted pendulum mobile platform,” *IEEE/ASME Trans. Mechatronics*, vol. 22, no. 6, pp. 2803–2808, 2017, doi: 10.1109/TMECH.2017.2767085.

[85] B. Stellato, T. Geyer, and P. J. Goulart, “High-Speed Finite Control Set Model Predictive Control for Power Electronics,” *IEEE Trans. Power Electron.*, vol. 32, no. 5, pp. 4007–4020, 2017, doi: 10.1109/TPEL.2016.2584678.

[86] Q. Gao, L. Liu, G. Feng, and Y. Wang, “Universal fuzzy integral sliding-mode controllers for stochastic nonlinear systems,” *IEEE Trans. Cybern.*, vol. 44, no. 12, pp. 2658–2669, 2014, doi: 10.1109/TCYB.2014.2313028.

[87] C. C. Chen, S. S. D. Xu, and Y. W. Liang, “Study of nonlinear integral sliding mode fault-tolerant control,” *IEEE/ASME Trans. Mechatronics*, vol. 21, no. 2, pp. 1160–1168, 2016, doi: 10.1109/TMECH.2015.2474700.

[88] A. Ferrara and G. P. Incremona, “Design of an Integral Suboptimal Second-Order Sliding Mode Controller for the Robust Motion Control of Robot Manipulators,” *IEEE Trans. Control Syst. Technol.*, vol. 23, no. 6, pp. 2316–2325, 2015, doi: 10.1109/TCST.2015.2420624.

[89] B. Qin *et al.*, “Robust h∞ control of doubly fed wind generator via state-dependent riccati equation technique,” *IEEE Trans. Power Syst.*, vol. 34, no. 3, pp. 2390–2400, 2019, doi: 10.1109/TPWRS.2018.2881687.

[90] Y. Batmani, “On the Design of Event-Triggered Suboptimal Controllers for Nonlinear Systems,” *Asian J. Control*, vol. 20, no. 3, pp. 1303–1311, 2018, doi: 10.1002/asjc.1632.

[91] S. R. Nekoo, “Model reference adaptive state-dependent Riccati equation control of nonlinear uncertain systems: Regulation and tracking of free-floating space manipulators,” *Aerosp. Sci. Technol.*, vol. 84, pp. 348–360, 2019, doi: 10.1016/j.ast.2018.10.005.

[92] S. M. H. Rostami, A. K. Sangaiah, J. Wang, and H. jin Kim, “Real-time obstacle avoidance of mobile robots using state-dependent Riccati equation approach,” *Eurasip J. Image Video Process.*, vol. 2018, no. 1, pp. 1–13, 2018, doi: 10.1186/s13640-018-0319-1.

[93] M. P. Kazmierkowski, “High Performance Control of ac Drives with MATLAB/Simulink Models [Book News],” *IEEE Ind. Electron. Mag.*, vol. 6, no. 4, pp. 68–69, 2012, doi: 10.1109/MIE.2012.2222252.

[94] “Mohan, N. and Raju, S. (2020). Induction Machine Equations in Phase Quantities. In Analysis and Control of Electric Drives (eds N. Mohan and S. Raju). https://doi.org/10.1002/9781119584575.ch11

[95] M. P. Kazmierkowski, T. Orłowska-Kowalska, and M. Kamińsaki, “Advanced and intelligent

control in power electronics and drives," in *Studies in Computational Intelligence*, vol. 531, no. 3, 2014, pp. 269–302. doi: 10.1007/978-3-319-03401-0_8.

[96] V. Yaramasu and B. Wu, "Basics of wind energy conversion systems (WECS)," in *Model Predictive Control of Wind Energy Conversion Systems*, John Wiley & Sons, Inc., 2016, pp. 1–467. doi: 10.1002/9781119082989.

[97] M. A. Abdullah, A. H. M. Yatim, C. W. Tan, and R. Saidur, "A review of maximum power point tracking algorithms for wind energy systems," *Renew. Sustain. Energy Rev.*, vol. 16, no. 5, pp. 3220–3227, 2012, doi: 10.1016/j.rser.2012.02.016.

[98] M. T. Hamayun, C. Edwards, H. Alwi, " A fault tolerant control allocation scheme with output integral sliding modes ,"*Automatica*, vol. 49, no. 6, pp. 1830-1837, 2013.

[99] P. Kshirsagar *et al.*, "Implementation and sensorless vector-control design and tuning strategy for SMPM machines in fan-type applications," *IEEE Trans. Ind. Appl.*, vol. 48, no. 6, pp. 2402–2413, 2012, doi: 10.1109/TIA.2012.2227135.

[100] B.-S. Jun, J. Park, J.-H. Choi, K.-D. Lee, and C.-Y. Won, "Temperature Estimation of Stator Winding in Permanent Magnet Synchronous Motors Using d-Axis Current Injection," Energies, vol. 11, no. 8, p. 2033, Aug. 2018, doi: 10.3390/en11082033.

[101] T. Chai and R. R. Draxler, "Root mean square error (RMSE) or mean absolute error (MAE)? – Arguments against avoiding RMSE in the literature," *Geosci. Model Dev.*, vol. 7, no. 3, pp. 1247–1250, 2014, doi: 10.5194/gmd-7-1247-2014.

[102] D. Zholtayev, M. Rubagotti, and T. D. Do, "Adaptive super-twisting sliding mode control for maximum power point tracking of PMSG-based wind energy conversion systems," *Renew. Energy*, vol. 183, pp. 877–889, 2022, doi: https://doi.org/10.1016/j.renene.2021.11.055.